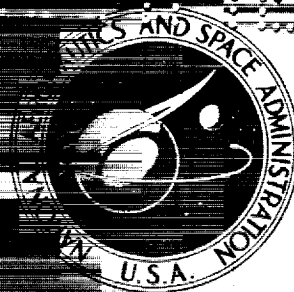


X66-1675

NASA TECHNICAL
MEMORANDUM



UB
NASA TM X-1227

UB
NASA TM X-1227

CASE FILE
COPY

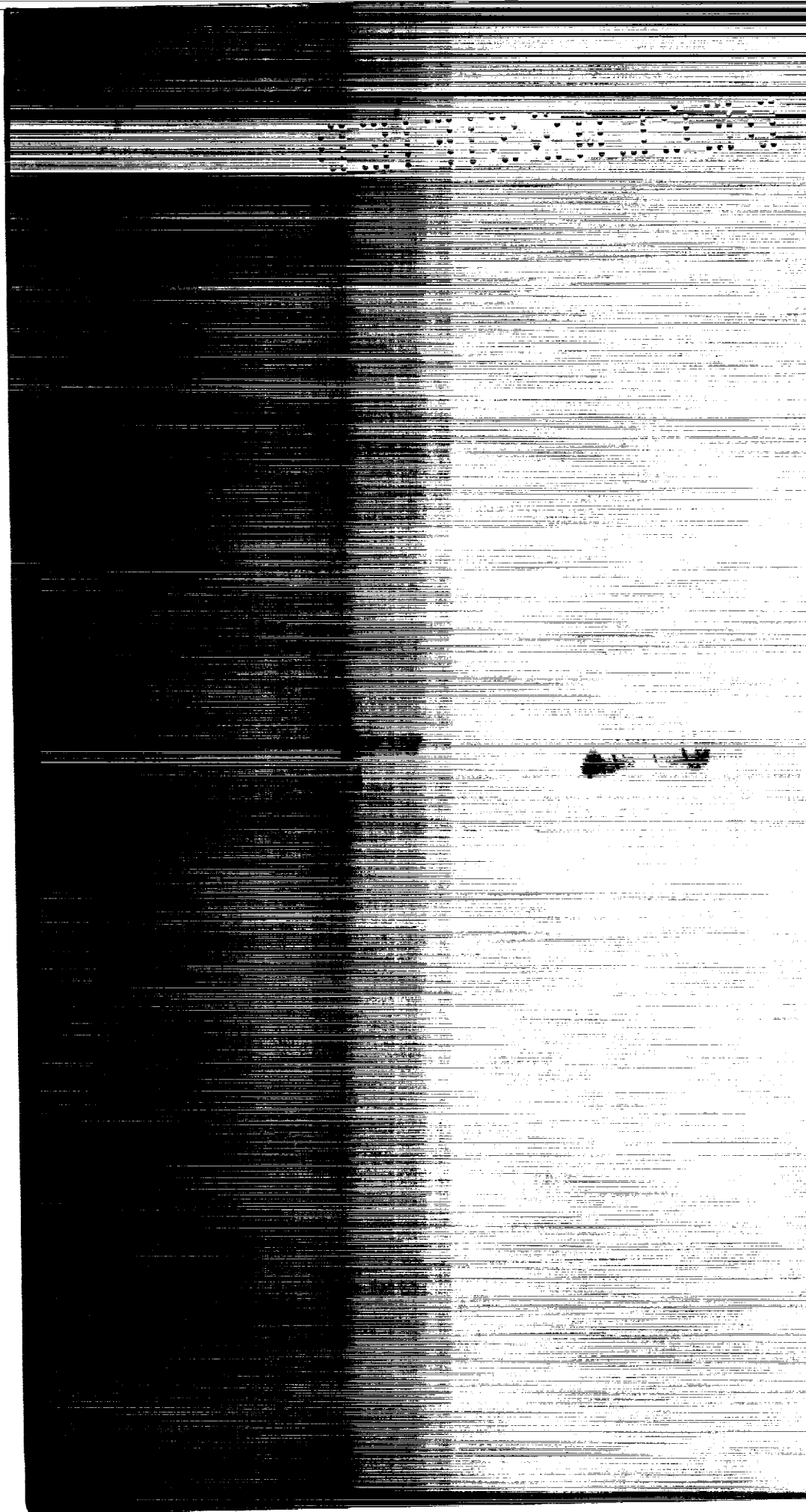
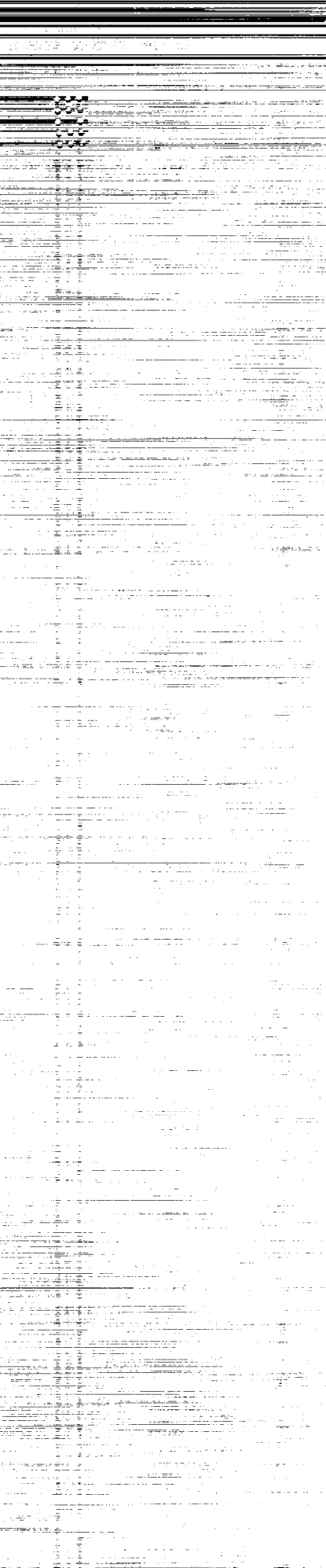
Declassified by authority of NASA
Classification Change Notices No. [REDACTED]
Dated ** [REDACTED] 15 DEC 1970 210 [REDACTED]

SUBSONIC LONGITUDINAL CONTROL
CHARACTERISTICS OF SEVERAL
ELEVON CONFIGURATIONS FOR A
MANNED LIFTING ENTRY VEHICLE

by Bernard Spencer, Jr., and Charles H. Fox, Jr.

Langley Research Center

Langley Station, Hampton, Va.



U
U
U

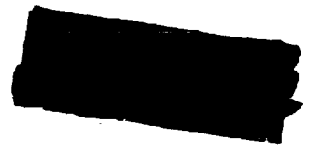
DECLASSIFIED

NASA TM X-1227

SUBSONIC LONGITUDINAL CONTROL CHARACTERISTICS
OF SEVERAL ELEVON CONFIGURATIONS FOR A
MANNED LIFTING ENTRY VEHICLE

By Bernard Spencer, Jr., and Charles H. Fox, Jr.

Langley Research Center
Langley Station, Hampton, Va.



NATIONAL AERONAUTICS AND SPACE ADMINISTRATION



[REDACTED]
031712Z1000

11

[REDACTED]

[REDACTED]

[REDACTED]

[REDACTED]

[REDACTED]

[REDACTED]

[REDACTED]

SUBSONIC LONGITUDINAL CONTROL CHARACTERISTICS
OF SEVERAL ELEVON CONFIGURATIONS FOR A
MANNED LIFTING ENTRY VEHICLE*

By Bernard Spencer, Jr., and Charles H. Fox, Jr.
Langley Research Center

SUMMARY

An investigation has been conducted at low subsonic speeds on a model of the HL-10 reentry vehicle configuration. The effects of increasing elevon and fin boat-tailing on the longitudinal stability and control effectiveness characteristics of both a one-fin and a three-fin configuration have been investigated. The tests were made in the Langley high-speed 7- by 10-foot tunnel at a Mach number of 0.35, corresponding to an average Reynolds number based on body length of 5.73×10^6 . The angle of attack ranged from approximately -6° to 23° at a 0° angle of sideslip.

For the three-fin configuration, boattailing the rudder of the center fin and the outer edge of the tip fins increased the maximum trimmed lift-drag ratio from approximately 3.2 to 4.0. A comparison of the effects of elevon boattail angle on both the three-fin and one-fin configurations indicated that the value of the maximum trimmed lift-drag ratio generally increased with increasing elevon boattail angle. For the highest boattail angle on the three-fin configuration, however, no stable trim existed in the region of maximum lift-drag ratio due to nonlinearities in the pitching moment and attendant losses in control effectiveness. A comparison of the three-fin and one-fin HL-10 maximum lift-drag ratio characteristics showed that the three-fin HL-10 had higher values of both trimmed and untrimmed maximum lift-drag ratio. The addition of small trailing-edge base extensions having varying degrees of boattailing to the original elevon provided values of both trimmed and untrimmed lift-drag ratio which were as high or higher than those of any other configuration tested.

INTRODUCTION

The National Aeronautics and Space Administration is presently engaged in numerous wind-tunnel investigations to obtain aerodynamic data on a manned lifting entry vehicle designated HL-10 (horizontal lander 10). The results of some of these investigations are reported in references 1 to 18. This configuration is designed to provide some

*Title, Unclassified.

[REDACTED]

hypersonic lift and lift-drag ratio and to have horizontal-landing capabilities. Low values of lift and lift-drag ratio inherent with this type of vehicle at subsonic speeds, however, produce problems since both lift and lift-drag ratio are of prime importance with regard to vehicle handling qualities and sink rate. Since the low values of the lift-curve slope cannot be increased for landing without resorting to some form of variable geometry or alteration in planform design, attention is currently focused on other methods of increasing the lift-drag ratio to improve the landing capabilities of the vehicle.

Results of an investigation on methods of increasing the subsonic lift-drag ratio of the HL-10 (ref. 11) have indicated that considerable improvement may be realized by boattailing regions of the center fin and tip fins to approximately a zero base thickness. These modifications can be made without penalizing the salient design points for entry or hypersonic flight by restoring the original surface with a movable flap. An investigation at a Reynolds number (based on body length) of 15×10^6 on the HL-10 configuration incorporating the modifications suggested in reference 11 has indicated that trimmed lift-drag ratios of 4.70 are obtainable. (See ref. 15.) The purpose of the present investigation is to extend the work of references 11 and 15 to study the effects of additional boattailing on the elevon surfaces and the resultant effects on longitudinal control effectiveness and stability. The elevon modifications have been investigated on both a three-fin and a one-fin configuration. All tests were made at a Mach number of 0.35, corresponding to an average test Reynolds number based on body length of 5.73×10^6 . The angle of attack was varied from approximately -6° to 23° at a 0° angle of sideslip.

SYMBOLS

All data are referred to the stability axis system, with all coefficients nondimensionalized with respect to the actual length and projected planform area of the body. The reference center of moments was located at 53 percent of the body length aft of the nose, and at 1.25 percent of the body length below the indicated body reference line. (See fig. 1(a).)

C_D	drag coefficient, $\frac{\text{Drag}}{q_\infty S}$
C_L	lift coefficient, $\frac{\text{Lift}}{q_\infty S}$
C_m	pitching-moment coefficient, $\frac{\text{Pitching moment}}{q_\infty S l}$
L/D	lift-drag ratio
l	length of vehicle, 30.54 in. (0.776 m)

q_∞	free-stream dynamic pressure, lb/ft^2 (N/m^2)
R	Reynolds number
r	radius
S	reference area, equal to projected planform area of body with elevons, 0.357ft^2 (2.31ft^2) (0.2145m^2)
α	angle of attack, deg
δ_e	elevon deflection angle, positive with trailing edge down, deg
δ_l	angle of elevon base extension lower surface, measured from elevon lower surface, deg
δ_u	angle of elevon base extension upper surface, measured from elevon upper surface with $\theta = 0^\circ$, deg
θ	angle of elevon upper surface boattail, measured from original elevon upper surface, deg

Subscripts:

max maximum condition

trim trimmed condition

Model component designations:

E_2 basic center fin

I_4 tip fins

MODEL

Design concepts and configuration geometry of the HL-10 are presented in reference 16. The designations for model components given in references 15 and 16 are used in the present paper where possible. Drawings of the model and various model components tested are presented in figure 1.

[REDACTED]

The body of the HL-10 configurations has a 74° delta planform with a thick negatively cambered airfoil section. Both the body with a center fin (one-fin configuration) and the body with a center fin and tip fins (three-fin configuration) have been tested with and without modifications to the fins. The basic center fin is designated E_2 (fig. 1(a)); this center fin boattailed to a 12° included angle on the rudder section is designated modified E_2 (fig. 1(c)). The basic tip fins are designated I_4 (fig. 1(b)), and the tip fins with 28.90° of outer edge boattailing are designated modified I_4 (fig. 1(c)). The configuration with both the center fin and the tip fins modified is designated mod ($E_2 + I_4$). This designation corresponds to the designation modified $E_2 + I_4$ in reference 15. Photographs of a model of the HL-10 showing several of the fin and elevon modifications are presented in figure 2.

The elevon was modified from the original thickness to have varying degrees of upper surface boattailing, with θ designating the boattail angle as measured from the original upper surface. Boattail angles of 0° , 4° , 8° , and 12° have been tested. The use of vortex generators to delay upper surface separation as noted in reference 11 has also been investigated for most of the configurations. (See fig. 1(b).) Several small trailing-edge extensions having various combinations of upper and lower surface boattailing were added to the original elevon ($\theta = 0^\circ$) in an effort to reduce the base drag associated with this elevon without inducing early upper surface separation.

TESTS AND CORRECTIONS

The present investigation was made in the Langley high-speed 7- by 10-foot tunnel at a Mach number of 0.35, corresponding to an average test Reynolds number based on body maximum length of 5.73×10^6 . The model was sting mounted, and forces and moments were measured by means of an internally mounted six-component strain-gage balance. The angle of attack ranged from approximately -6° to 23° at a 0° angle of sideslip.

Jet-boundary and solid-blockage corrections, determined by the methods described in references 19 and 20, respectively, have been applied to the data. The angle of attack has also been corrected for the effects of sting and balance bending under load. All drag data of this investigation represent gross drag, and have not been corrected for static pressures in the balance cavity. Transition strips of No. 100 carborundum grains were utilized on the model nose only. They were placed 10.0 percent of the body length aft of the body nose unless otherwise noted.

RESULTS AND DISCUSSION

The effects of various fin and elevon modifications on the basic subsonic aerodynamic characteristics of the three-fin HL-10 configuration are presented in figure 3 for an elevon deflection angle of 0° . The alterations of the center fin and tip fins are modifications of suggestions presented in reference 11 for improving the HL-10 subsonic lift-drag ratio characteristics. Data on the effect of elevon boattail angle on the longitudinal control characteristics for both the three-fin and the one-fin configurations are presented in figures 4 to 13 and summarized in figures 14 to 20 in the form of plots of the trimmed lift and lift-drag ratio as a function of the angle of attack. Most of the discussion is confined to the summary figures.

Performance and Control Effectiveness Characteristics

The effects of boattailing the rudder of center fin E_2 and the outer edge of tip fin I_4 on the trimmed lift coefficient, lift-drag ratio, and corresponding angle of attack are shown in figure 14 for the three-fin configuration having the original elevon. For the configuration with no vortex generators, an increase in trimmed $(L/D)_{\max}$ from approximately 3.2 to 4.0 is shown. The addition of the vortex generators further increased the trimmed $(L/D)_{\max}$ to approximately 4.3 by delaying flow separation on the body upper surface at the higher angles of attack and thus reducing the drag.

The effects of increasing the elevon boattail angle on the trimmed lift coefficient, lift-drag ratio, and angle of attack for the three-fin HL-10 configuration having modified fins E_2 plus I_4 with and without vortex generators are presented in figures 15 to 17. These data for the configuration with vortex generators on are summarized as a function of boattail angle θ in figure 20. The value of trimmed $(L/D)_{\max}$ increases from approximately 4.4 for $\theta = 0^\circ$ to 4.75 for $\theta = 8^\circ$ (fig. 20). For $\theta = 12^\circ$, however, no stable trim points exist in the angle-of-attack region of $(L/D)_{\max}$ because of the increased instability and attendant losses in control effectiveness for this highest elevon boattail angle. (See figs. 9(b) and 17.) The values of untrimmed $(L/D)_{\max}$ for the three-fin HL-10 configuration are also shown in figure 20 and indicate little or no change in $(L/D)_{\max}$ with increased elevon boattailing. The elevon deflection associated with the highest value of untrimmed $(L/D)_{\max}$ is dependent on the boattail angle θ , as may be noted from the basic data of figures 4 to 9.

In an effort to retain the favorable linear pitching-moment variations with δ_e and α of the configuration with $\theta = 0^\circ$ while reducing the elevon base areas, several small trailing-edge extensions having varying degrees of boattailing were attached to the elevon bases. The effects of adding these extensions to the original elevon ($\theta = 0^\circ$) are summarized in figures 18 and 20 for the three-fin HL-10 configuration having modified

[REDACTED]

fins E₂ plus I₄ and vortex generators on. The extension showing the most improvement in performance had 15° and 26° of lower and upper surface boattailing, respectively, and a resultant value of trimmed $(L/D)_{\max}$ of 4.65 (fig. 18). This configuration provided values of both trimmed and untrimmed lift-drag ratio that were as high as or higher than those of any other configuration investigated. (See fig. 20.)


Data on the effects of elevon boattailing on the trimmed lift coefficient, maximum lift-drag ratio, and angle of attack for the one-fin HL-10 configuration with and without vortex generators are presented in figure 19 and compared with the three-fin configuration data in figure 20. The value of trimmed $(L/D)_{\max}$ increases from approximately 4.0 for $\theta = 0^\circ$ to 4.30 for $\theta = 12^\circ$ for the one-fin configuration. (See fig. 19.) The data of figure 20 indicate that the values of both the trimmed and untrimmed $(L/D)_{\max}$ noted for the three-fin arrangement are significantly higher than the values obtainable with the one-fin configuration. For the highest elevon boattail angle tested ($\theta = 12^\circ$), trim existed to the maximum test angle of attack on the one-fin HL-10 configuration because of the low level of longitudinal stability and resultant low elevon settings required for trim. (See figs. 13 and 19.) Larger penalties in L/D due to trim for the one-fin configuration may be expected if the level of longitudinal stability were adjusted to that for the three-fin configurations.

Reynolds Number Effects

The data of the present investigation obtained on the three-fin HL-10 configuration having modified fins E₂ plus I₄ and $\theta = 4^\circ$ at a Reynolds number of approximately 5.73×10^6 are compared in figure 15 with data obtained on the same configuration at a Reynolds number of approximately 15×10^6 (as presented in ref. 15). For the configuration in the present test, a value of trimmed $(L/D)_{\max}$ of 4.3 was obtained at a Reynolds number of approximately 5.73×10^6 . (See fig. 15(a).) The tests of reference 15 ($R = 15 \times 10^6$) indicate higher values of the trimmed L/D at angles of attack above 13° and an increase in the value of the trimmed $(L/D)_{\max}$ from 4.3 to 4.7 at an angle of attack of approximately 16° . These increases in the value of the lift-drag ratio are a result of the increase in Reynolds number, which causes a reduction in skin-friction drag and a delay in trailing-edge flow separation. The delay in trailing-edge flow separation is evidenced by the fact that the addition of vortex generators to the configuration in the present tests results in a similar but lower increase in the value of $(L/D)_{\text{trim}}$ at the high angles of attack. (See fig. 15(a).)

CONCLUDING REMARKS

An investigation has been conducted at low subsonic speeds on a model of the HL-10 reentry configuration. The effects of increasing elevon and fin boattailing on the



longitudinal stability and control effectiveness characteristics of both a one-fin and a three-fin arrangement have been investigated. The tests were made in the Langley high-speed 7- by 10-foot tunnel at a Mach number of 0.35, corresponding to an average Reynolds number based on body length of 5.73×10^6 . The angle of attack ranged from approximately -6° to 23° at a 0° angle of sideslip. Results of the investigation may be summarized as follows:

1. For the three-fin configuration, boattailing the rudder of the center fin and the outer edge of the tip fins increased the maximum trimmed lift-drag ratio from approximately 3.2 to 4.0.
2. A comparison of the effects of elevon boattail angle on the longitudinal control characteristics for both the three-fin and one-fin configurations indicates that the values of the maximum trimmed lift-drag ratio generally increased with increasing elevon boattail angle. For the three-fin configuration having the highest elevon boattail angle, no stable trim exists in the region of maximum lift-drag ratio due to nonlinearities in the pitching moment and attendant losses in control effectiveness.
3. A comparison of the three-fin and one-fin HL-10 maximum lift-drag ratio characteristics shows that the three-fin HL-10 configuration exhibited considerably higher values of both trimmed and untrimmed maximum lift-drag ratio.
4. The addition of small trailing-edge base extensions having varying degrees of boattailing to the original elevon provided values of both trimmed and untrimmed lift-drag ratio that were as high or higher than those of any other configuration tested.

Langley Research Center,
National Aeronautics and Space Administration,
Langley Station, Hampton, Va., January 25, 1966.

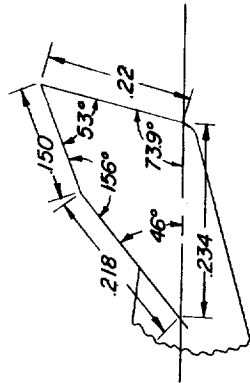
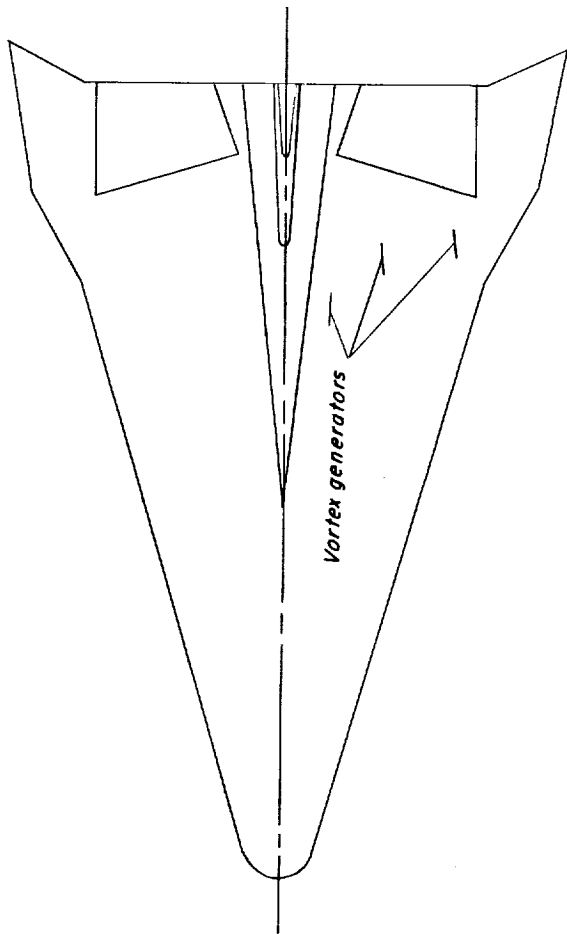
REFERENCES

1. Johnston, Patrick J.: Stability Characteristics of a Manned Lifting Entry Vehicle at a Mach Number of 20.3 in Helium. NASA TM X-1156, 1965.
2. Harris, Julius E.: Longitudinal Aerodynamic Characteristics of a Manned Lifting Entry Vehicle at a Mach Number of 19.7. NASA TM X-1080, 1965.
3. Rainey, Robert W.; and Ladson, Charles L.: Preliminary Aerodynamic Characteristics of a Manned Lifting Entry Vehicle at a Mach Number of 6.8. NASA TM X-844, 1963.
4. Ladson, Charles L.: Aerodynamic Characteristics of a Manned Lifting Entry Vehicle at a Mach Number of 6.8. NASA TM X-915, 1964.
5. McShera, John T., Jr.; and Campbell, James F.: Stability and Control Characteristics of a Manned Lifting Entry Vehicle at Mach Numbers From 2.29 to 4.63. NASA TM X-1019, 1964.
6. Campbell, James F.; and McShera, John T., Jr.: Stability and Control Characteristics From Mach Number 1.50 to 2.86 of a Model of a Manned Lifting Entry Vehicle. NASA TM X-1117, 1965.
7. Silvers, H. Norman; and Campbell, James F.: Stability Characteristics of a Manned Lifting Entry Vehicle With Various Fins at Mach Numbers From 1.50 to 2.86. NASA TM X-1161, 1965.
8. Rainey, Robert W.; and Ladson, Charles L.: Aerodynamic Characteristics of a Manned Lifting Entry Vehicle at Mach Numbers From 0.2 to 1.2. NASA TM X-1015, 1964.
9. Ware, George M.: Aerodynamic Characteristics of Models of Two Thick 74° Delta Manned Lifting Entry Vehicles at Low-Subsonic Speeds. NASA TM X-914, 1964.
10. Ware, George M.: Effect of Fin Arrangements on Aerodynamic Characteristics of a Thick 74° Delta Manned Lifting Entry Vehicle at Low-Subsonic Speeds. NASA TM X-1020, 1965.
11. Spencer, Bernard, Jr.: An Investigation of Methods of Improving Subsonic Performance of a Manned Lifting Entry Vehicle. NASA TM X-1157, 1965.
12. Moul, Martin T.; and Brown, Lawrence W.: Some Effects of Directional Instability on Lateral Handling Qualities of an Early Version of a Manned Lifting Entry Vehicle. NASA TM X-1162, 1965.

- 
13. Dunavant, James C.; and Everhart, Philip E.: Investigation of the Heat Transfer to the HL-10 Manned Lifting Entry Vehicle at a Mach Number of 8. NASA TM X-998, 1964.
14. Everhart, Philip E.; and Hamilton, H. Harris: Investigation of Roughness-Induced Turbulent Heating to the HL-10 Manned Lifting Entry Vehicle at a Mach Number of 8. NASA TM X-1101, 1965.
15. Ware, George M.: Full-Scale Wind-Tunnel Investigation of the Aerodynamic Characteristics of the HL-10 Manned Lifting Entry Vehicle. NASA TM X-1160, 1965.
16. Rainey, Robert W.: Summary of an Advanced Manned Lifting Entry Vehicle Study. NASA TM X-1159, 1965.
17. McShera, John T., Jr.; and Campbell, James F.: Aerodynamic Characteristics From Mach 1.50 to 2.86 of a Lifting Entry Vehicle Alone, With Adapter Sections, and With a Saturn Launch Vehicle. NASA TM X-1125, 1965.
18. Campbell, James F.: Effects of Tip-Fin Geometry on Stability Characteristics of a Manned Lifting Entry Vehicle From Mach 1.50 to 2.86. NASA TM X-1176, 1965.
19. Gillis, Clarence L.; Polhamus, Edward C.; and Gray, Joseph L., Jr.: Charts for Determining Jet-Boundary Corrections for Complete Models in 7- by 10-Foot Closed Rectangular Wind Tunnels. NACA WR L-123, 1945. (Formerly NACA ARR L5G31.)
20. Herriot, John G.: Blockage Corrections for Three-Dimensional-Flow Closed-Throat Wind Tunnel, With Consideration of the Effect of Compressibility. NACA Rept. 995, 1950. (Supersedes NACA RM A7B28.)

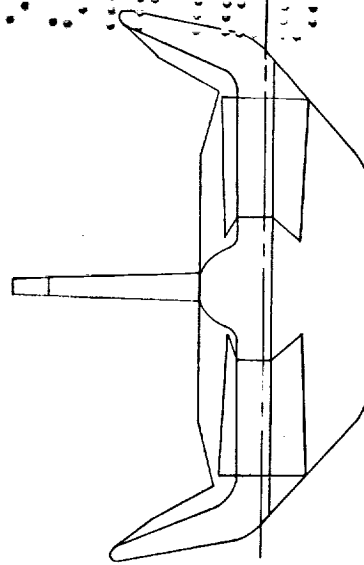
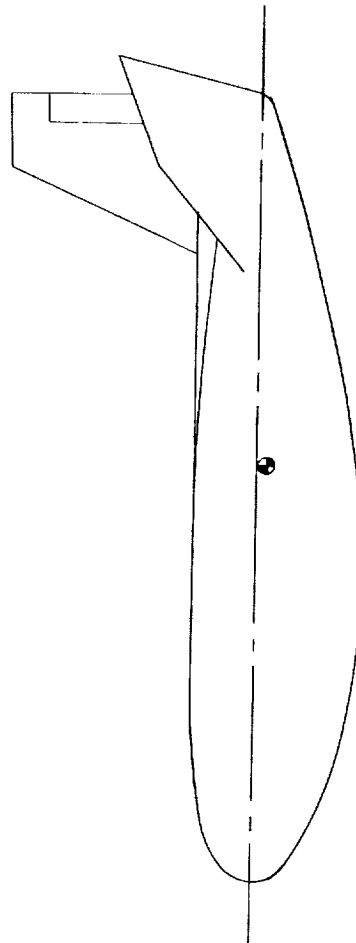


(a) One-fin HL-10. Center fin E2.



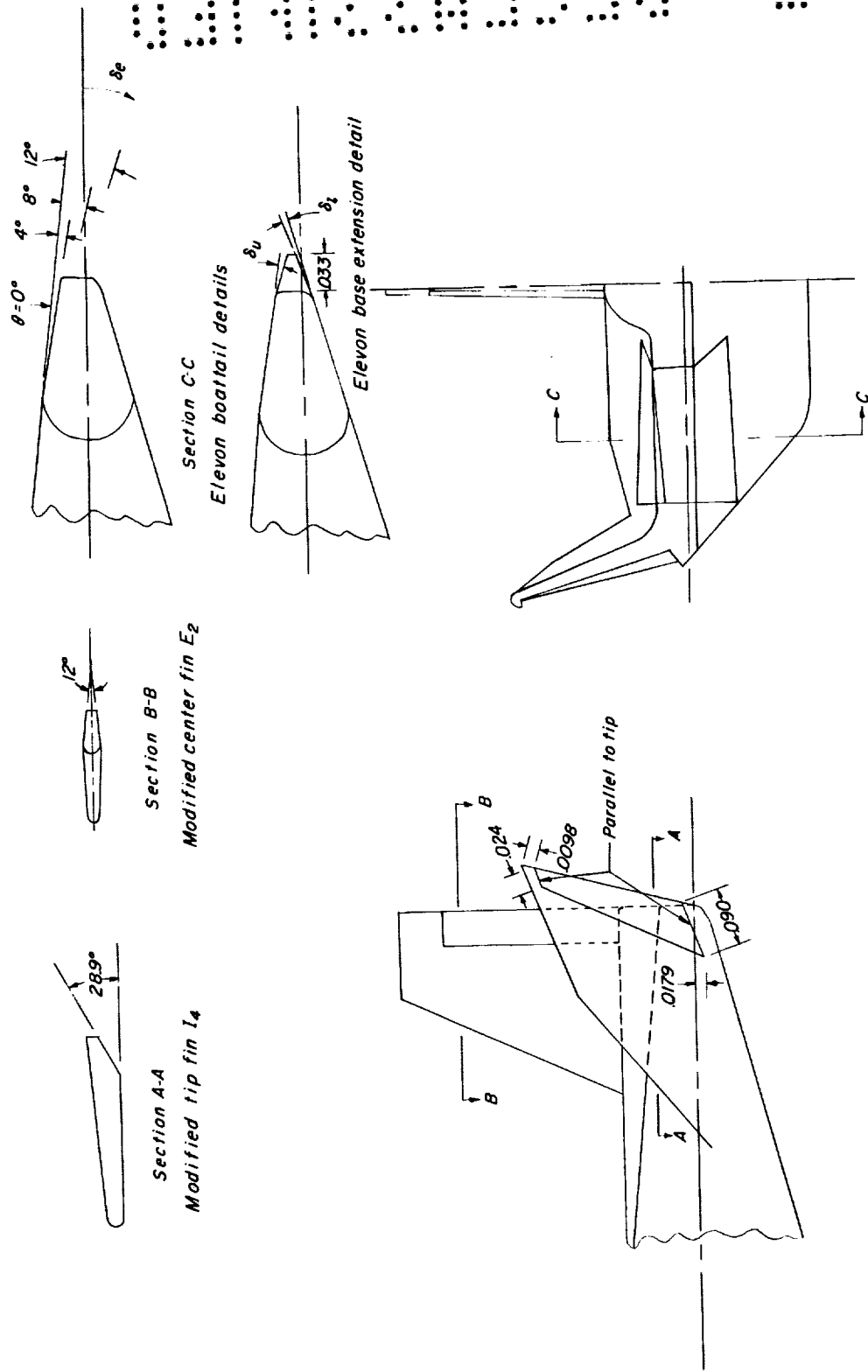
Tip fin I₄

Dimensions are in plane of fin



(b) Three-fin HL-10. Center fin E₂; tip fin I₄.

Figure 1.- Continued.



(c) Modified fins E₂ plus I₄ and elevon details showing various degrees of boattailing.

Figure 1.- Concluded.

SECRET

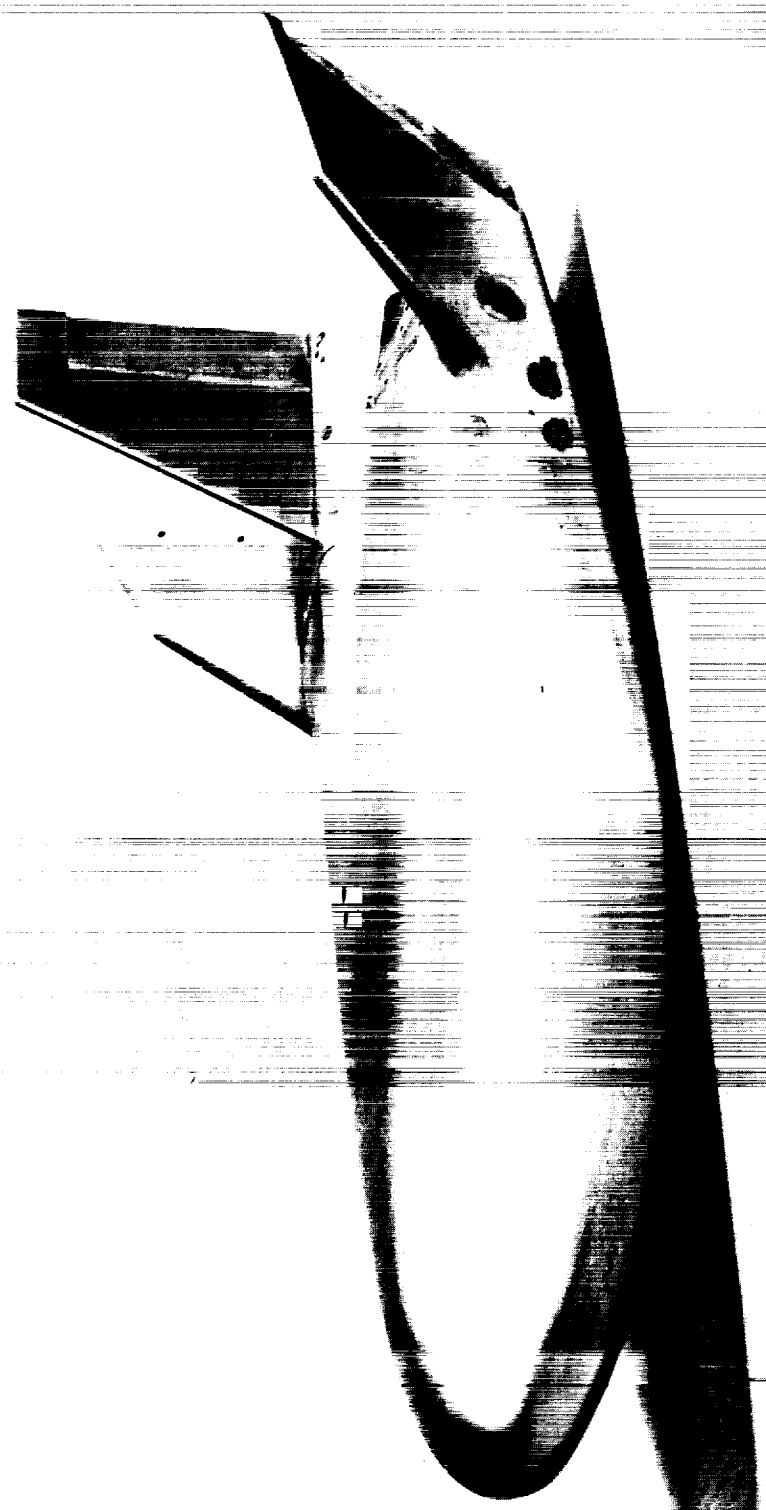


(a) Three-fin configuration. Original elevon; $\theta = 0^\circ$; original fins E_2 plus I_4 .

Figure 2.- Photographs of model.

L-65-3607

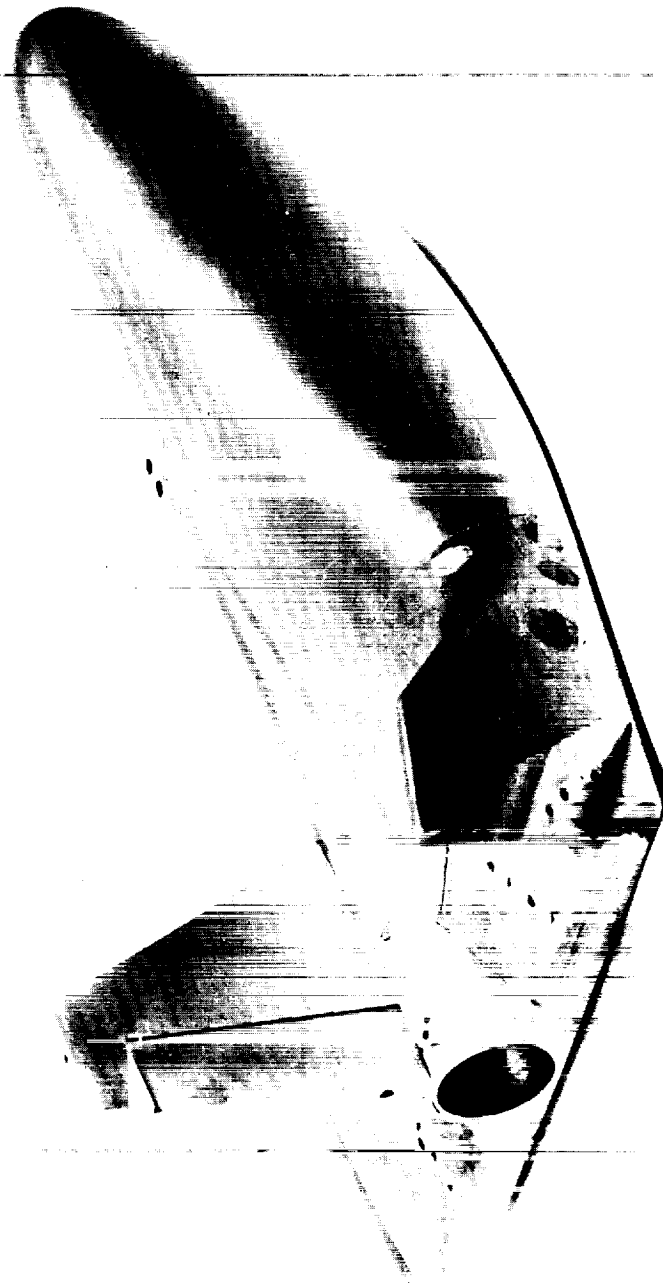
0317281001



L-65-3608

(b) Three-fin configuration. Modified elevon; $\theta = 40^\circ$, modified fins E_2 plus I_4 .

Figure 2.- Continued.



(c) Three-fin configuration. Modified elevon; $\theta = 40^\circ$; modified fins E_2 plus I_4 .

Figure 2.- Concluded.

L-65-3609

θ, deg Transition

- \circ $E_2 + I_4$ Off
- \square $E_2 + I_4$ On
- \diamond Mod $E_2 + I_4$ On
- \triangle Mod $(E_2 + I_4)$ On
- ∇ Mod $(E_2 + I_4)$ On

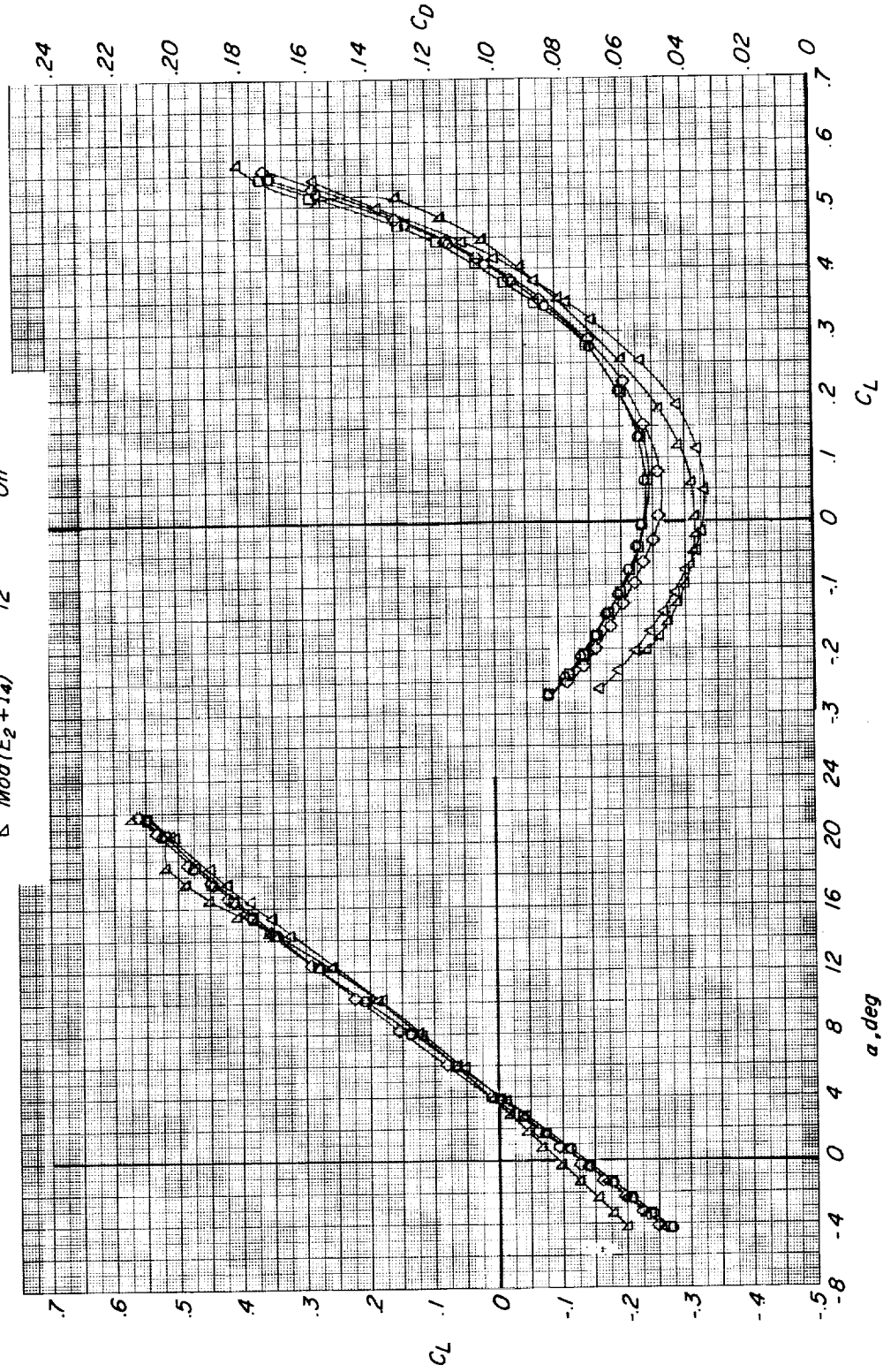


Figure 3.- Effects of various combinations of geometric changes on basic three-fin HL-10 configuration. $\delta_e = 0^\circ$.

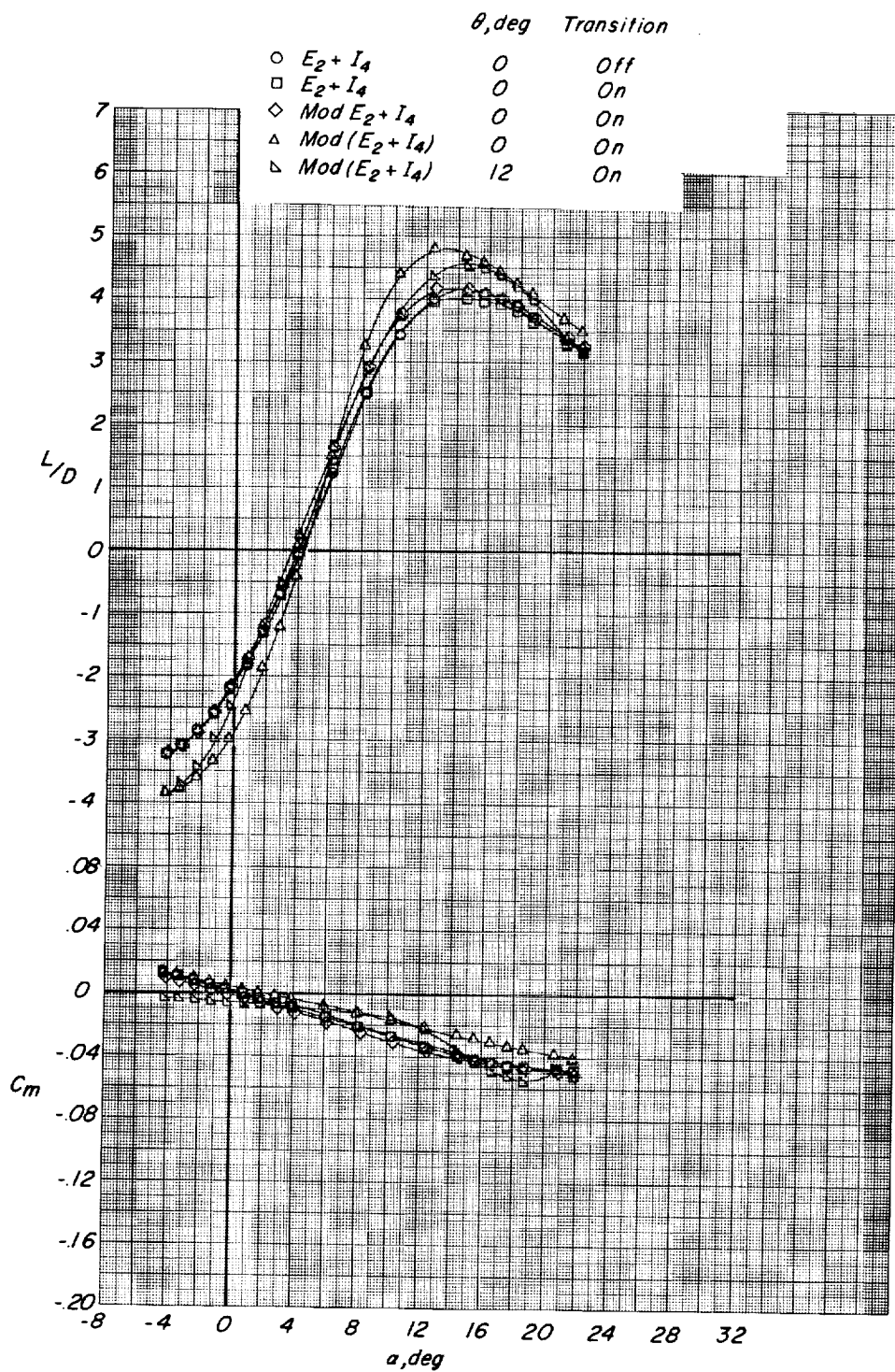


Figure 3.- Continued.

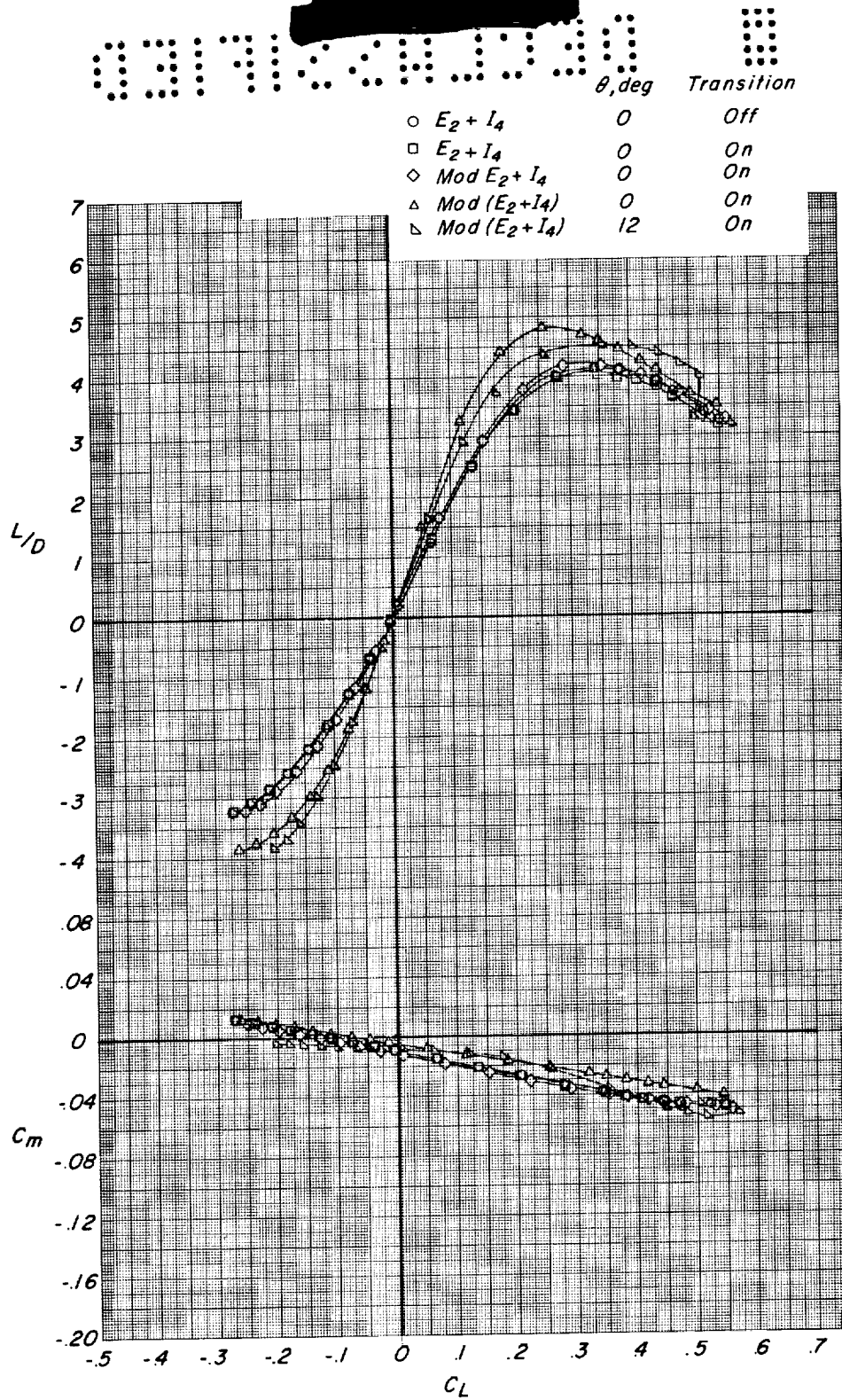


Figure 3.- Concluded.

$\delta e, \text{deg}$ Nose probe
 0 Off
 -5 Off
 -10 Off
 -10 On
 -20 On
 5 On

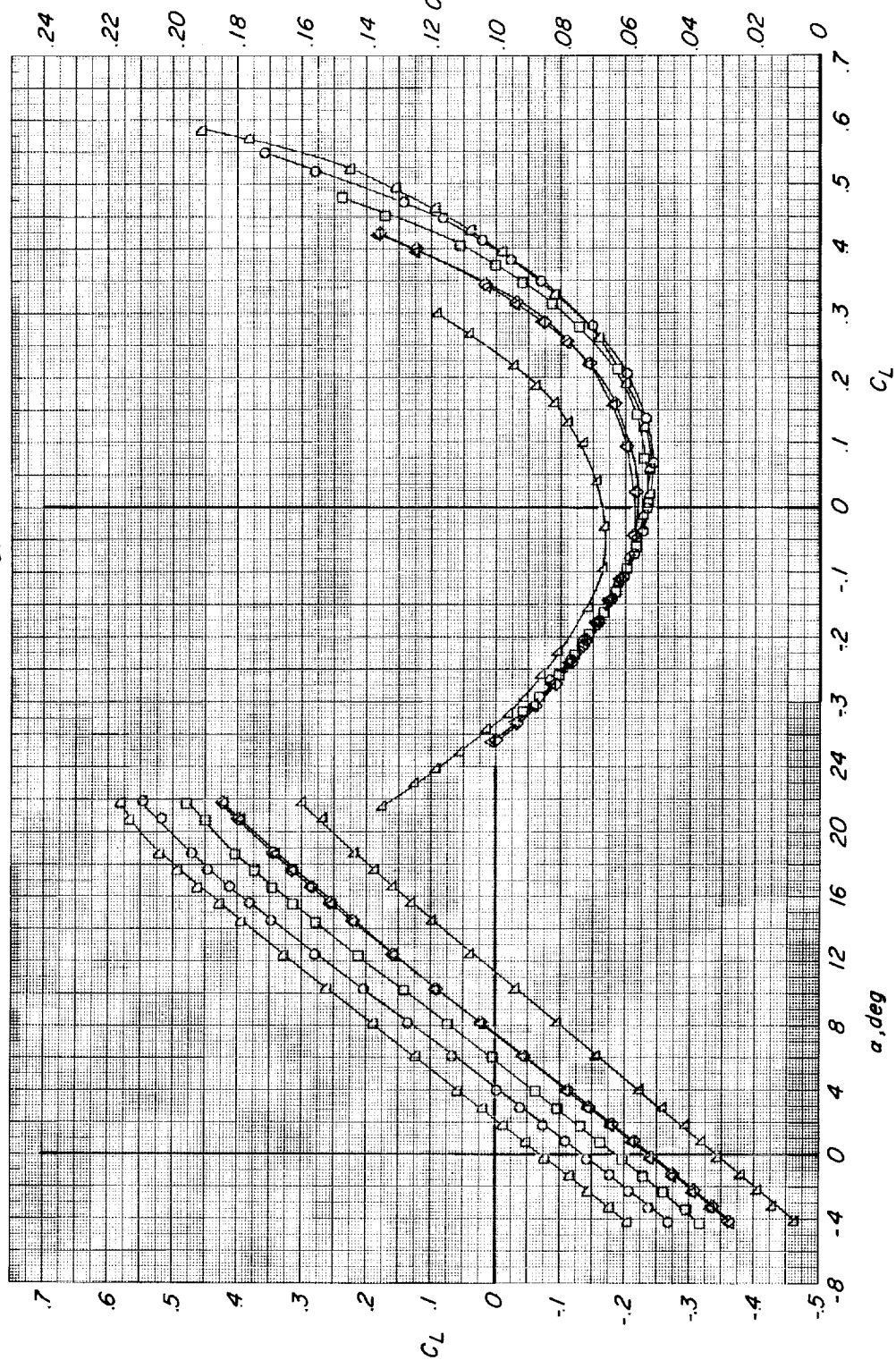


Figure 4.- Longitudinal control characteristics associated with deflection of original HL-10 elevon. $\theta = 0^\circ$; vortex generators off; three-fin HL-10; fins E2 plus I4.

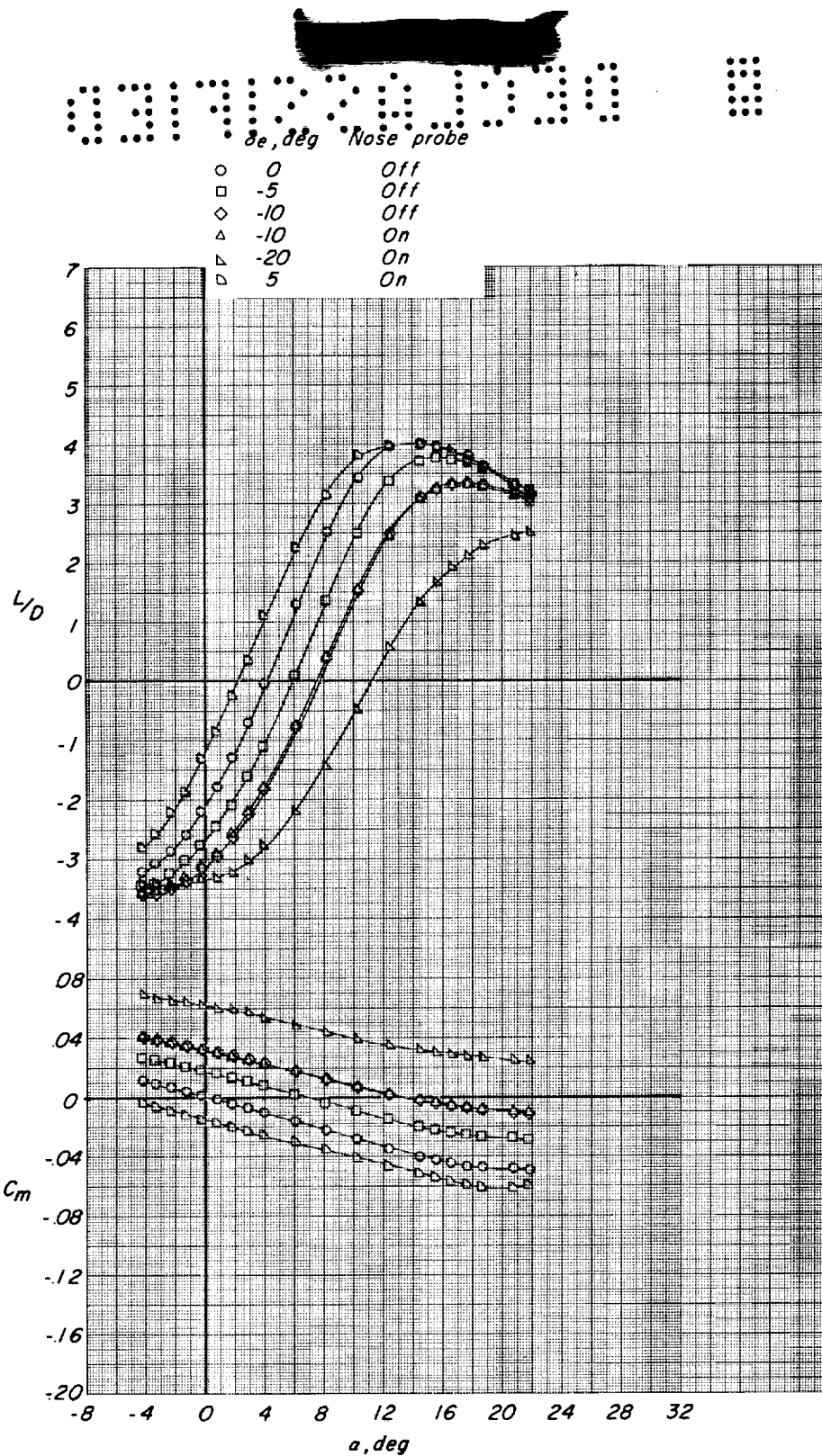


Figure 4.- Continued.

δ_e, deg

- \circ 0
 \square -5
 \diamond -10
 \triangle 5

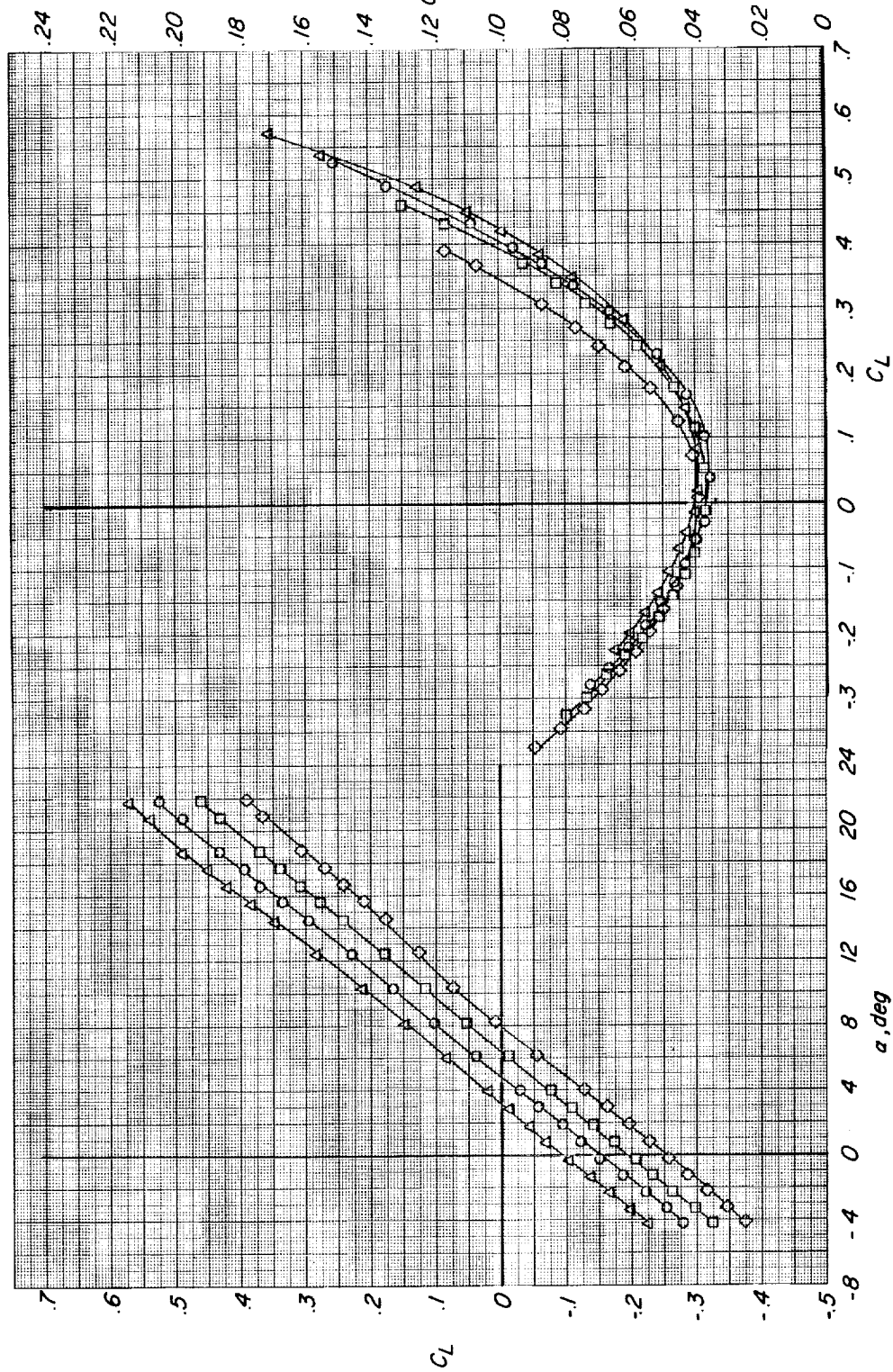


Figure 5.- Longitudinal control characteristics associated with deflection of original HL-10 elevon. $\theta = 0^\circ$; vortex generators off; three-fin HL-10; fins E_2 plus modified I_4 .

○	0
□	-5
◇	-10
△	5

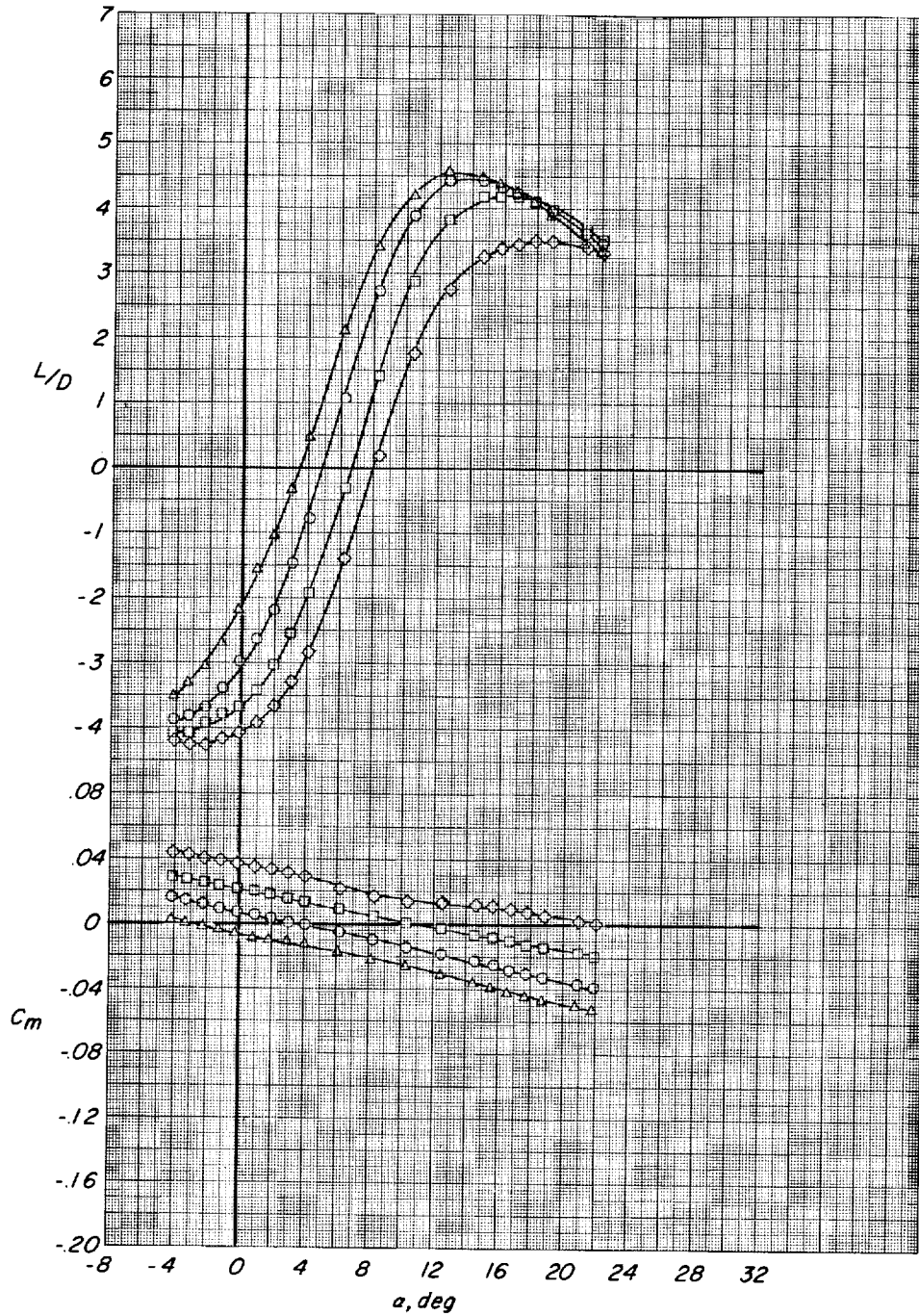


Figure 5.- Continued.

[REDACTED]

037105000

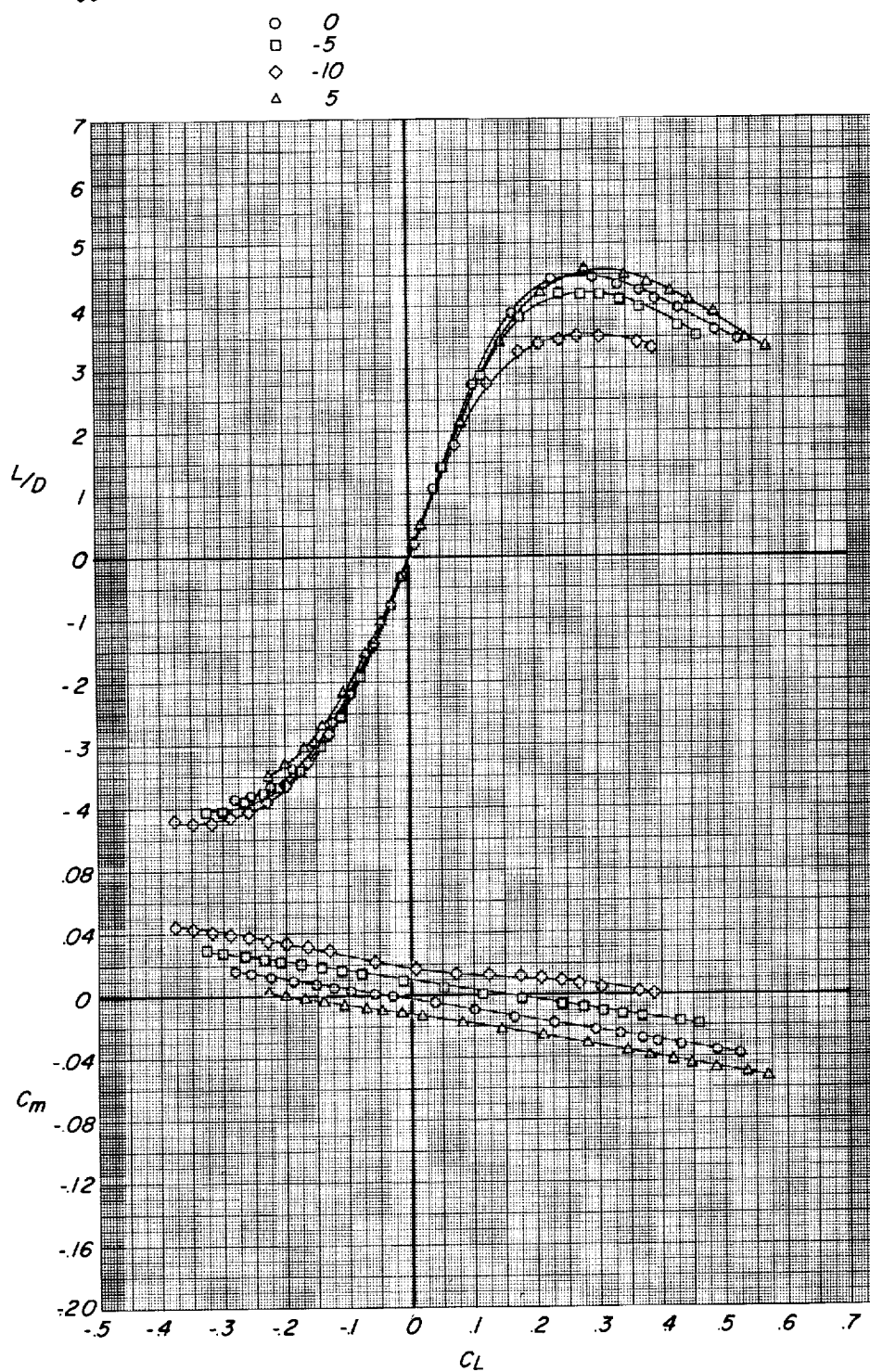
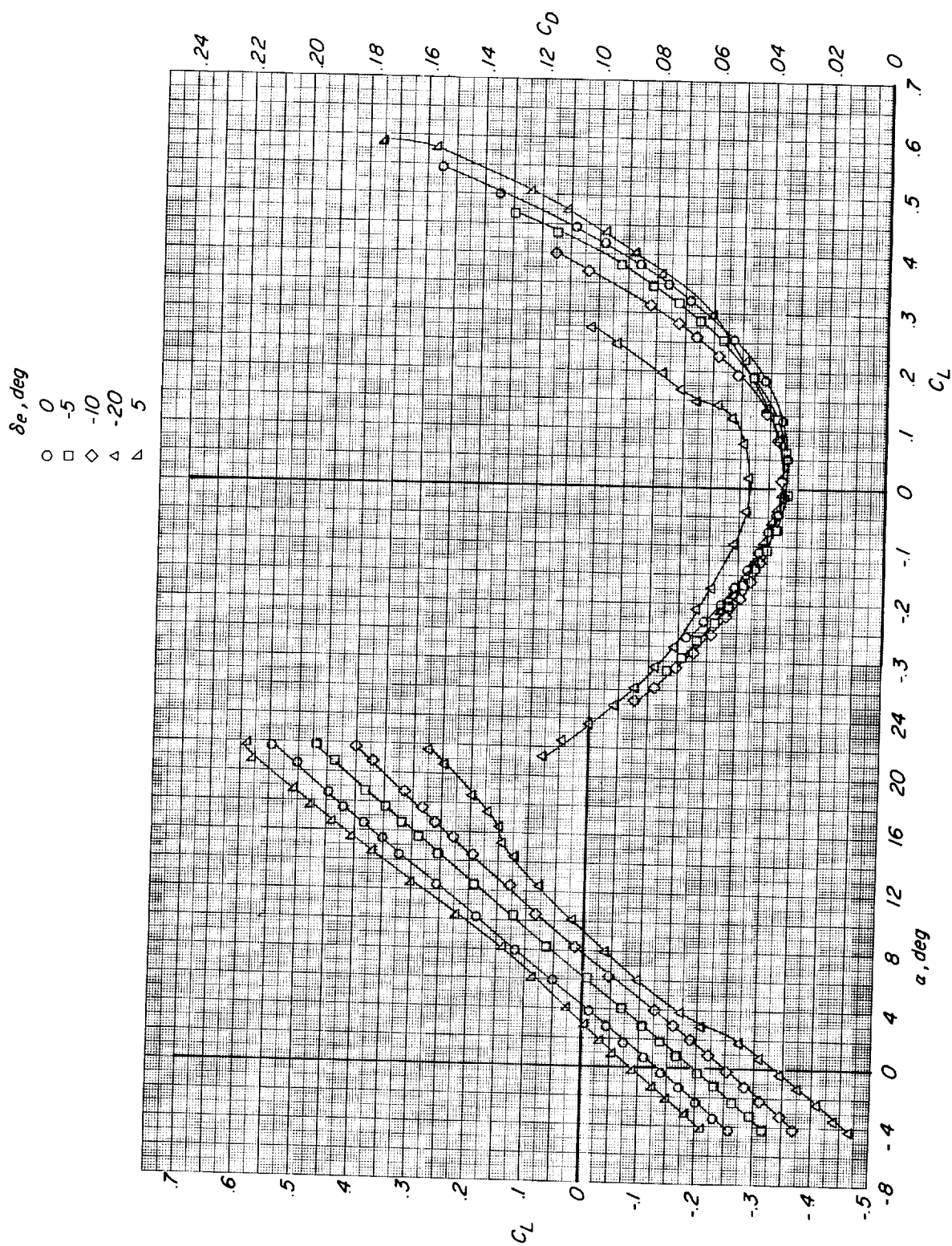
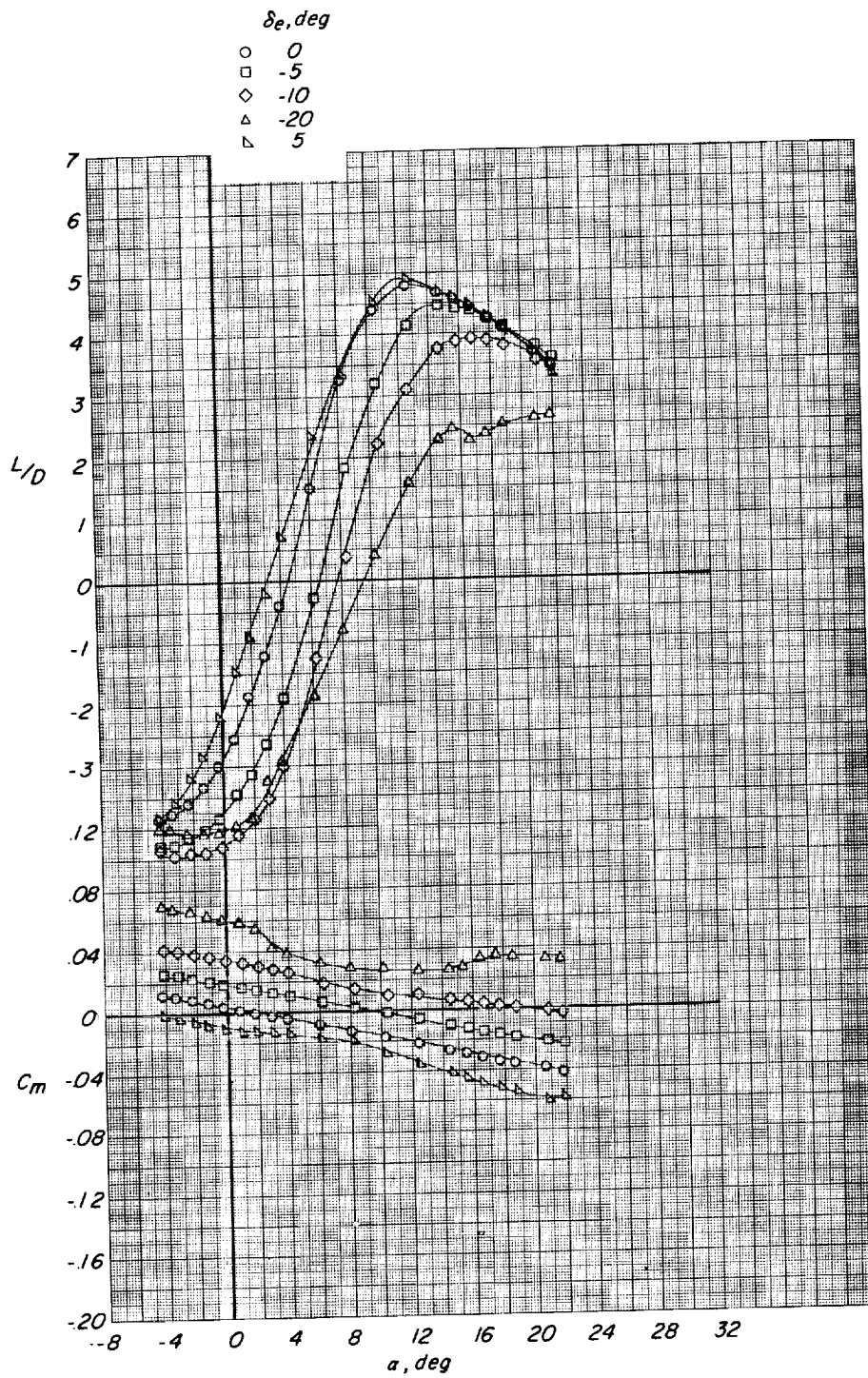


Figure 5.- Concluded.



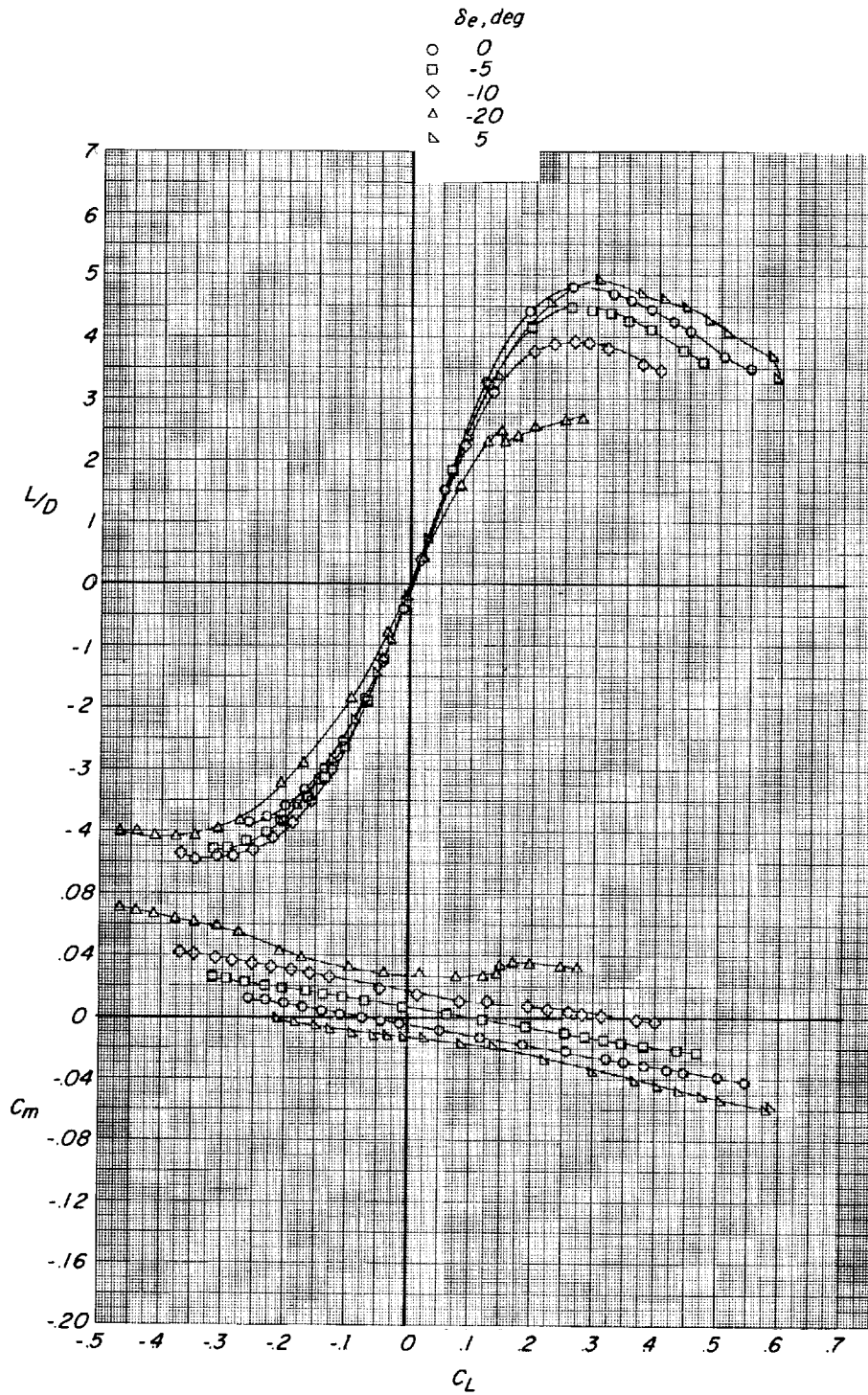
(a) Vortex generators off.

Figure 6.- Longitudinal control characteristics associated with deflection of original HL-10 elevator. $\theta = 0^\circ$; three-fin HL-10; modified fins E_2 plus I_4 .



(a) Continued.

Figure 6.- Continued.

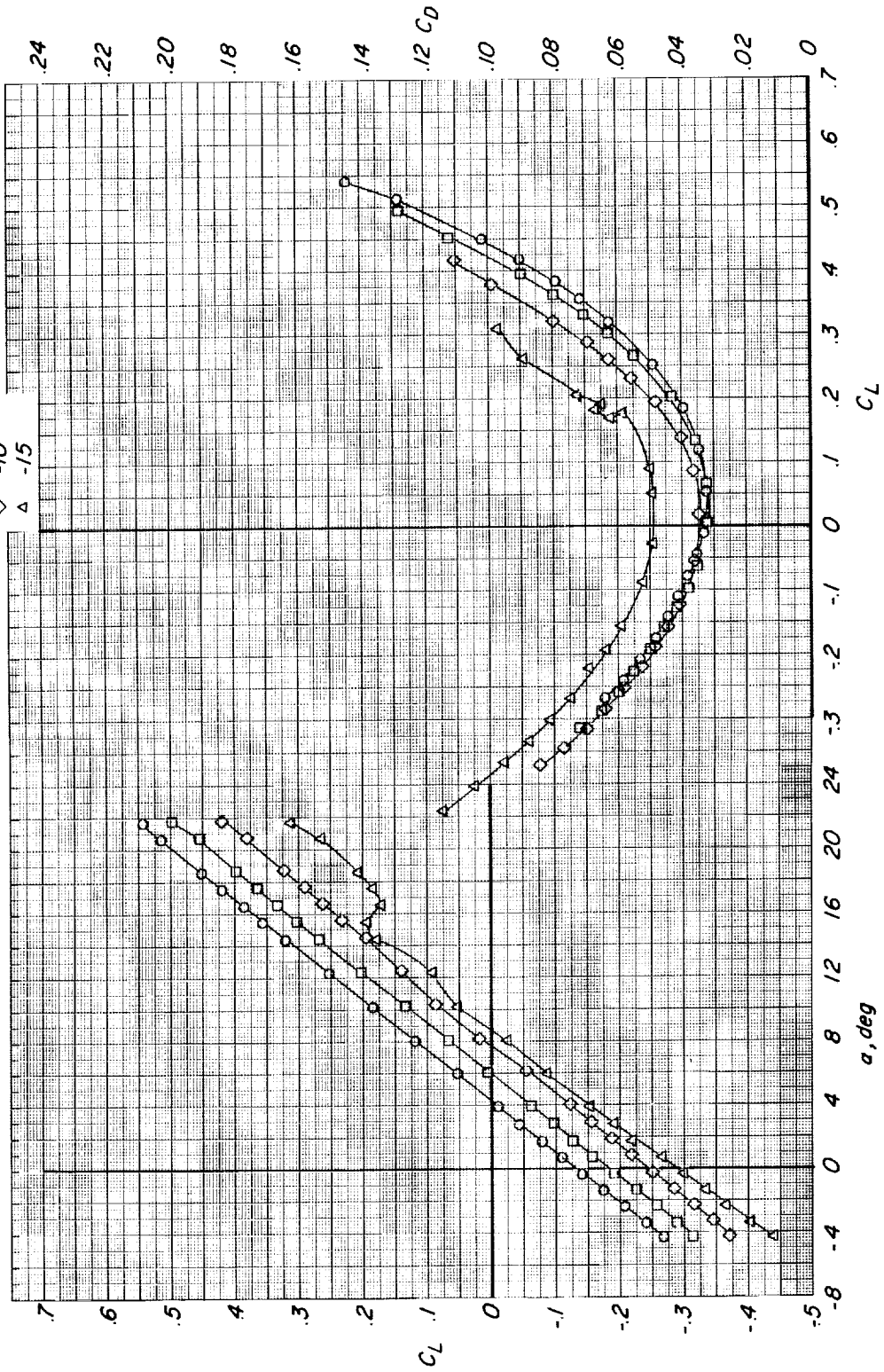


(a) Concluded.

Figure 6.- Continued.

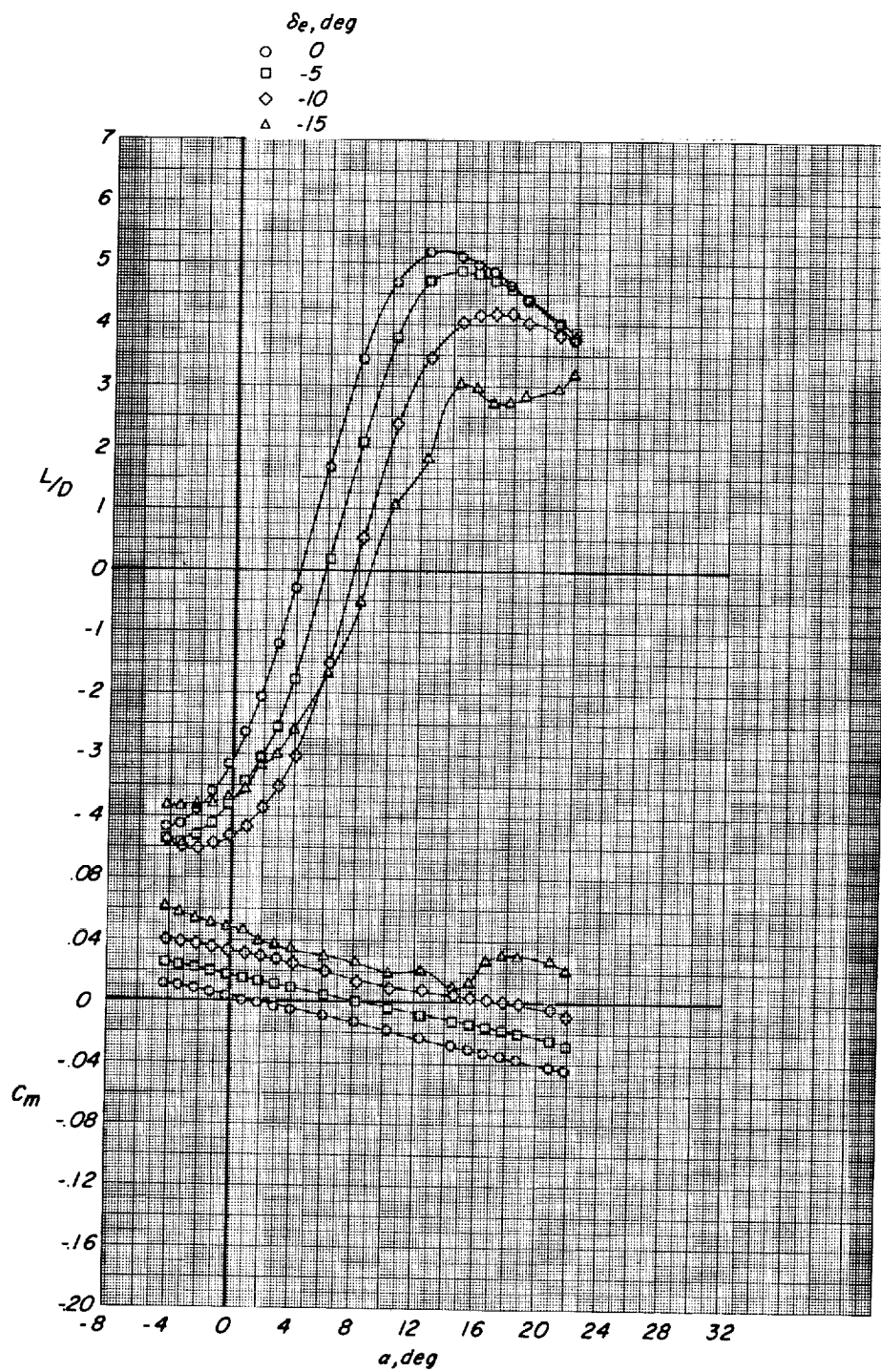
$\delta e, \text{deg}$

○ 0
 □ -5
 ◇ -10
 △ -15



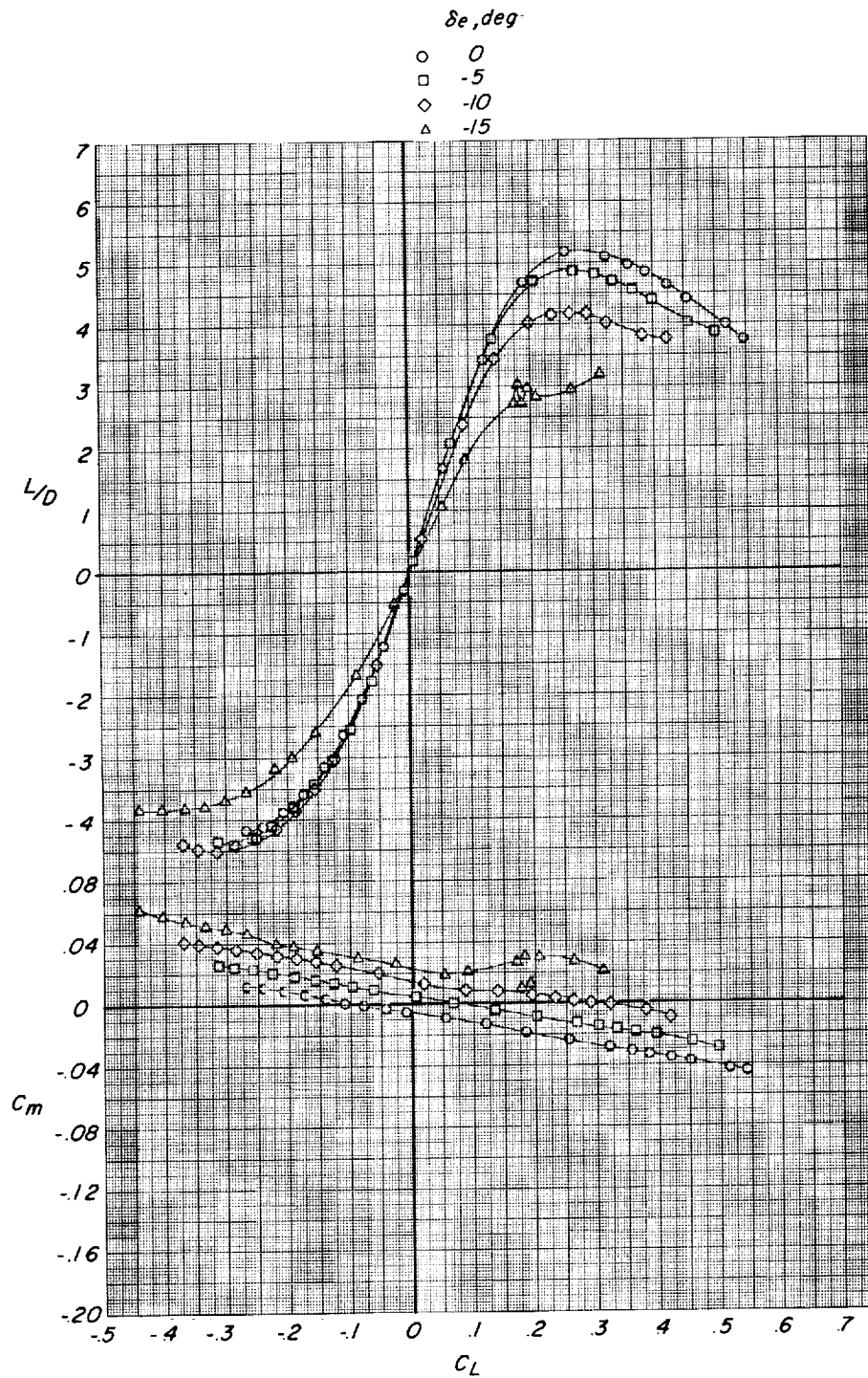
(b) Vortex generators on.

Figure 6.- Continued.



(b) Continued.

Figure 6.- Continued.

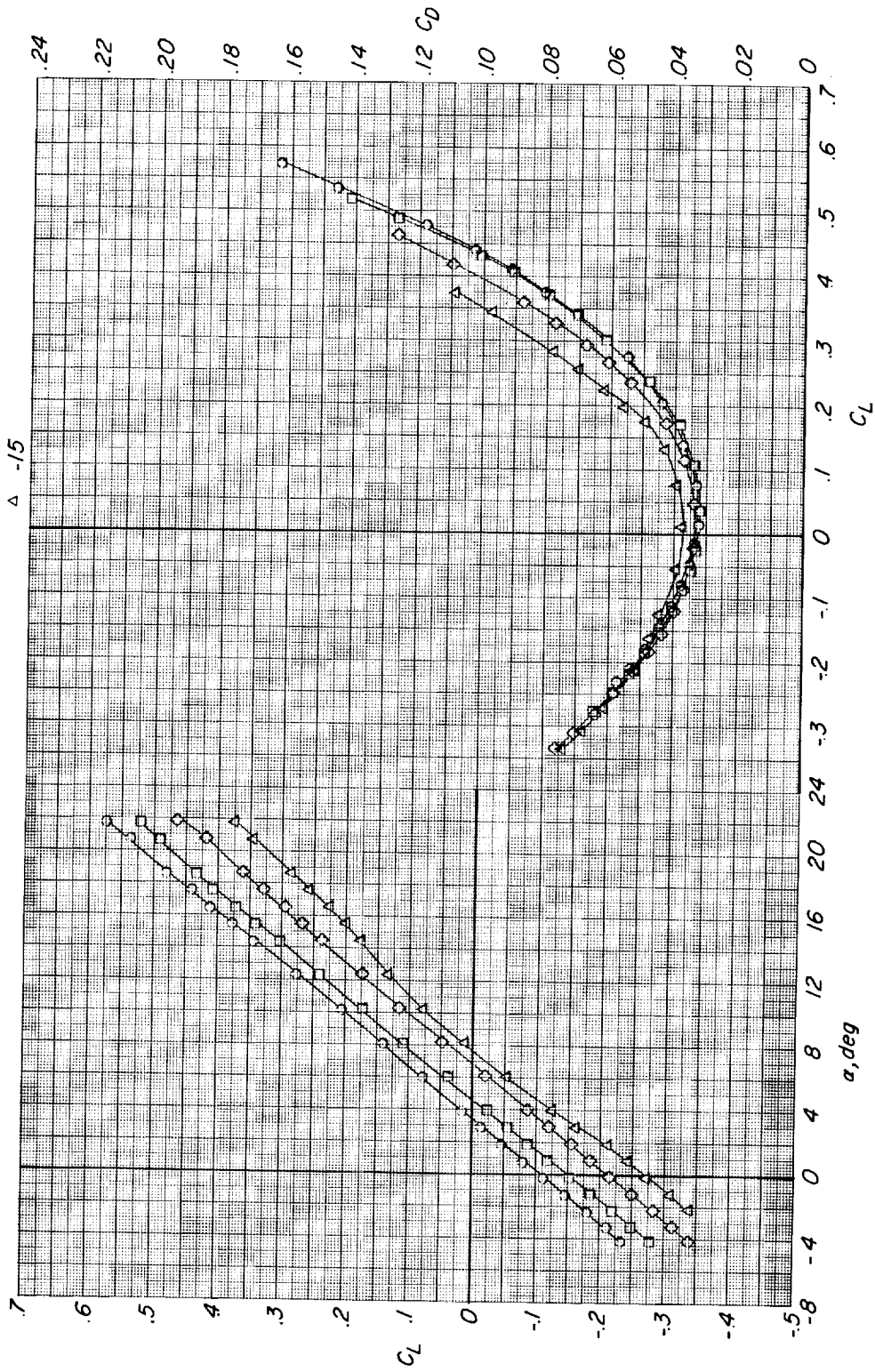


(b) Concluded.

Figure 6.- Concluded.

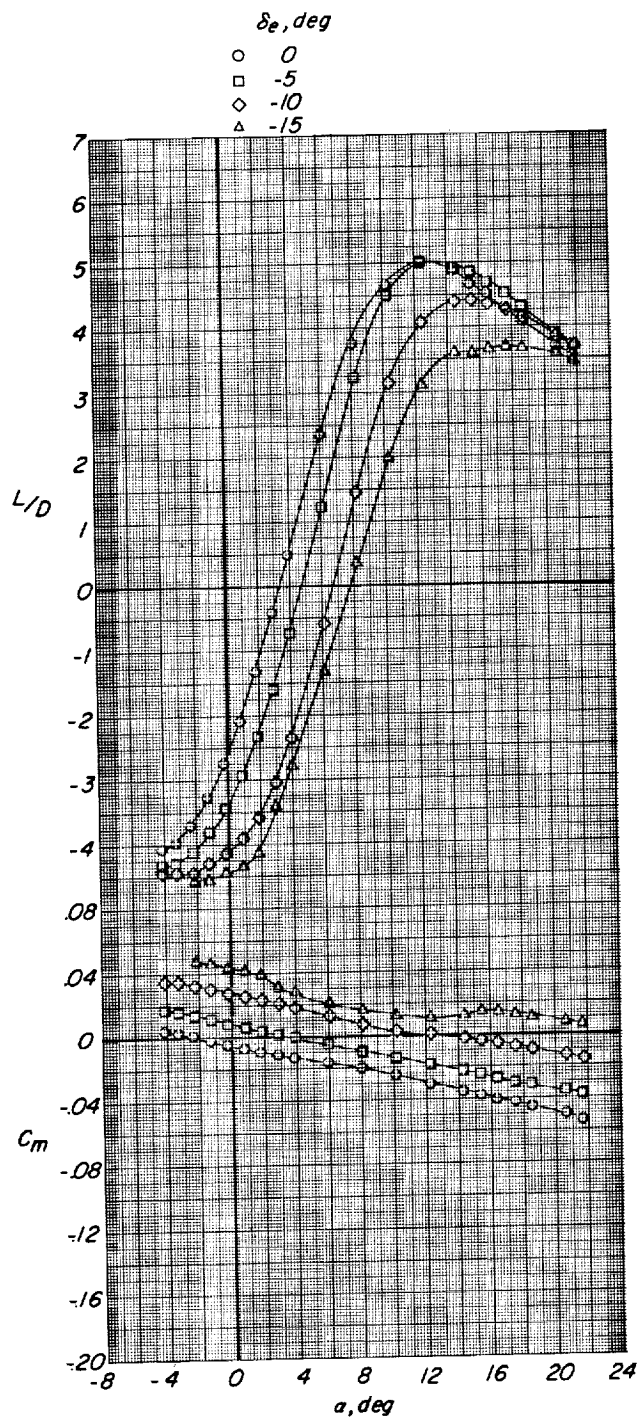
δ_e, deg

- 0
- -5
- ◇ -10
- △ -15



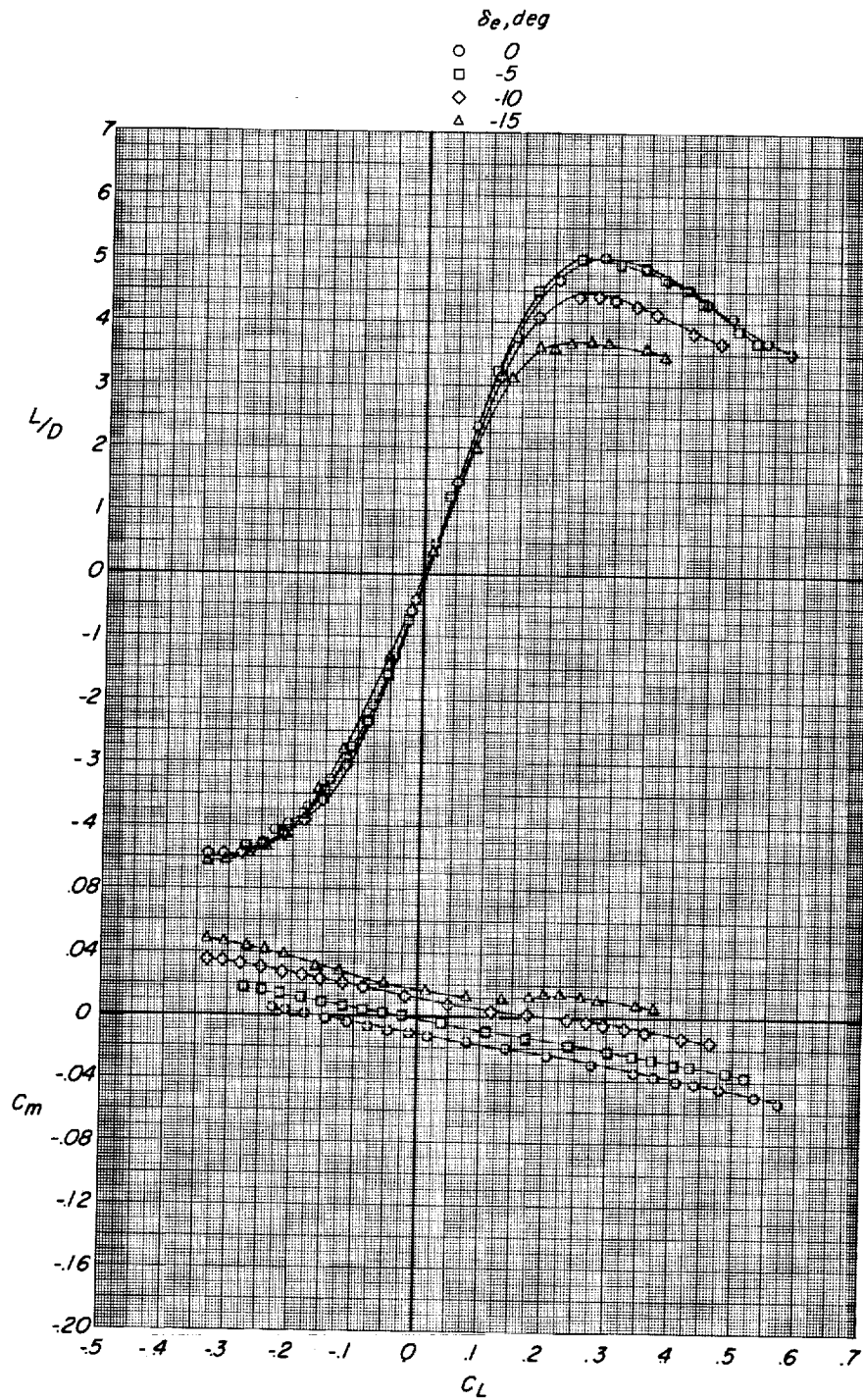
(a) Vortex generators off.

Figure 7.- Longitudinal control characteristics associated with deflection of modified HL-10 elevon. $\theta = 4^\circ$; three-fin HL-10; modified fins E_2 plus I_4 .



(a) Continued.

Figure 7.- Continued.

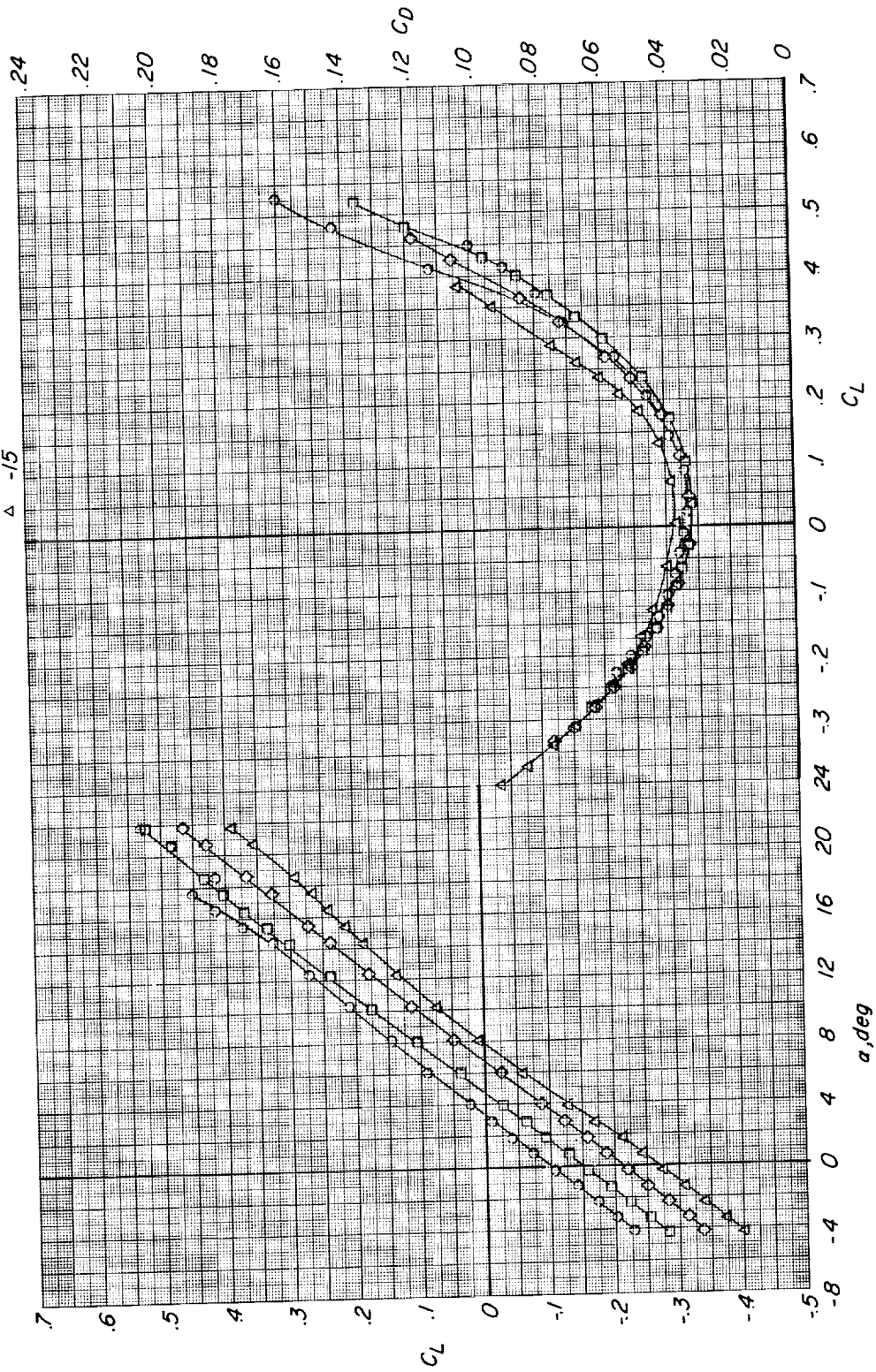


(a) Concluded.

Figure 7.- Continued.

δ_e, deg

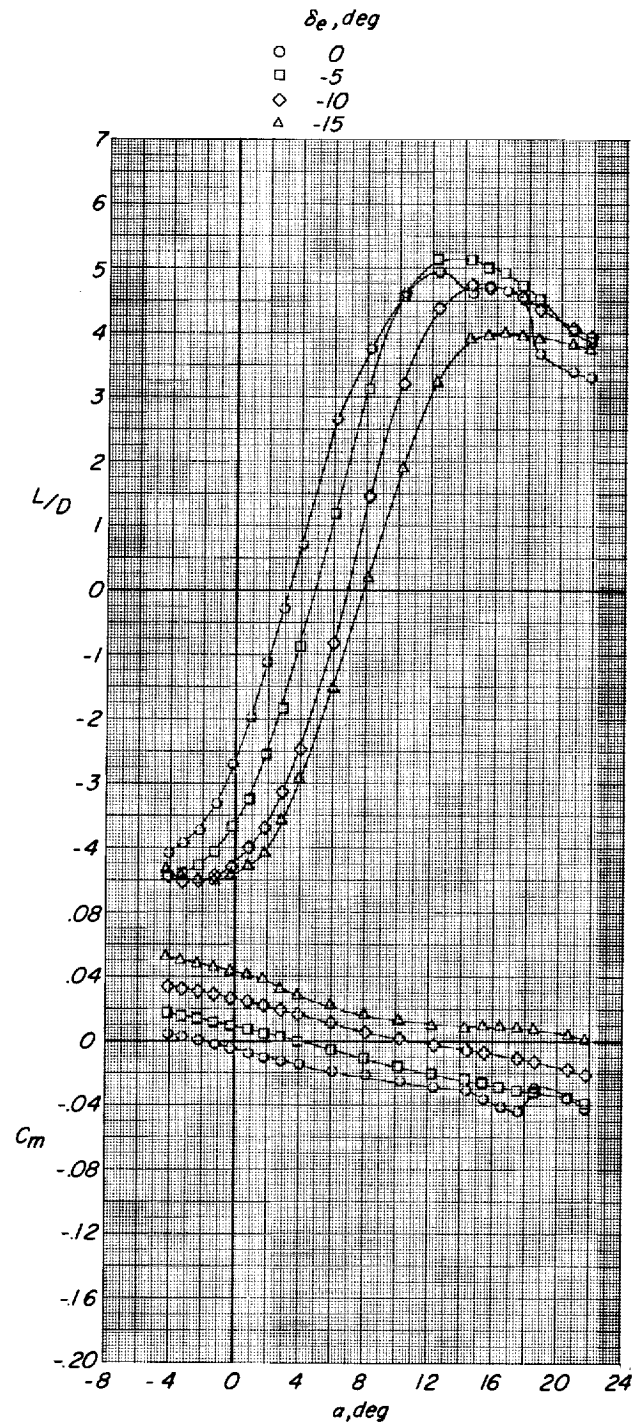
- 0
- -5
- ◇ -10
- △ -15



(b) Vortex generator on.

Figure 7.- Continued.

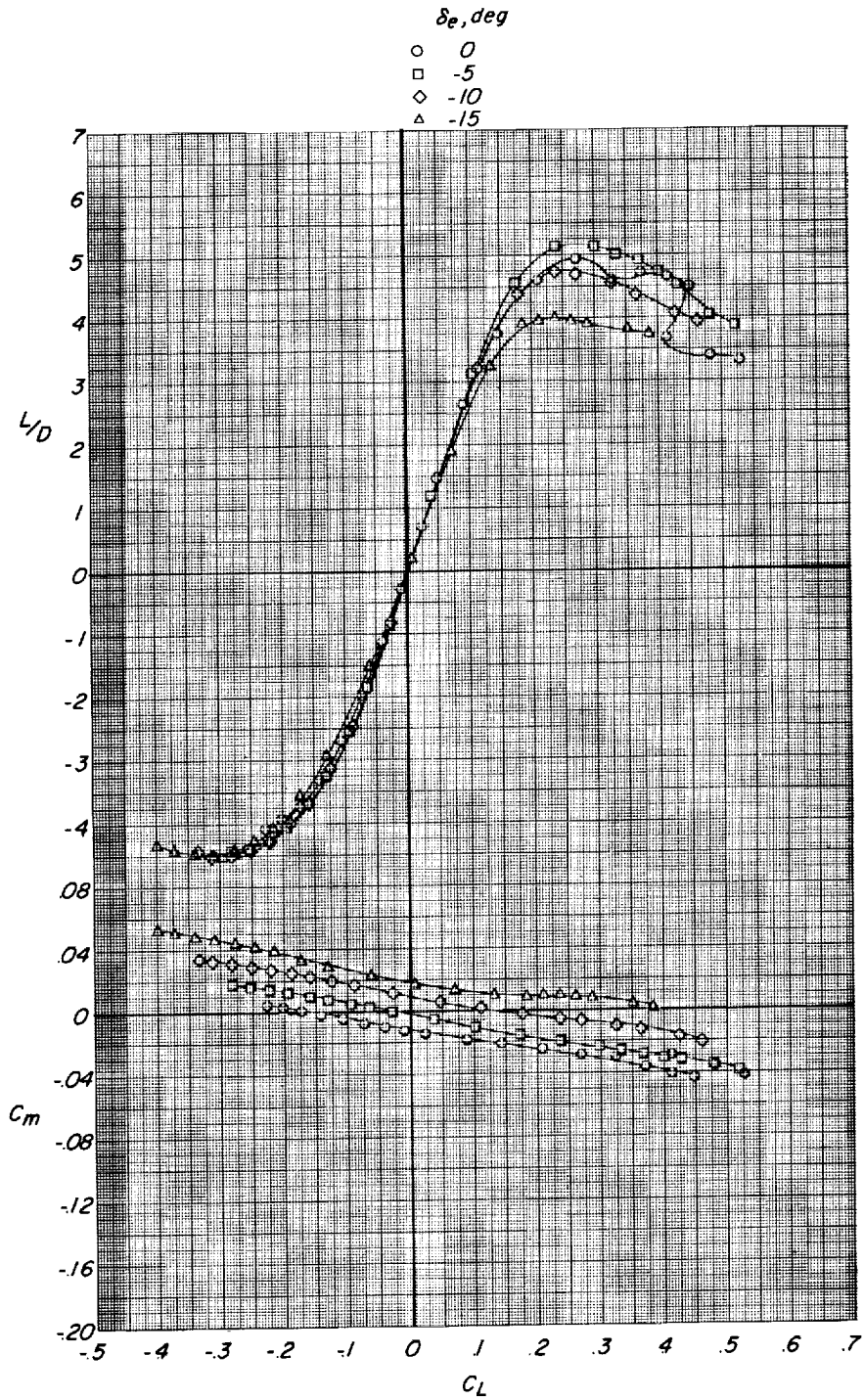
CONFIDENTIAL



(b) Continued.

Figure 7.- Continued.

CONFIDENTIAL

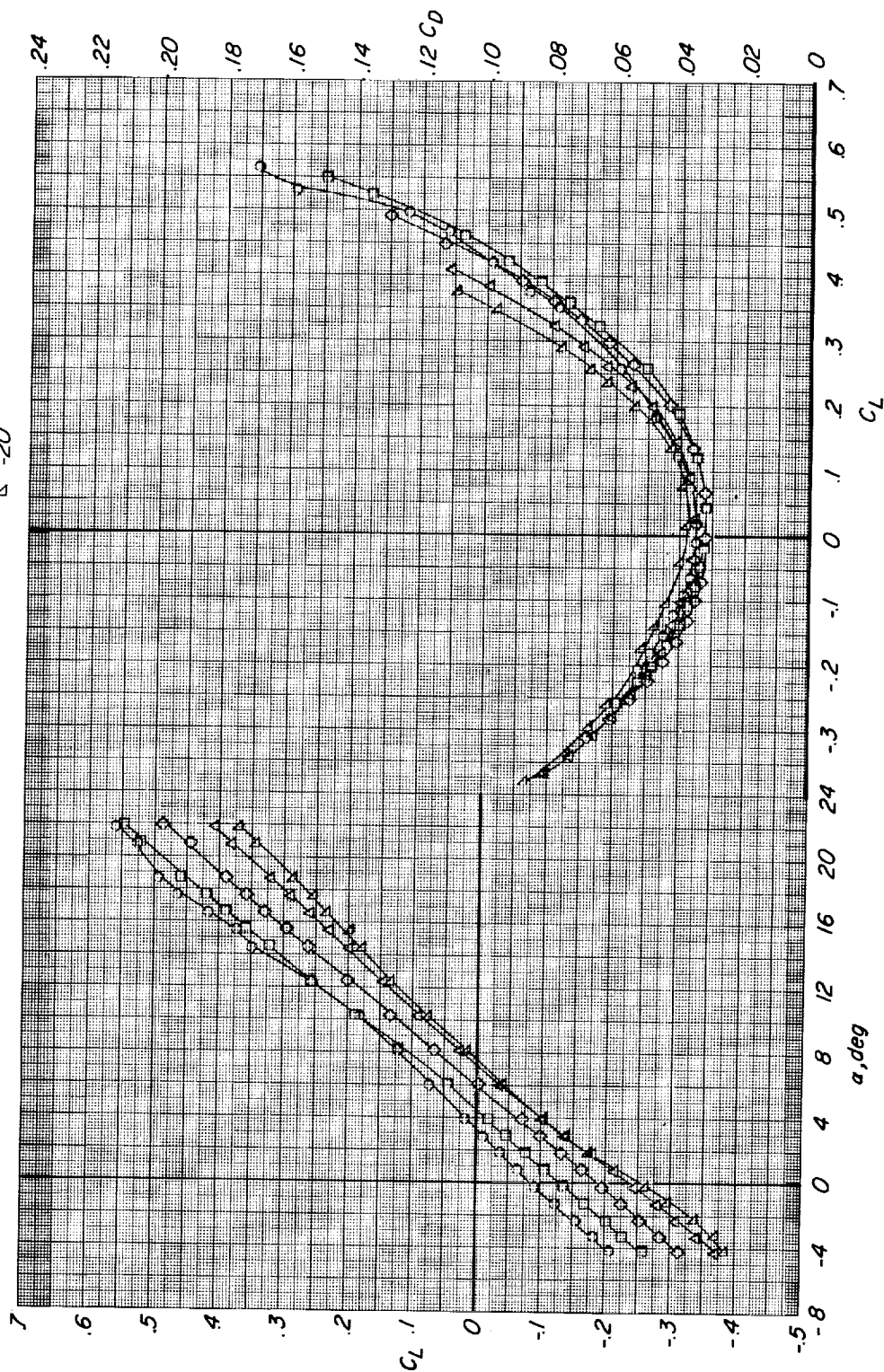


(b) Concluded.

Figure 7.- Concluded.

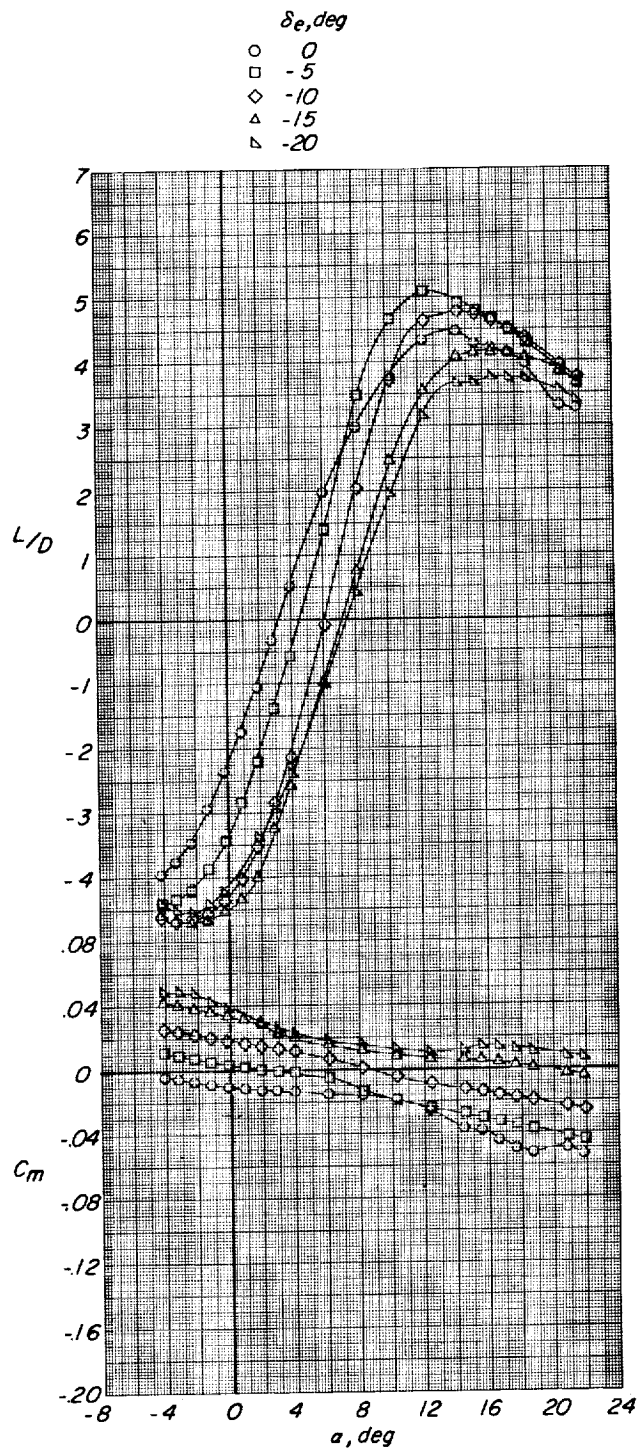
δ_e, deg

- 0
- -5
- ◇ -10
- △ -15
- ▽ -20



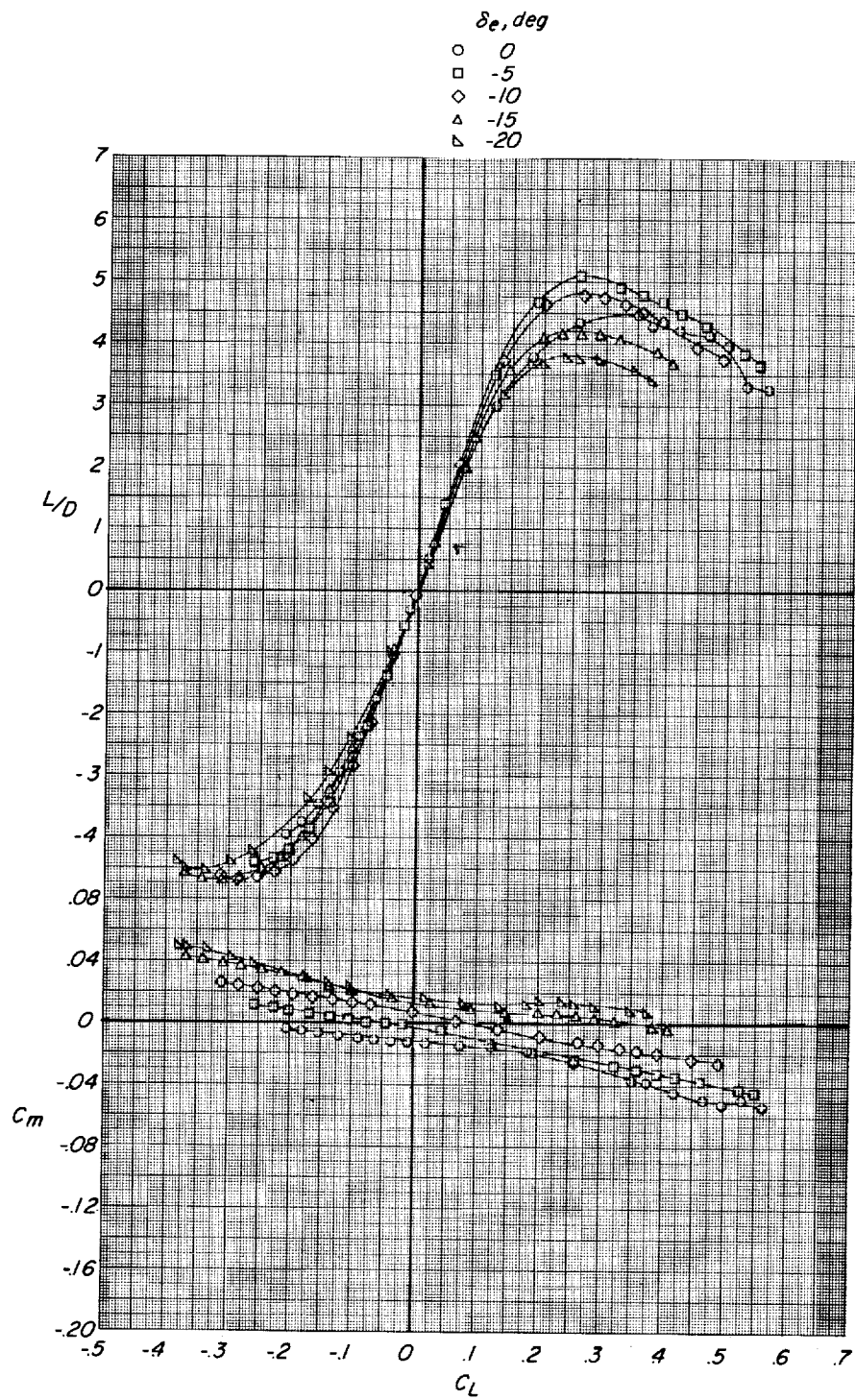
(a) Vortex generators off.

Figure 8.- Longitudinal control characteristics associated with deflection of modified HL-10 elevon. $\theta = 8^\circ$, three-fin HL-10, modified fins E2 plus I4.



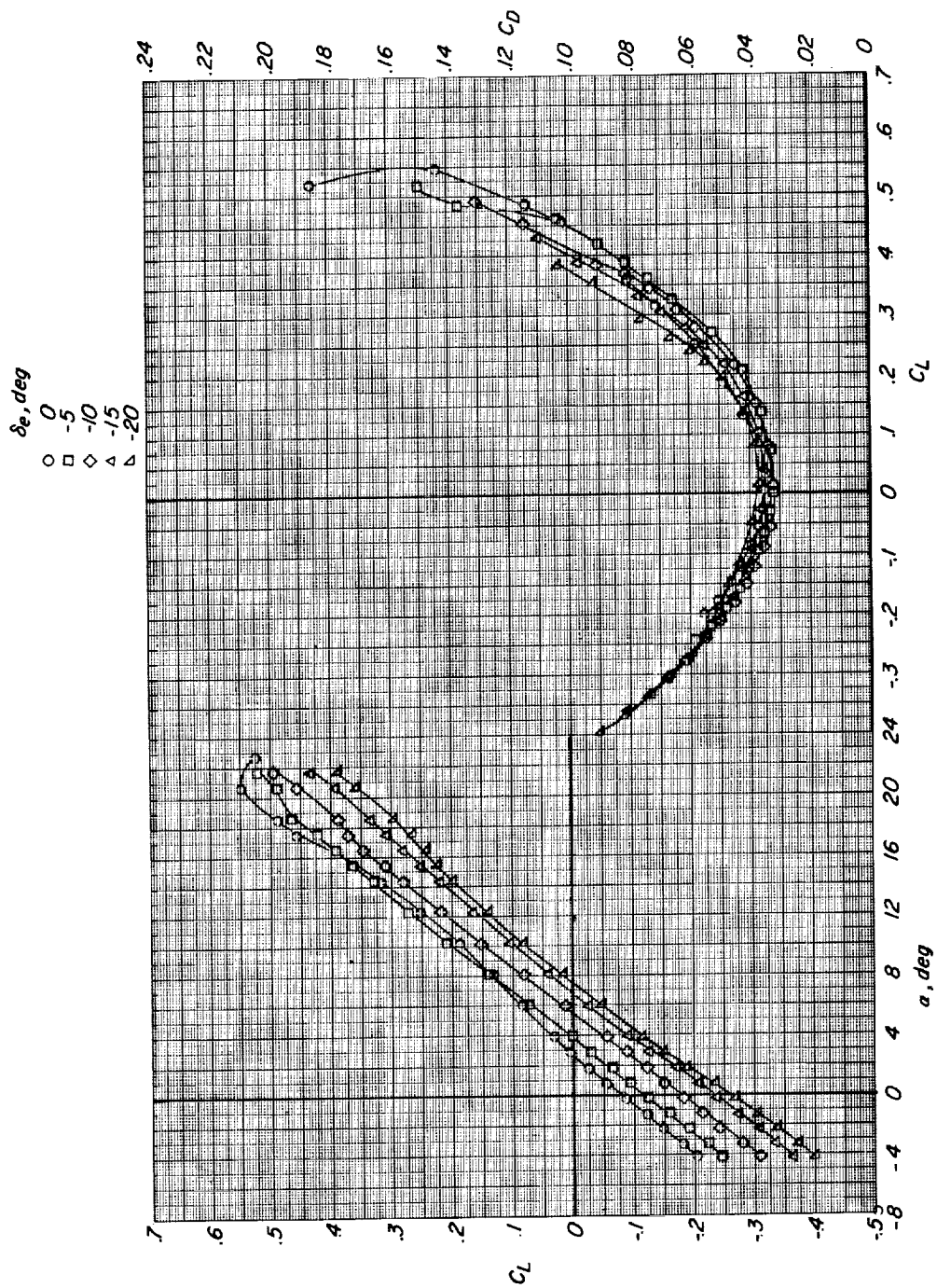
(a) Continued.

Figure 8.- Continued.



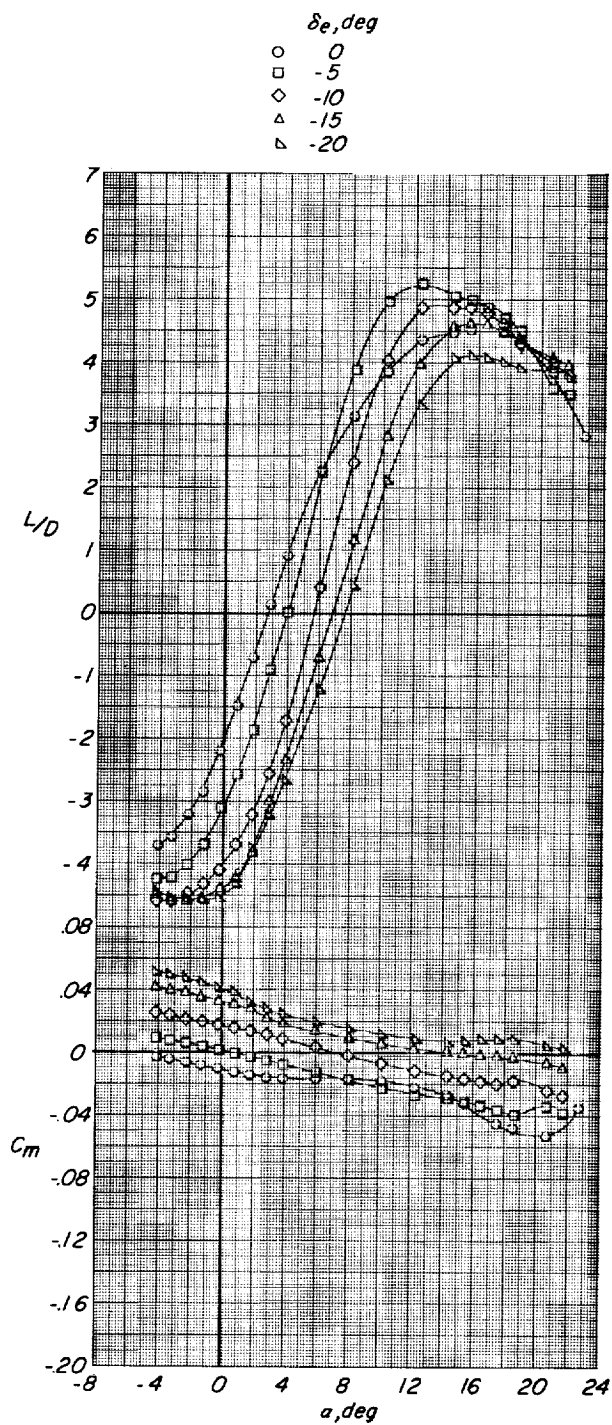
(a) Concluded.

Figure 8.- Continued.



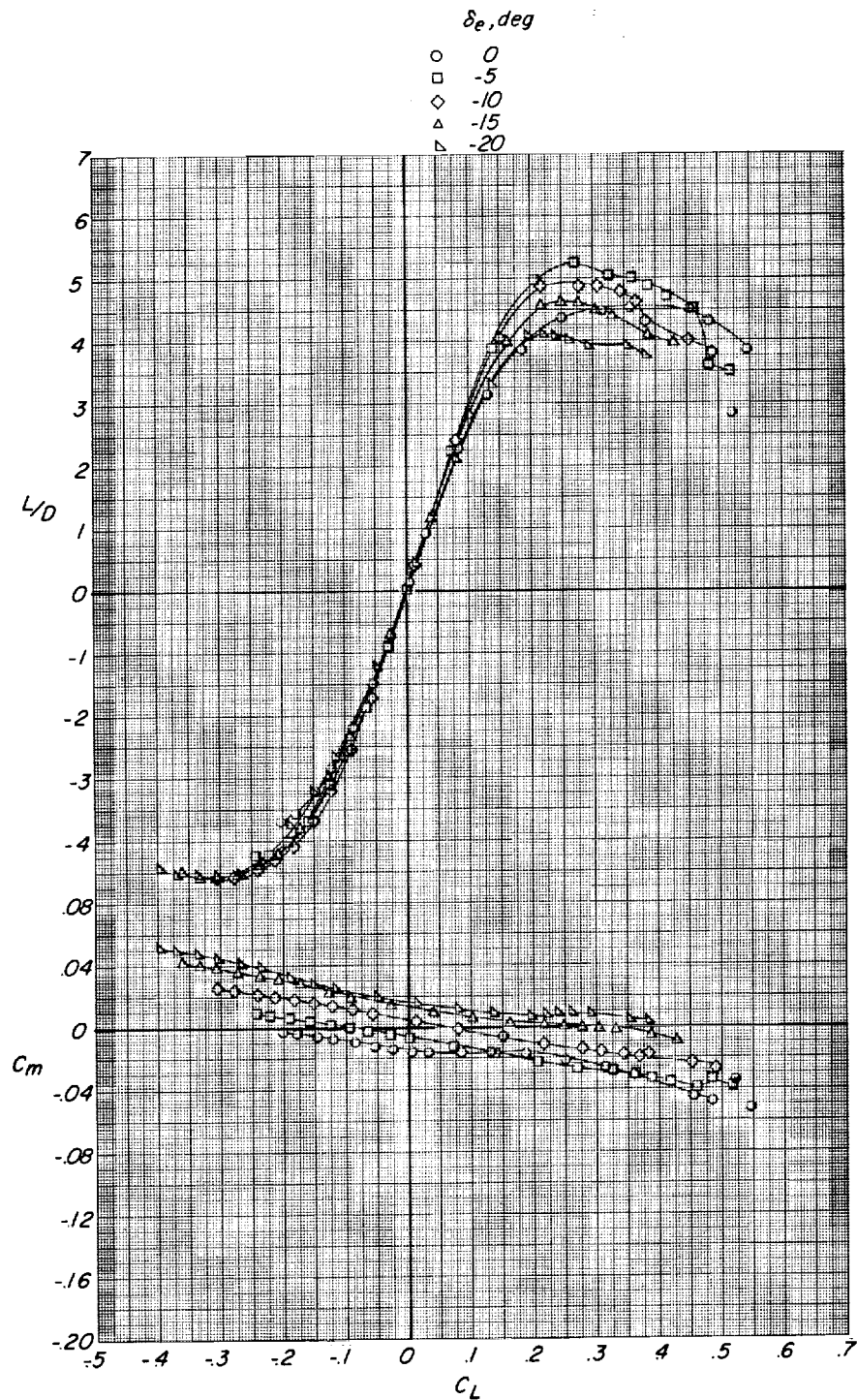
(b) Vortex generators on.

Figure 8.- Continued.



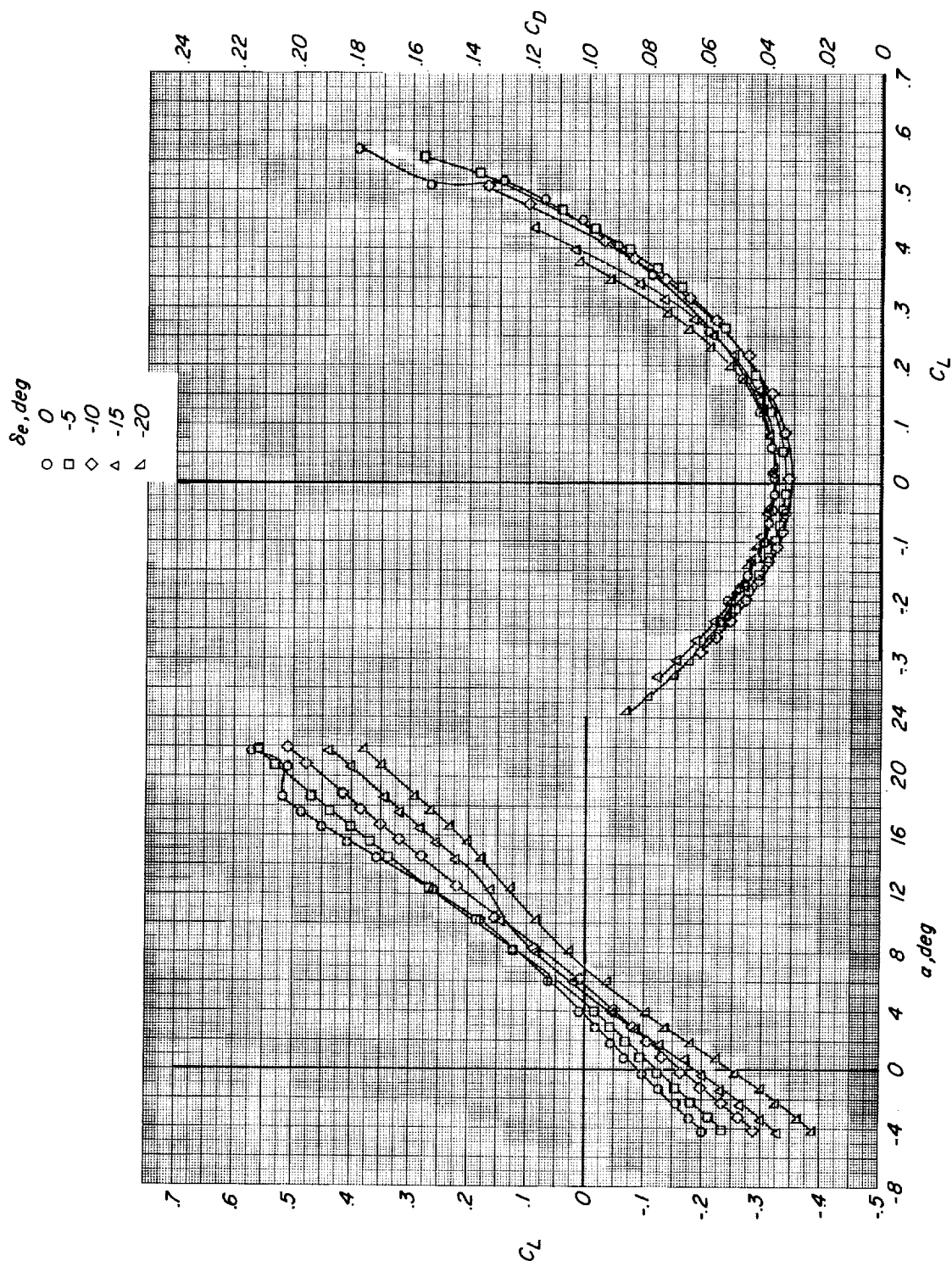
(b) Continued.

Figure 8.- Continued.



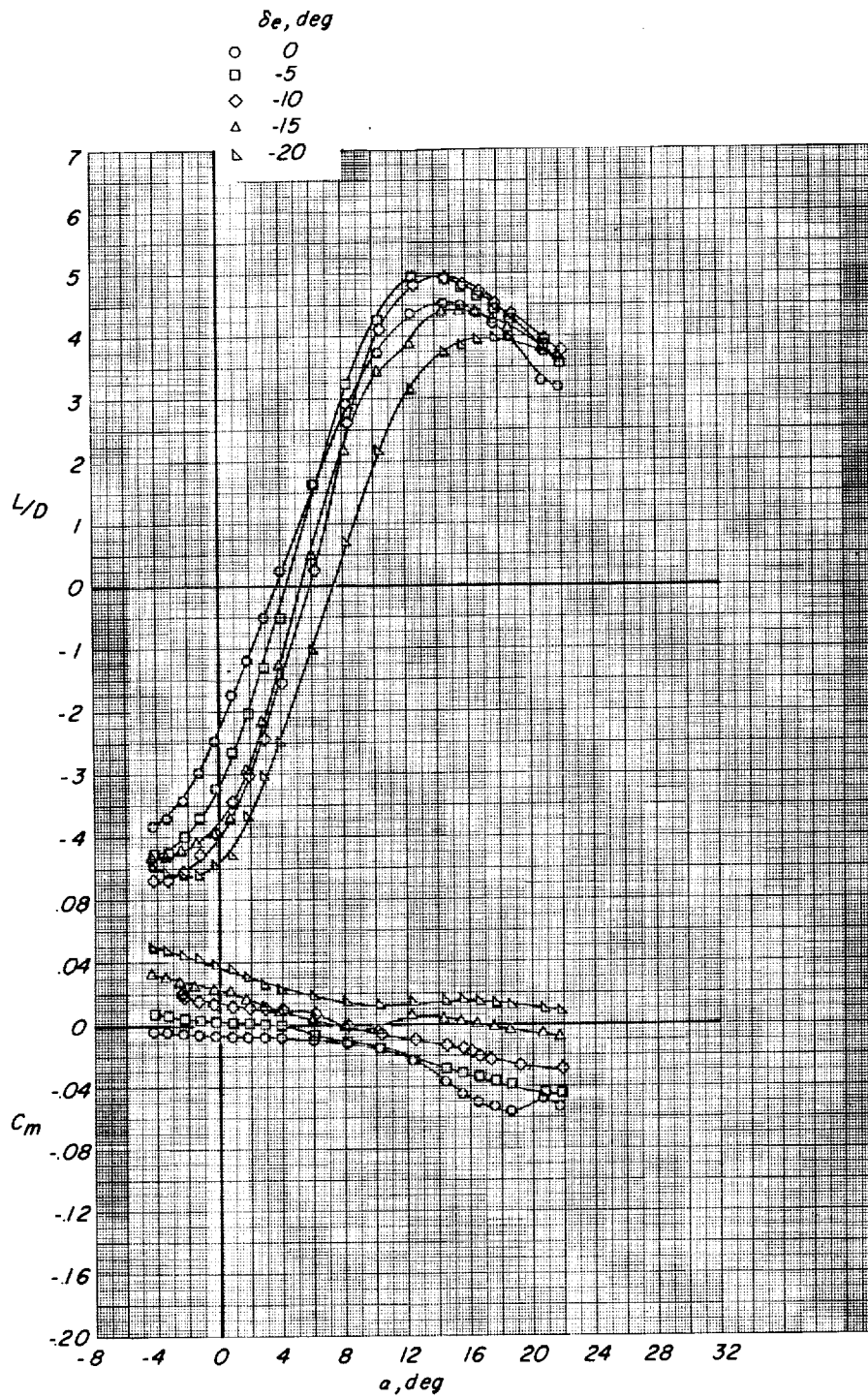
(b) Concluded.

Figure 8.- Concluded.



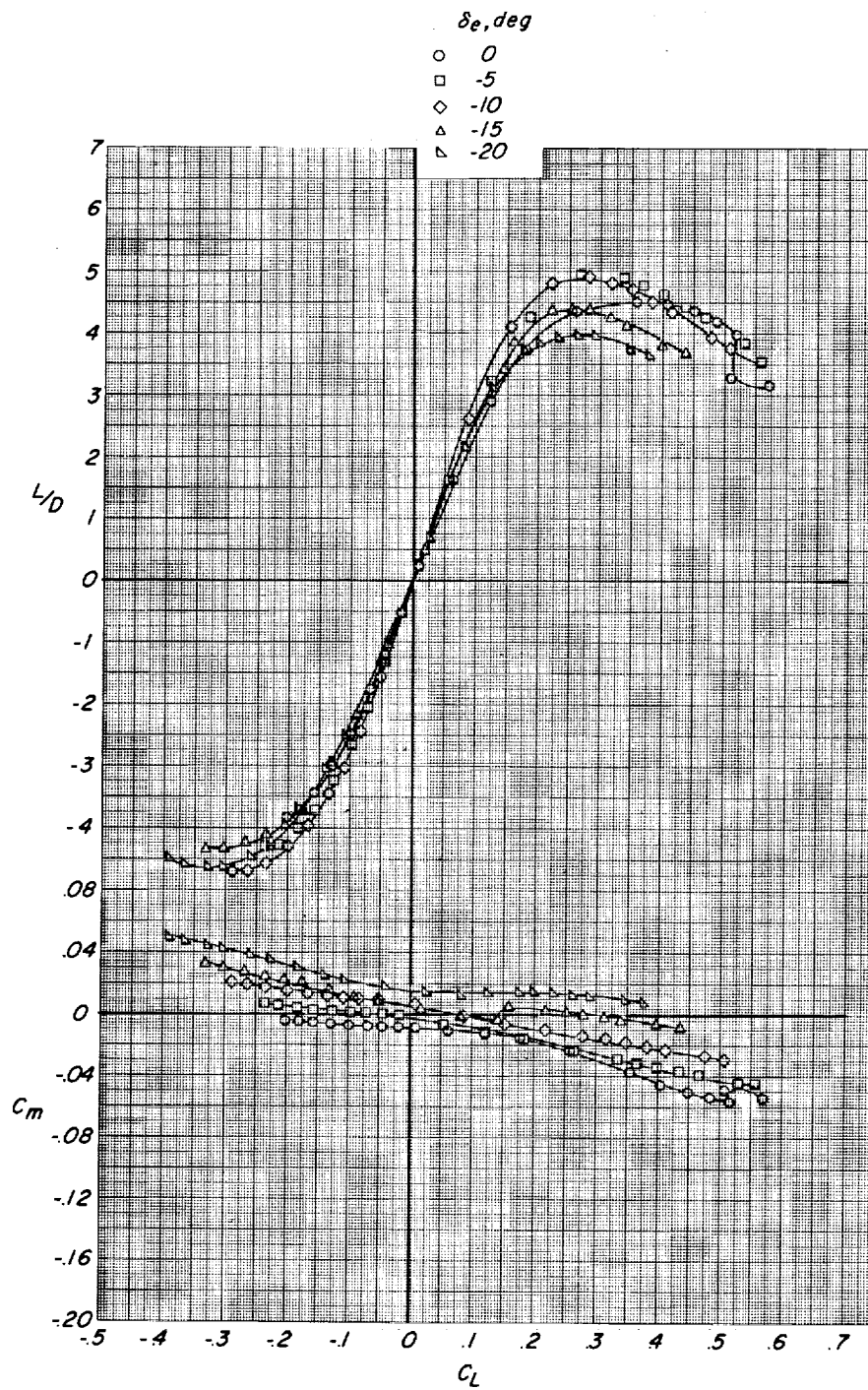
(a) Vortex generators off.

Figure 9.- Longitudinal control characteristics associated with deflection of modified HL-10 elevon. $\theta = 12^\circ$; three-fin HL-10; modified fins E2 plus 14.



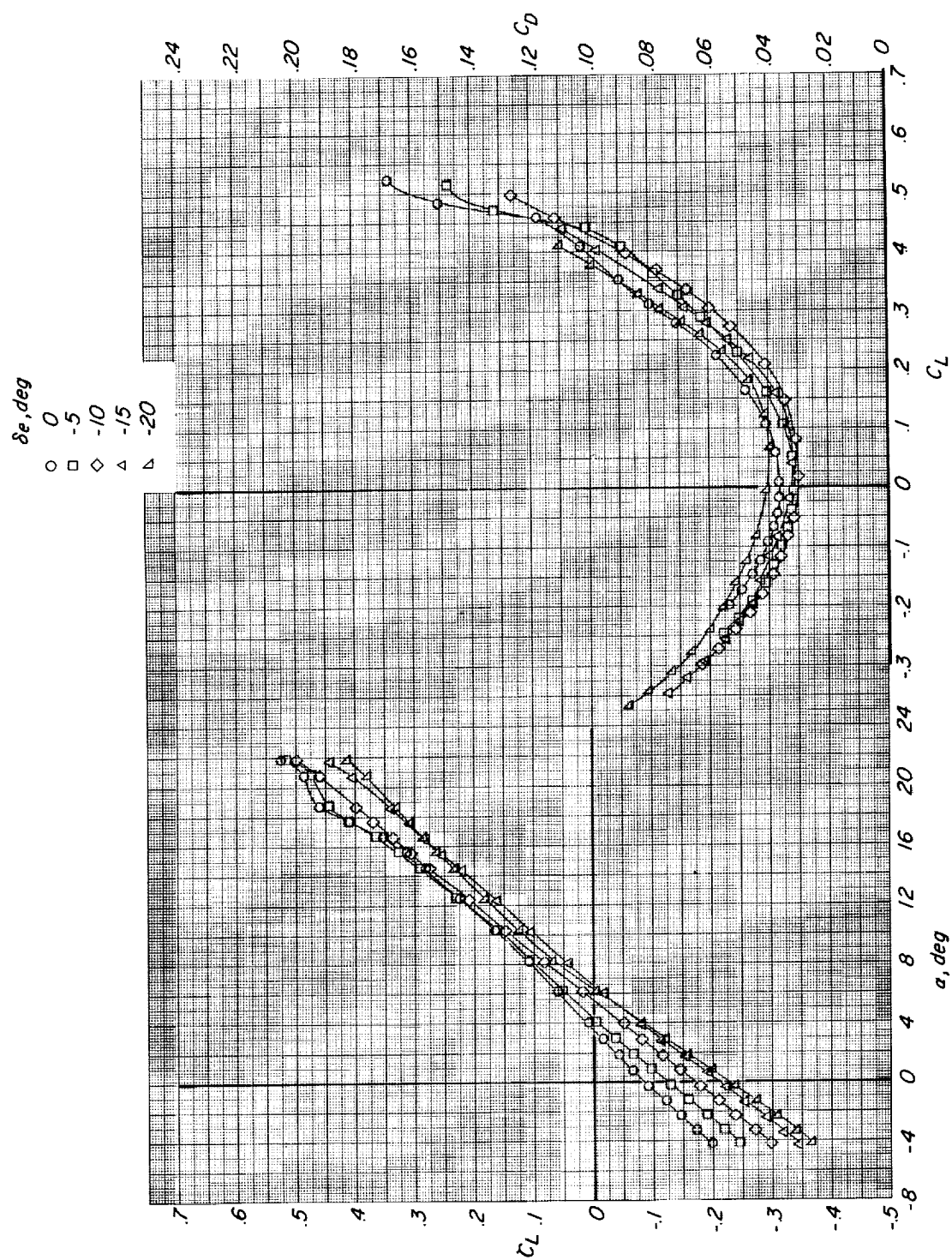
(a) Continued.

Figure 9.- Continued.



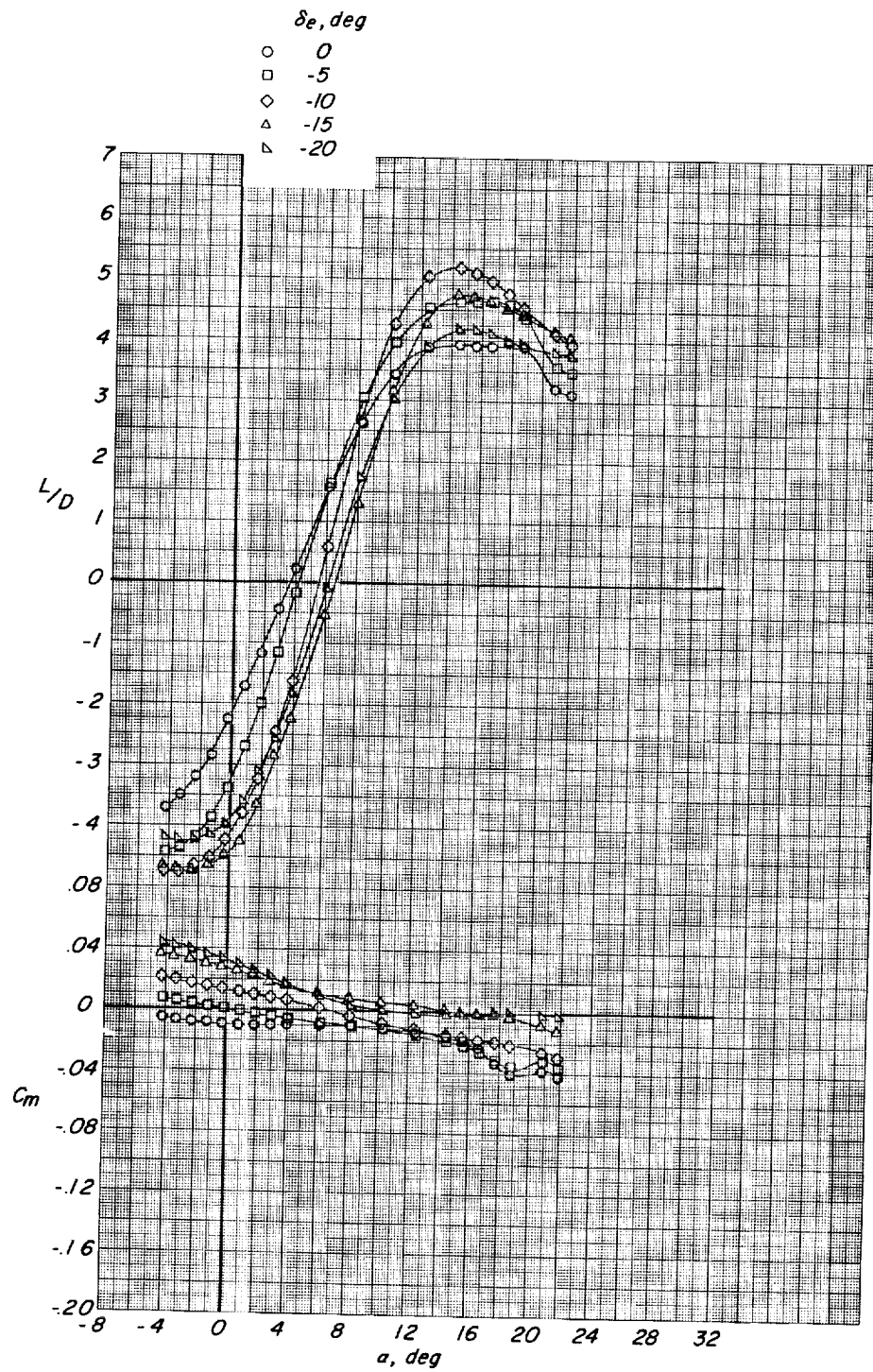
(a) Concluded.

Figure 9.- Continued.



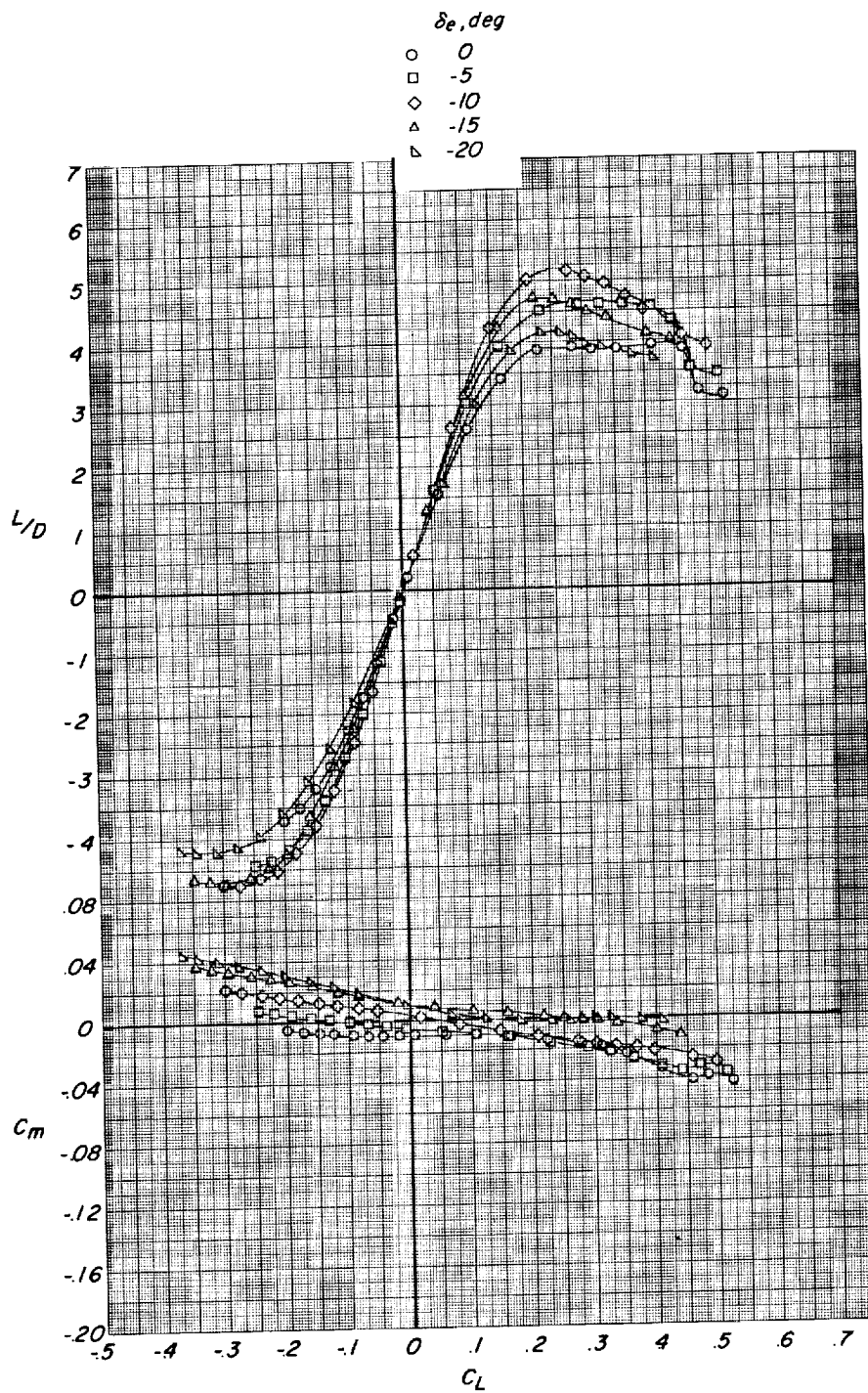
(b) Vortex generators on.

Figure 9.- Continued.



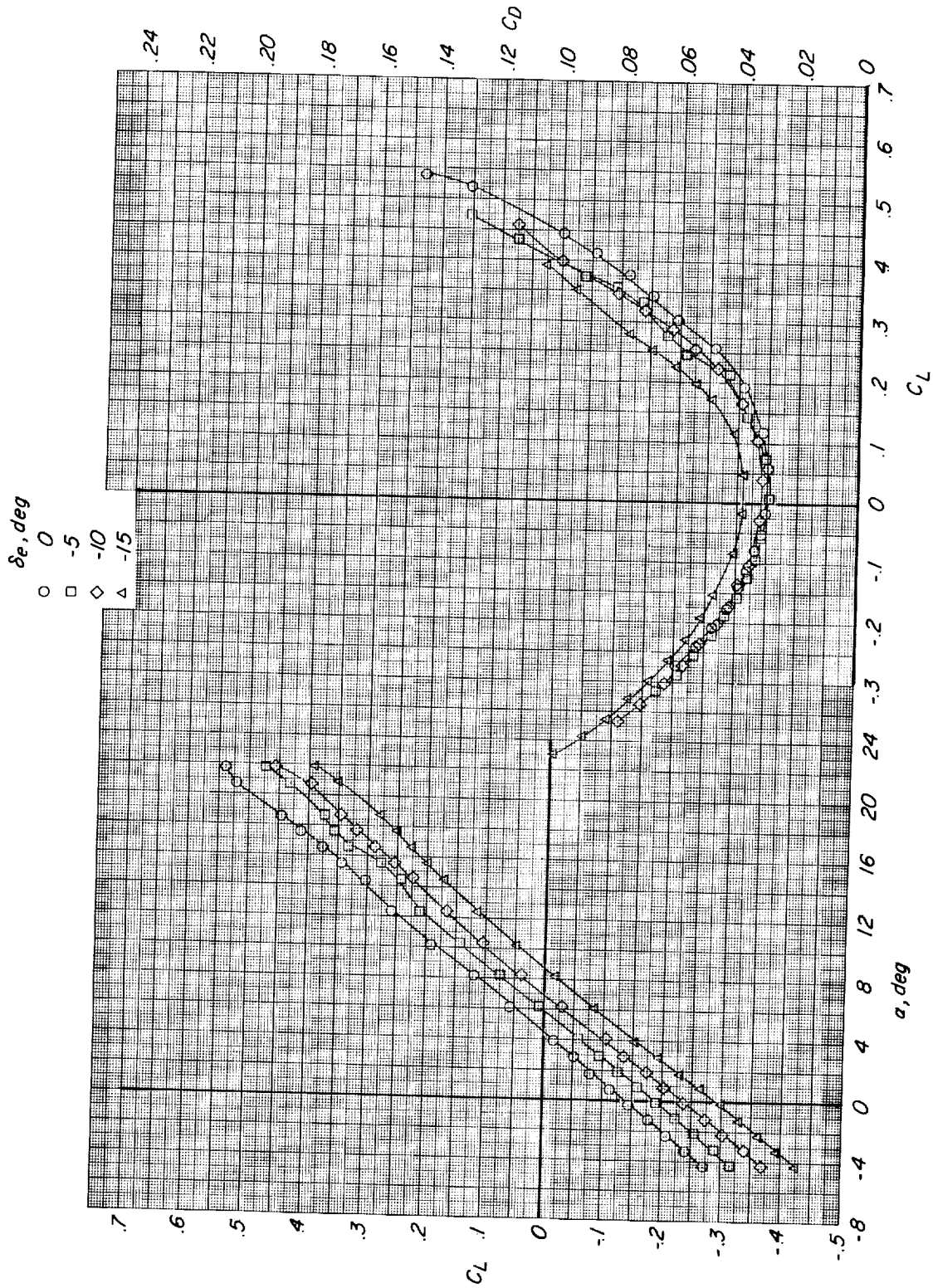
(b) Continued.

Figure 9.- Continued.



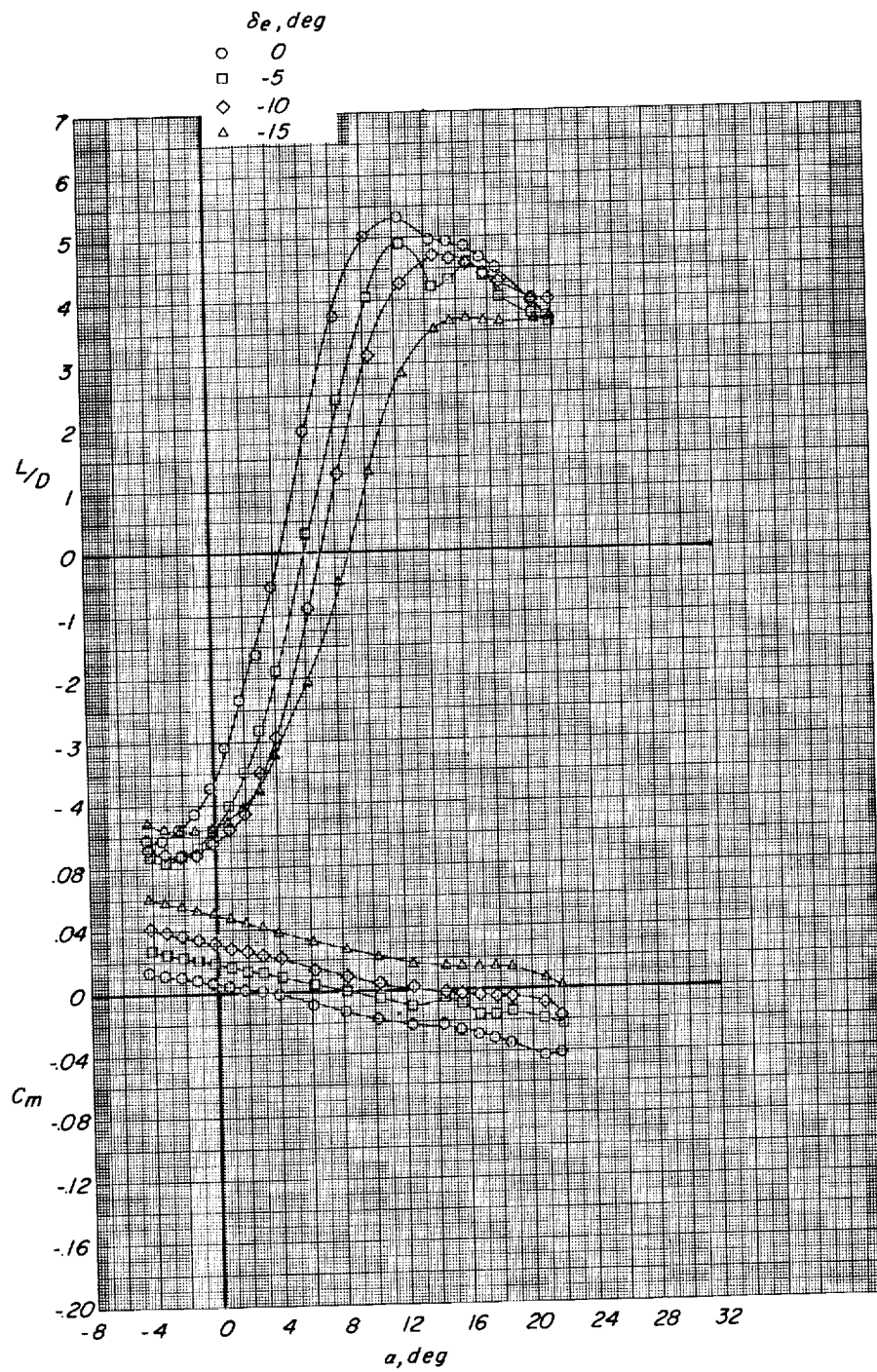
(b) Concluded.

Figure 9.- Concluded.



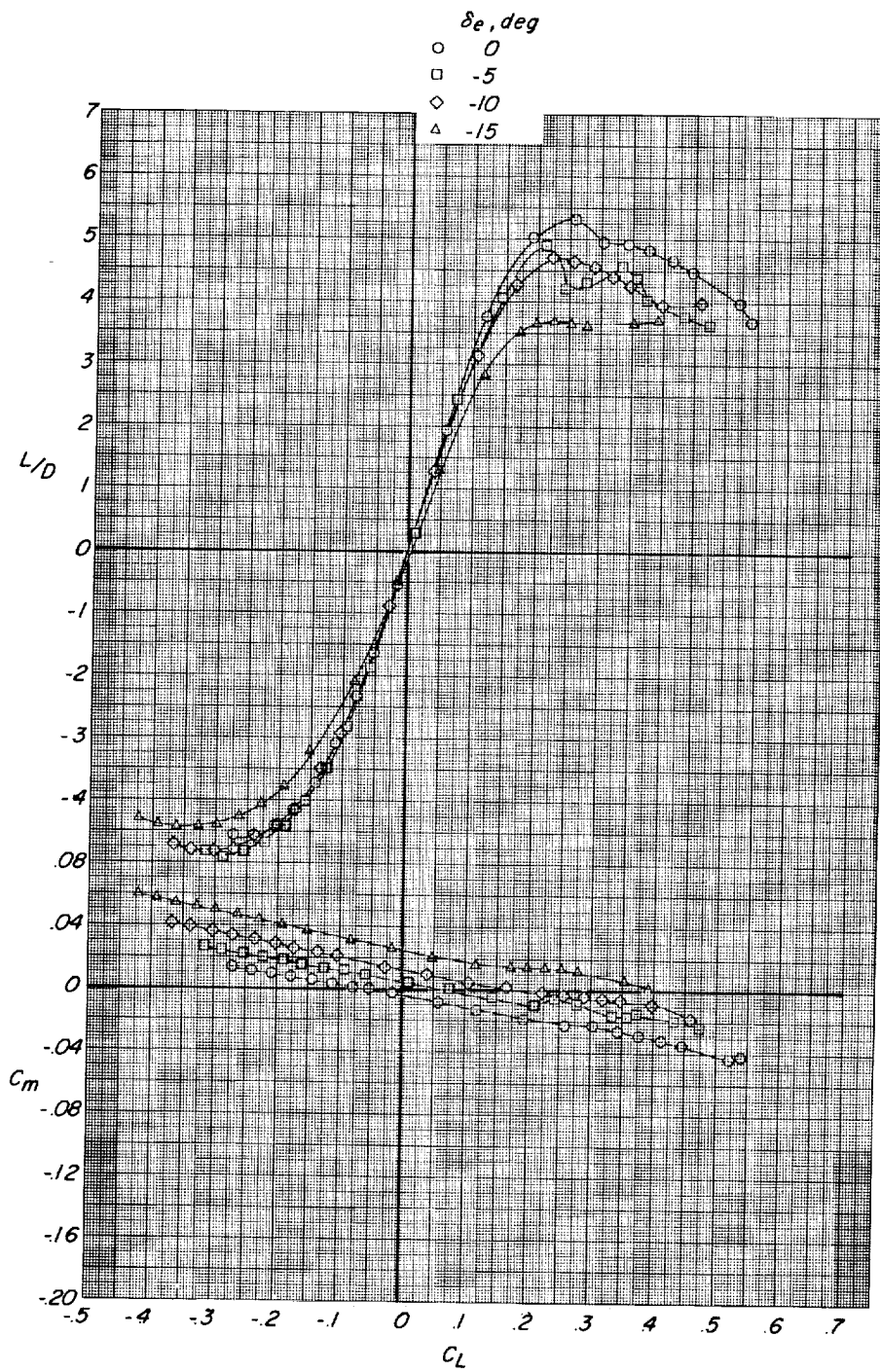
(a) Elevon base extension having $\delta_L = 25^\circ$ and $\delta_U = 16^\circ$.

Figure 10.- Longitudinal control characteristics associated with deflection of original HL-10 elevon with various base extensions added. $\theta = 0^\circ$; vortex generators on; three-fin HL-10; modified fins E_2 plus I_4 .



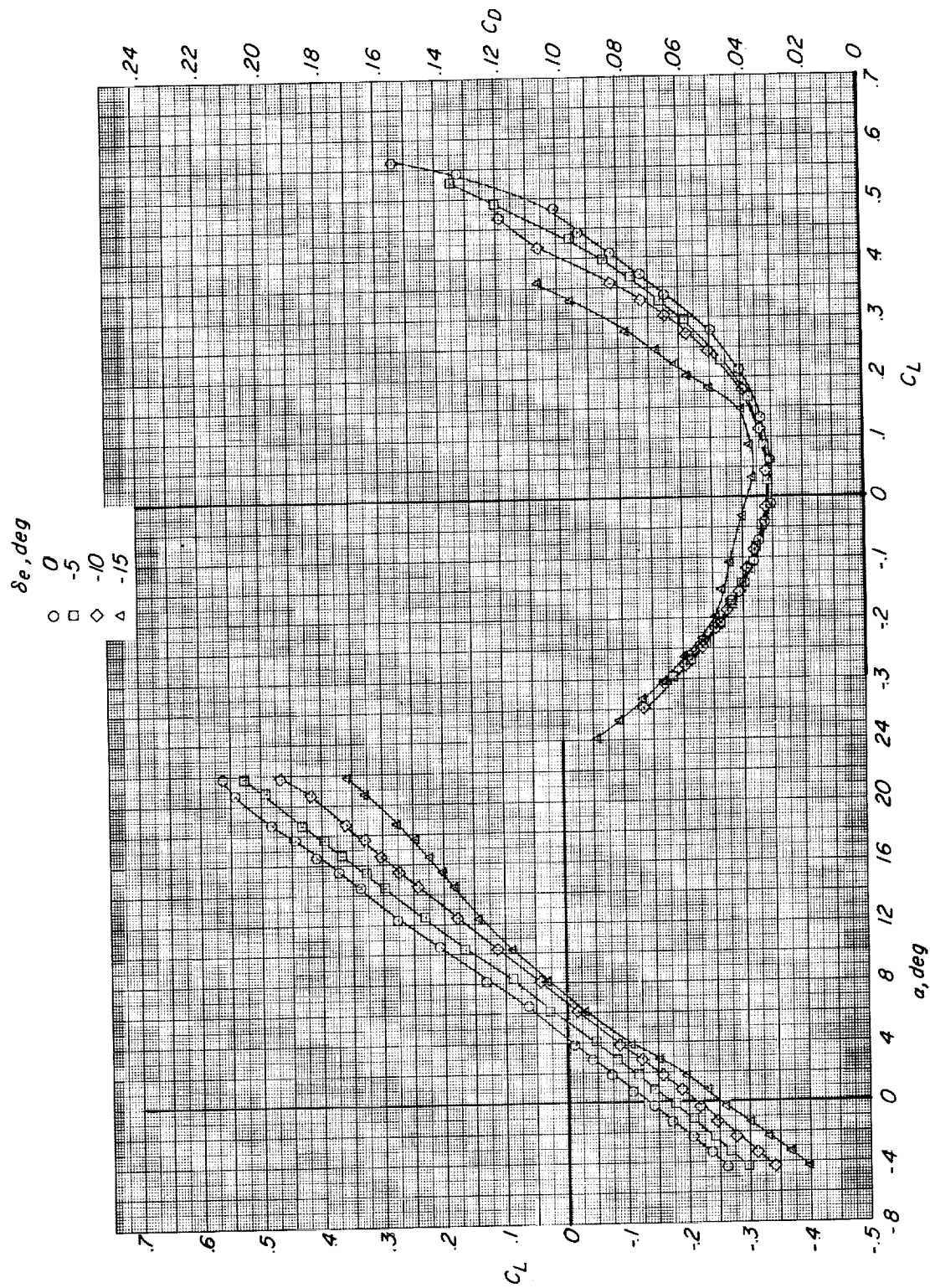
(a) Continued.

Figure 10.- Continued.



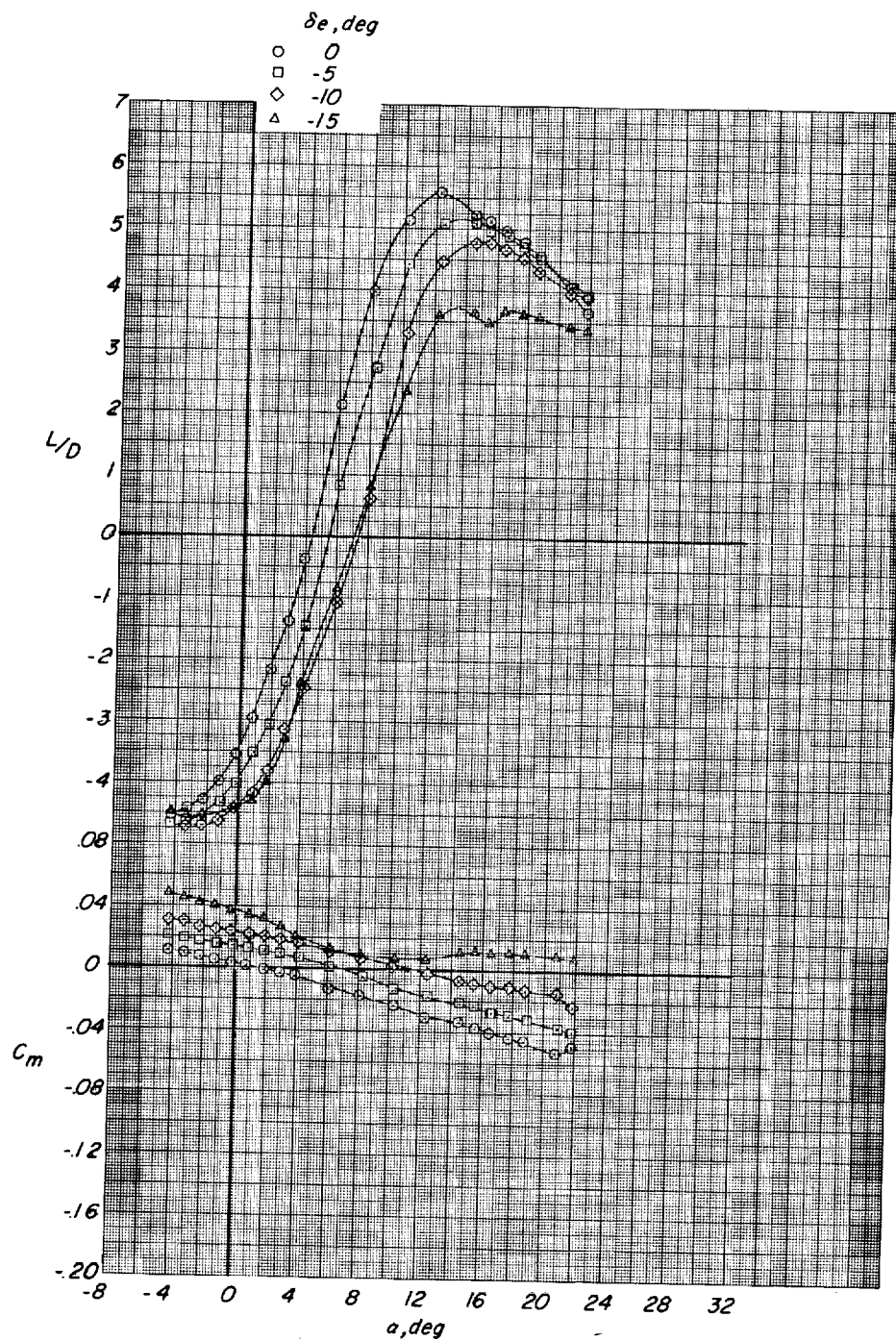
(a) Concluded.

Figure 10.- Continued.



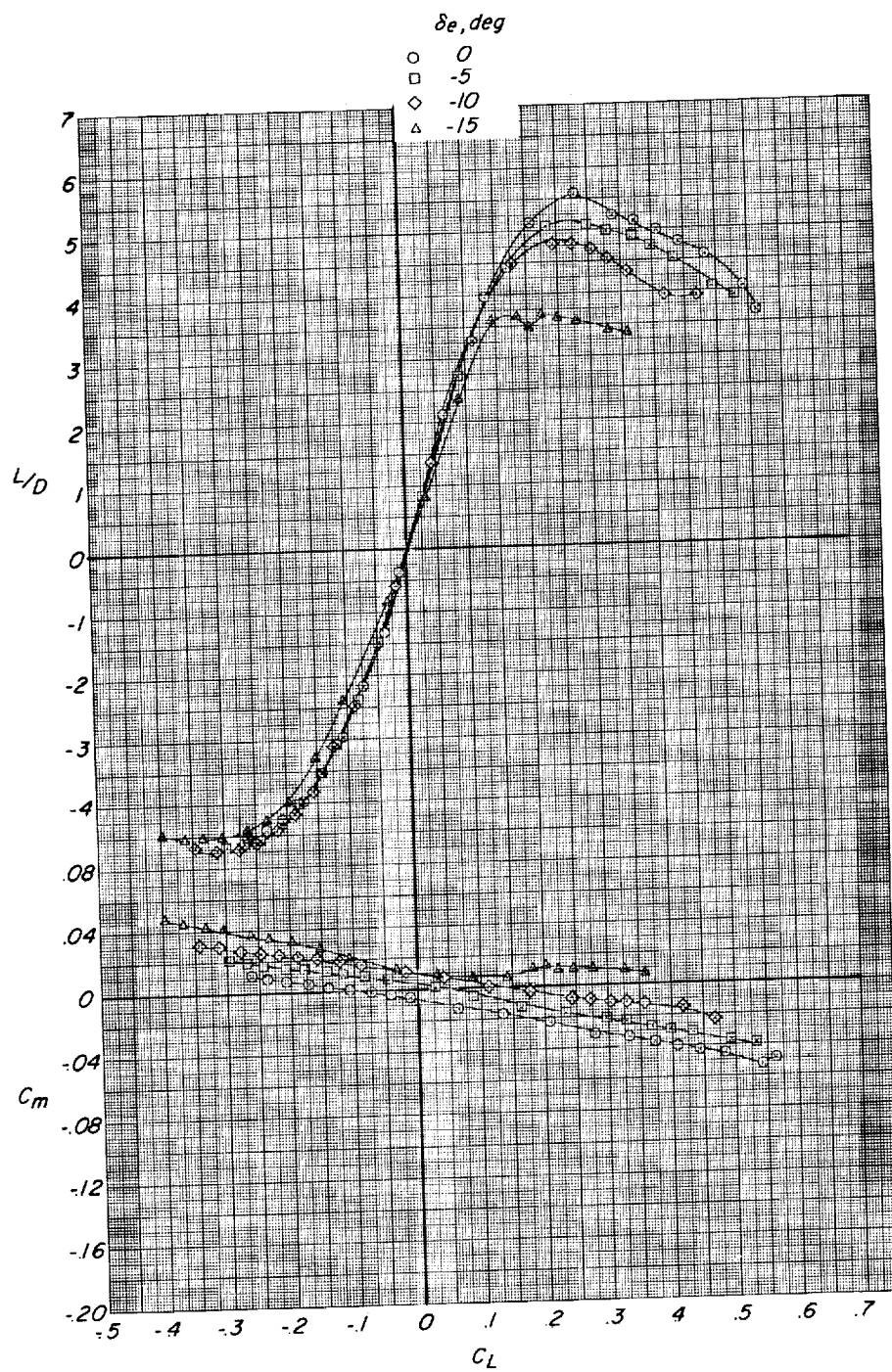
(b) Elevon base extension having $\delta_L = 35^\circ$ and $\delta_U = 26^\circ$.

Figure 10.- Continued.



(b) Continued.

Figure 10.- Continued.

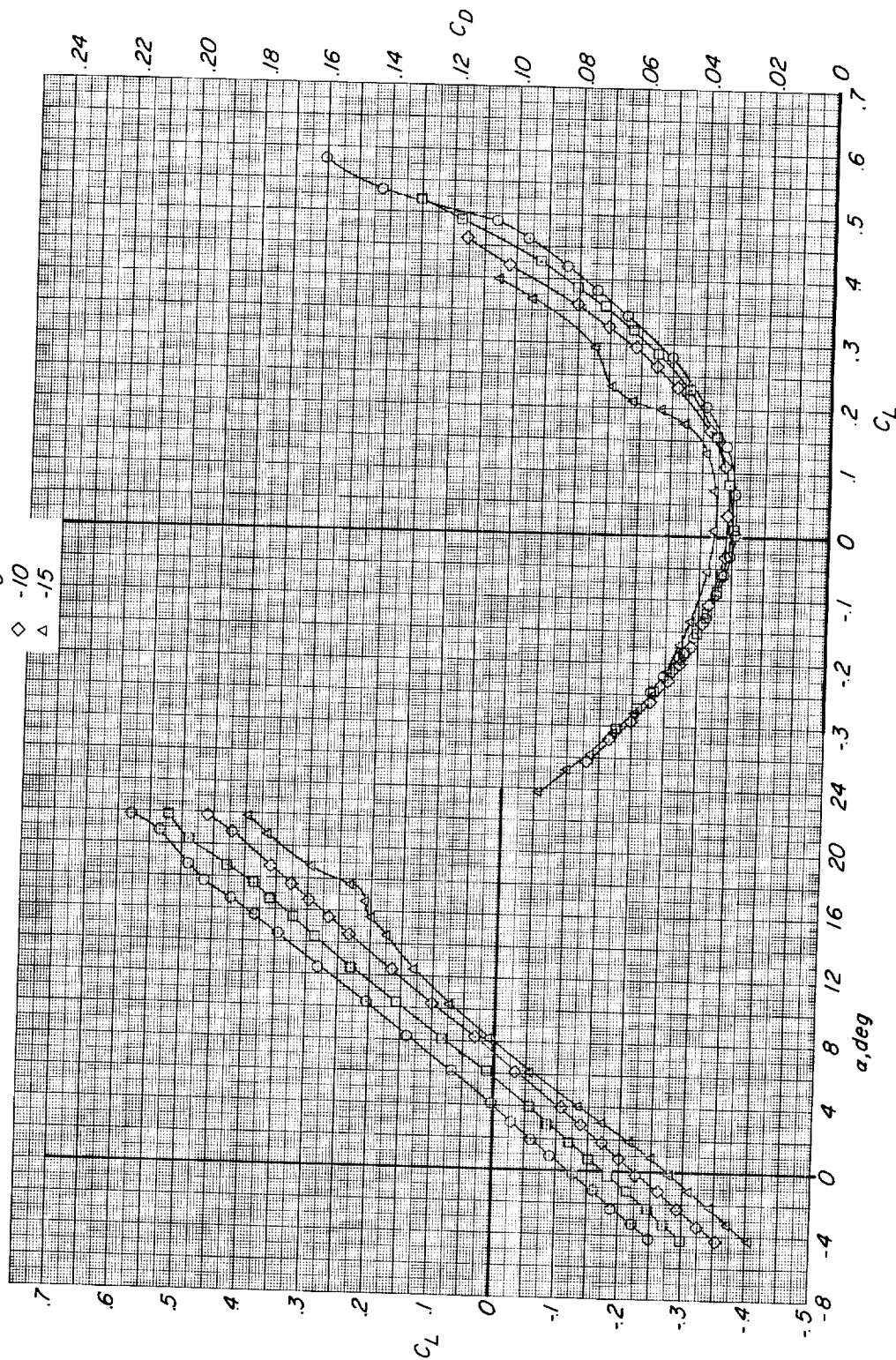


(b) Concluded.

Figure 10.- Continued.

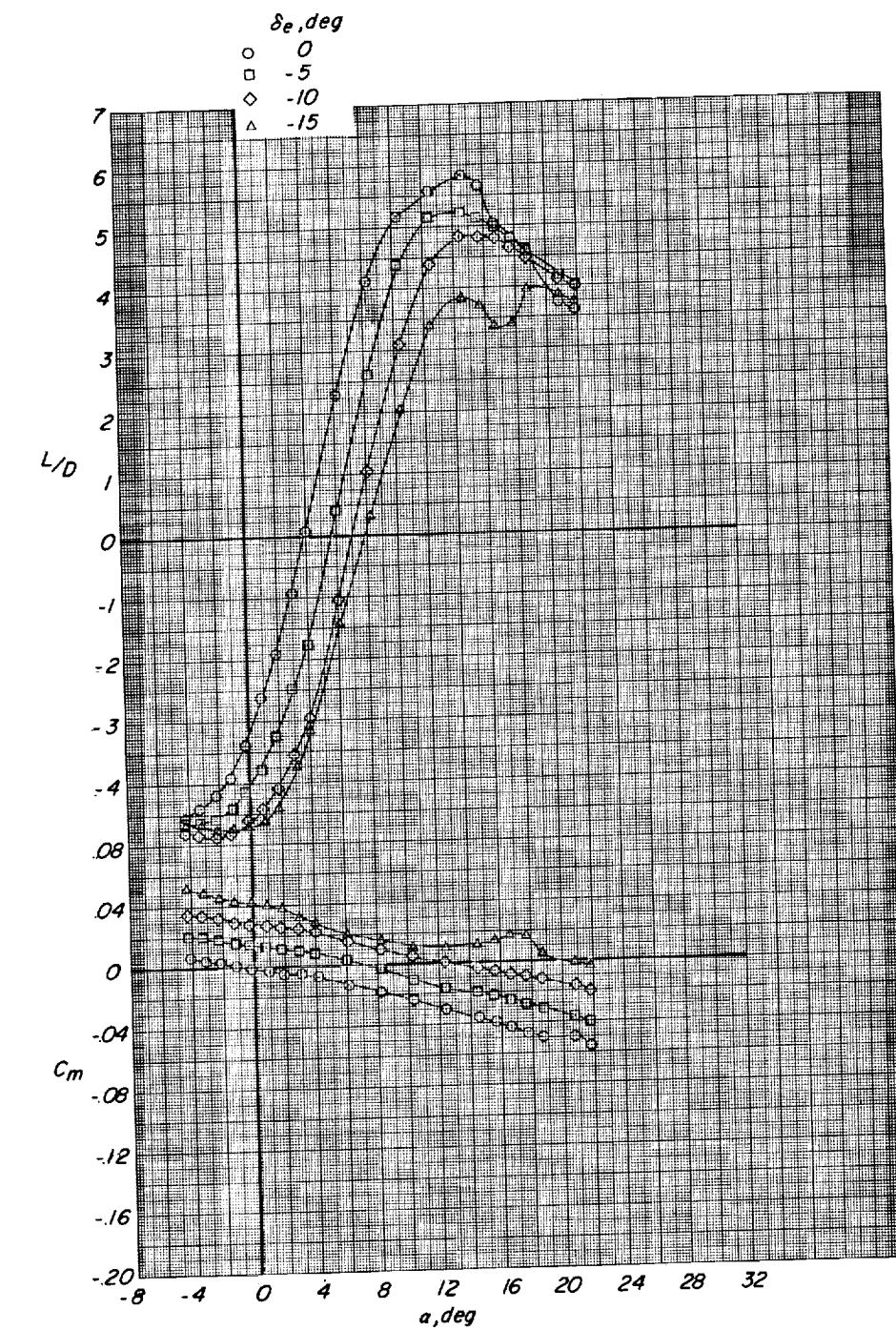
δ_e, deg

- 0
- -5
- ◇ -10
- △ -15



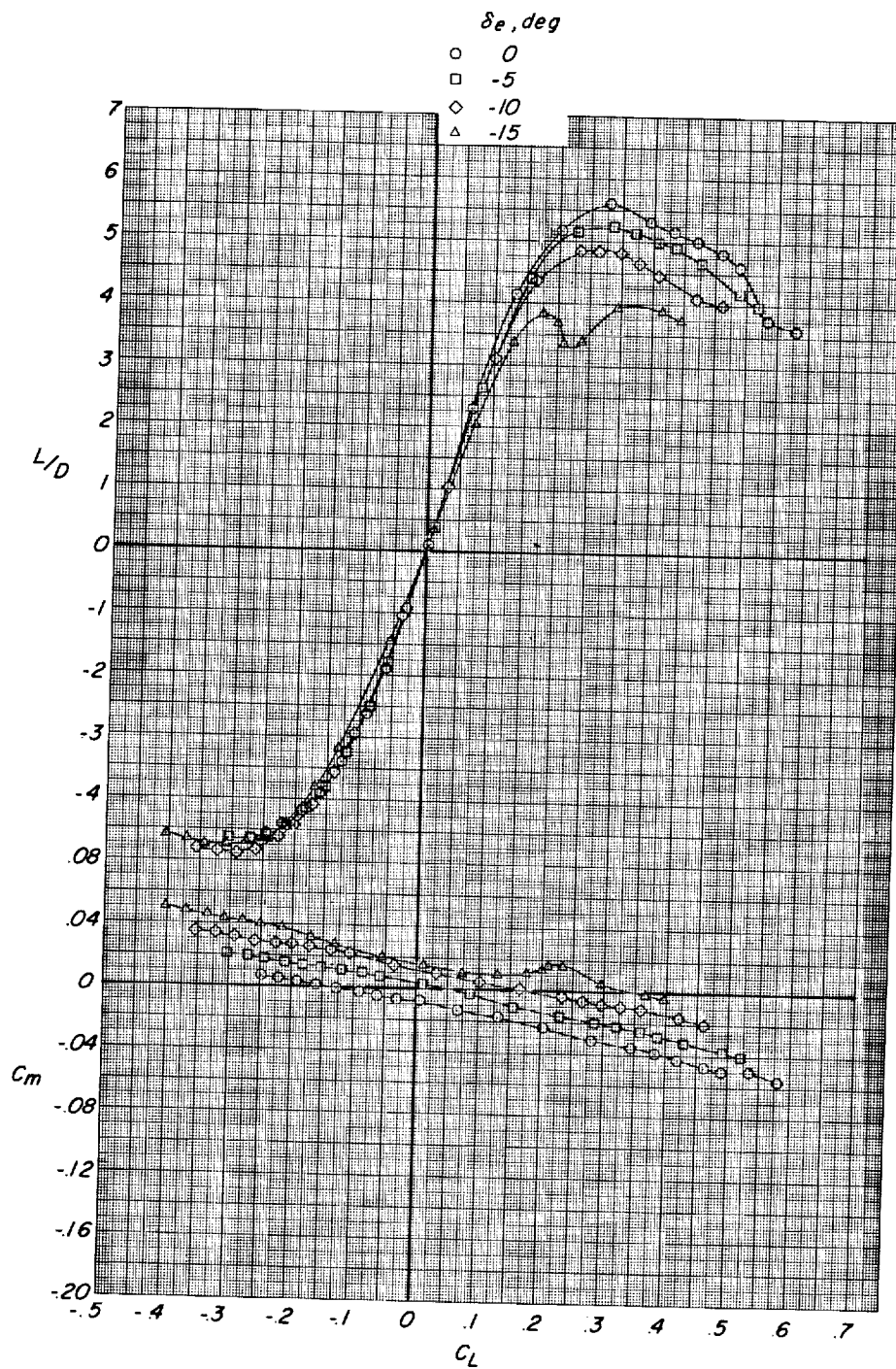
(c) Elevon base extension having $\delta_L = 15^\circ$ and $\delta_U = 26^\circ$.

Figure 10.- Continued.



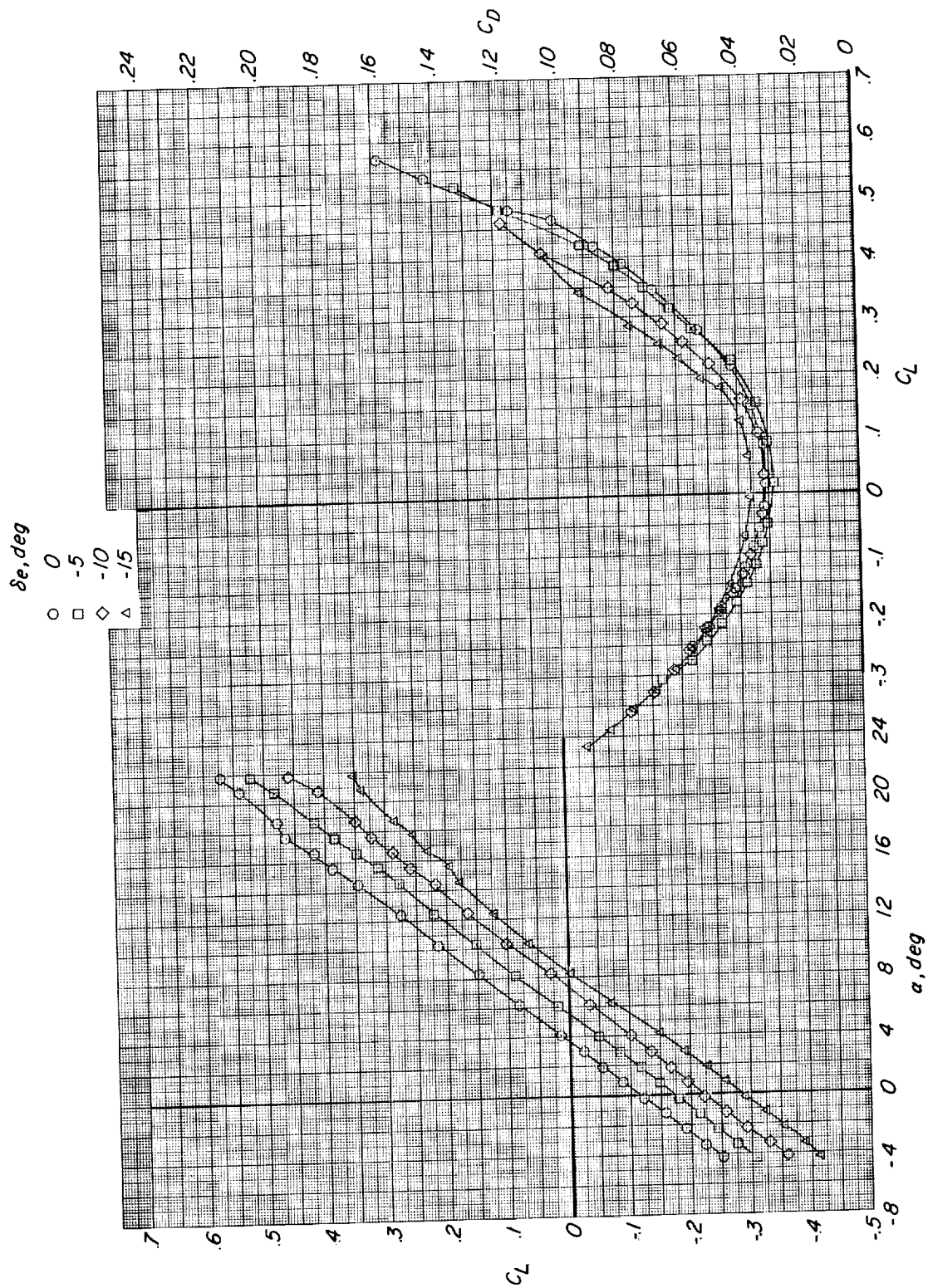
(c) Continued.

Figure 10.- Continued.



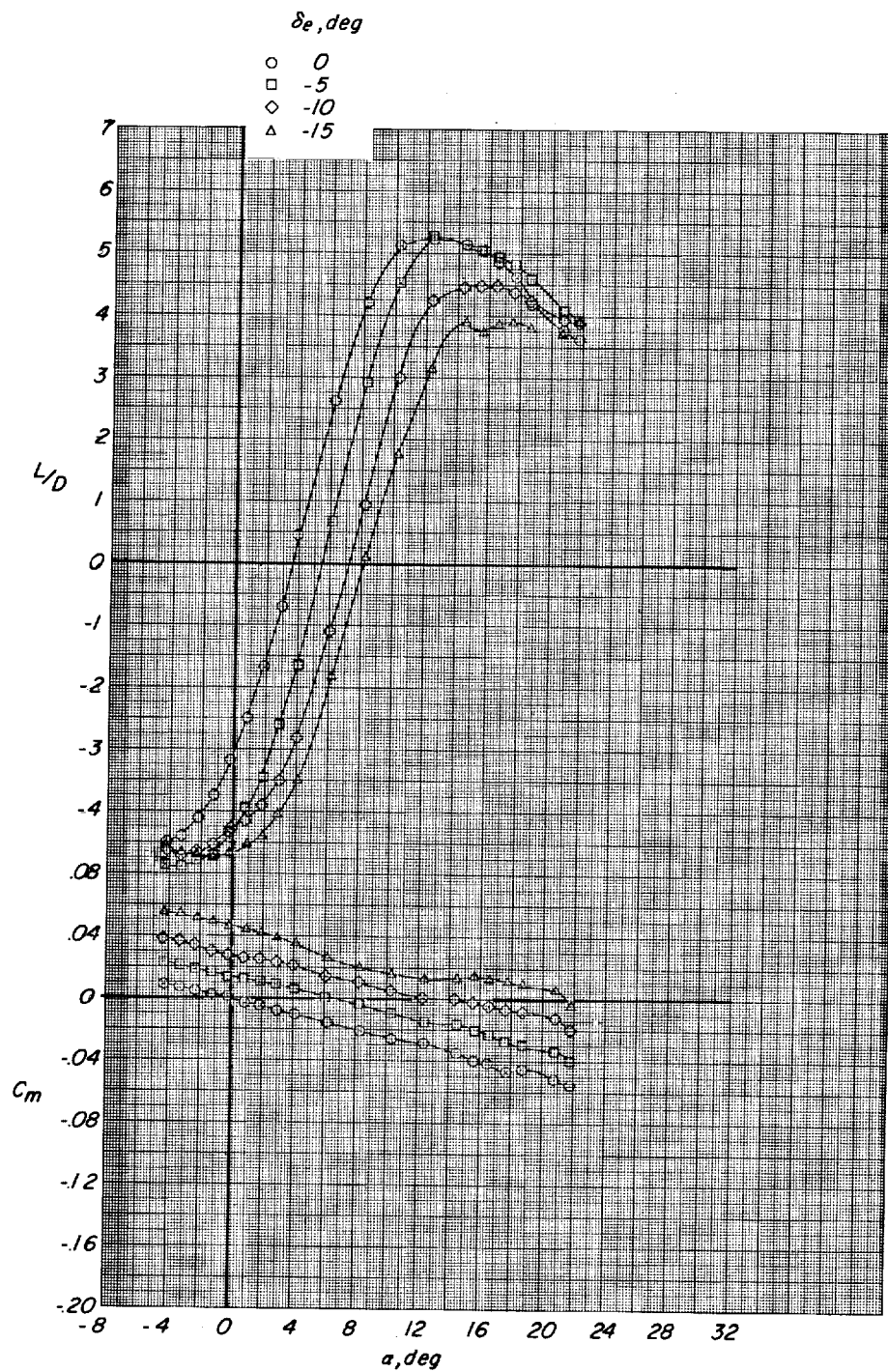
(c) Concluded.

Figure 10.- Continued.



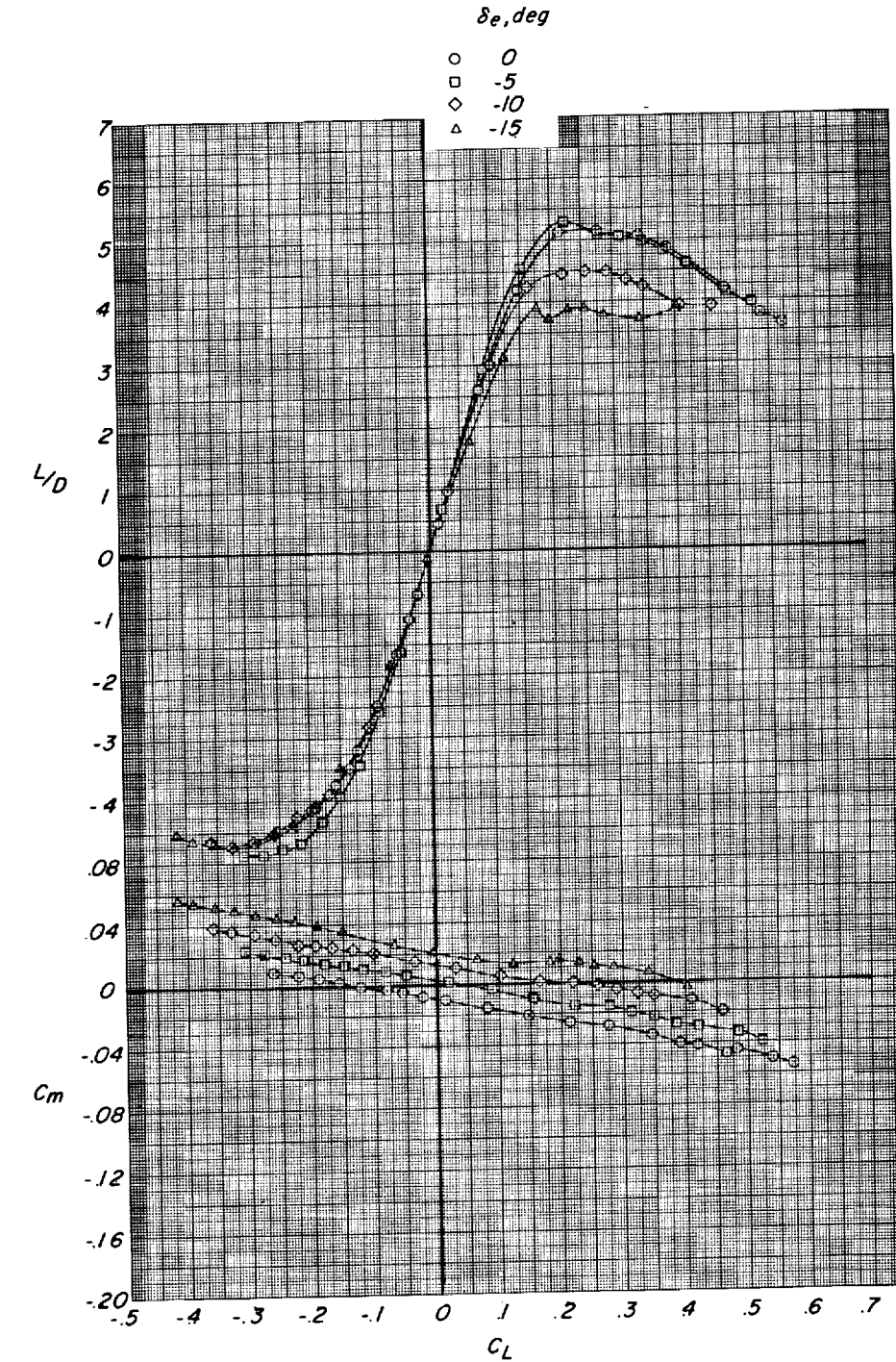
(d) Elevon base extension having $\delta_L = 15^\circ$ and $\delta_U = 16^\circ$.

Figure 10.- Continued.



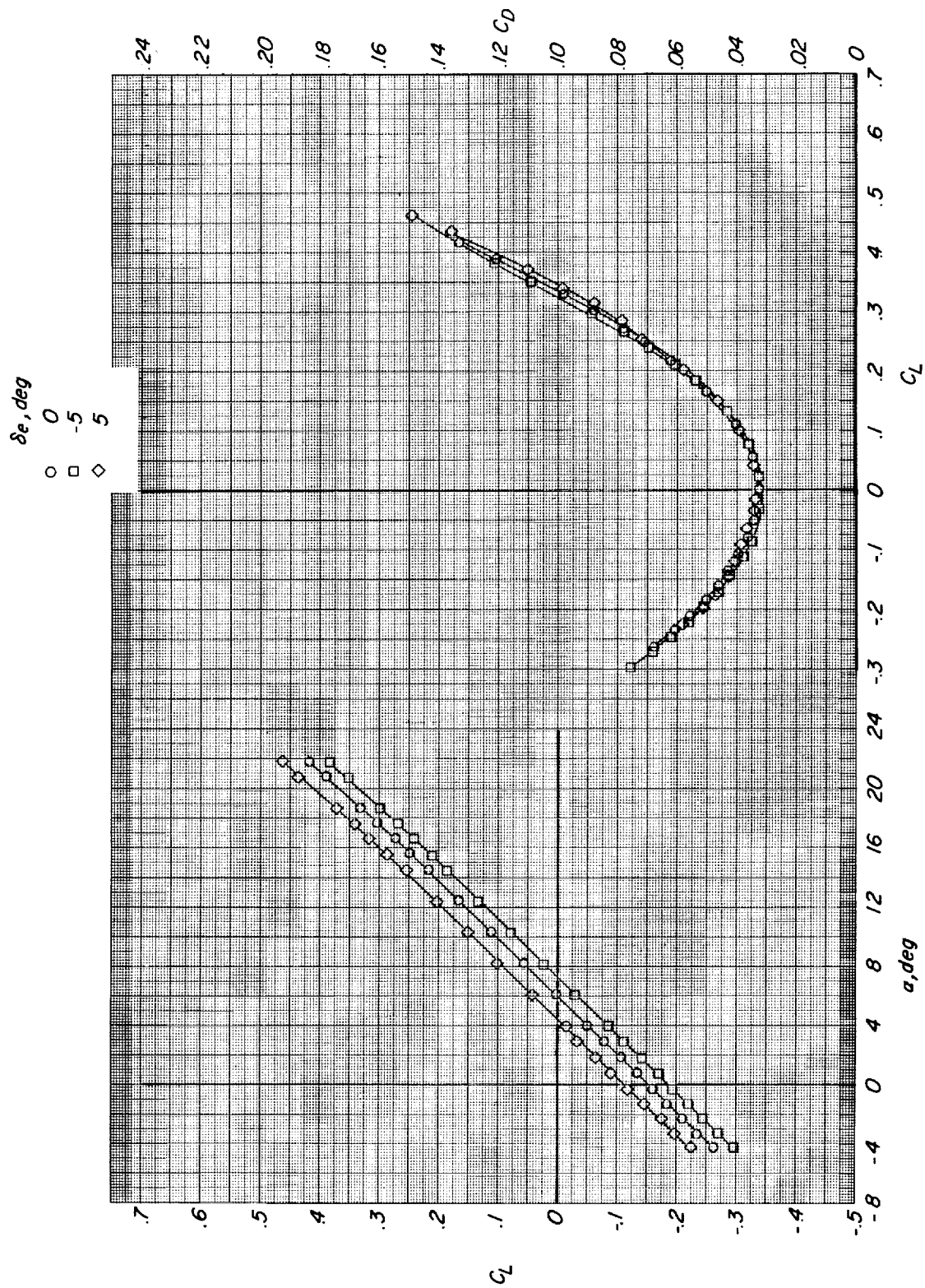
(d) Continued.

Figure 10.- Continued.



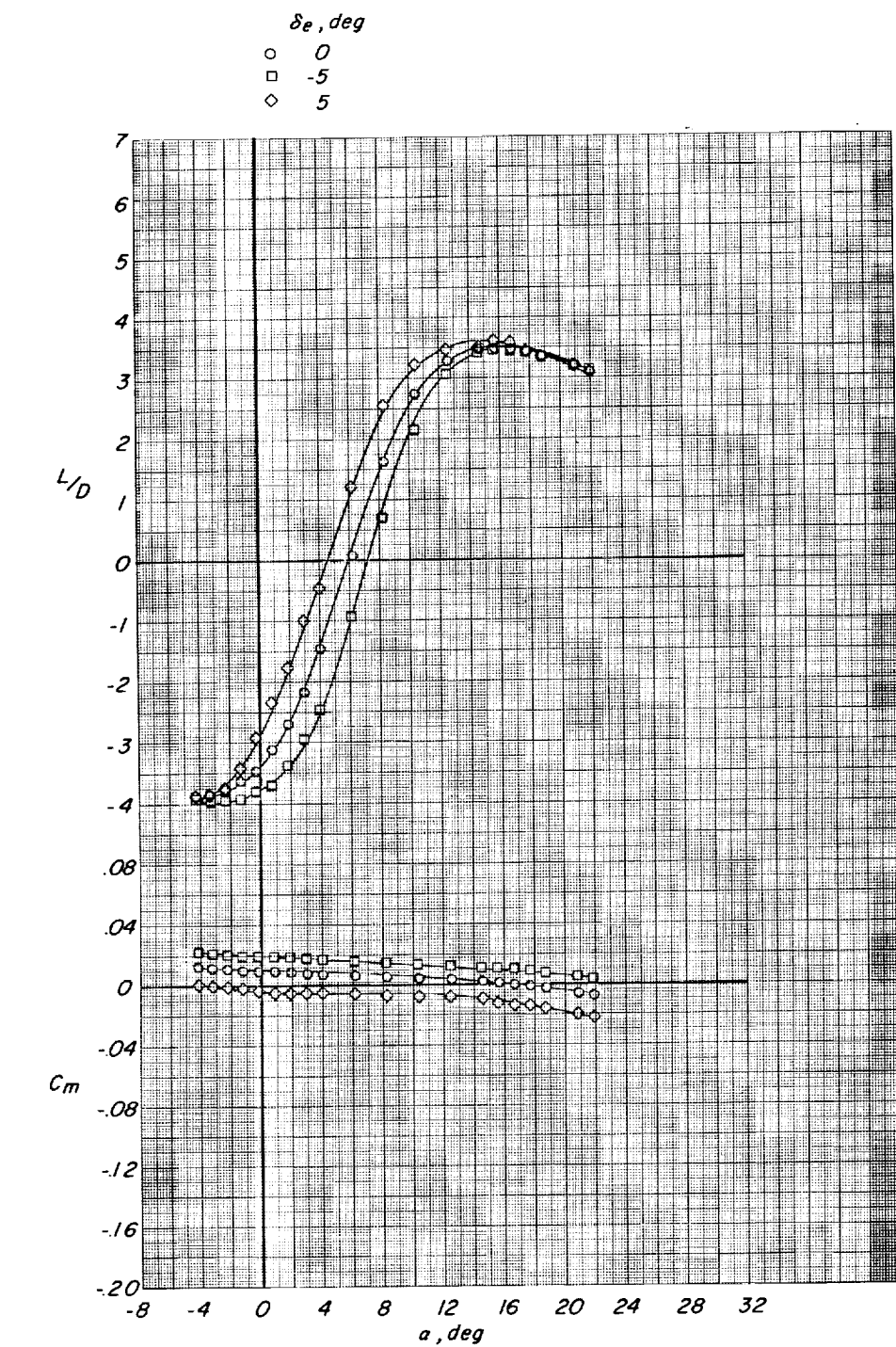
(d) Concluded.

Figure 10.- Concluded.



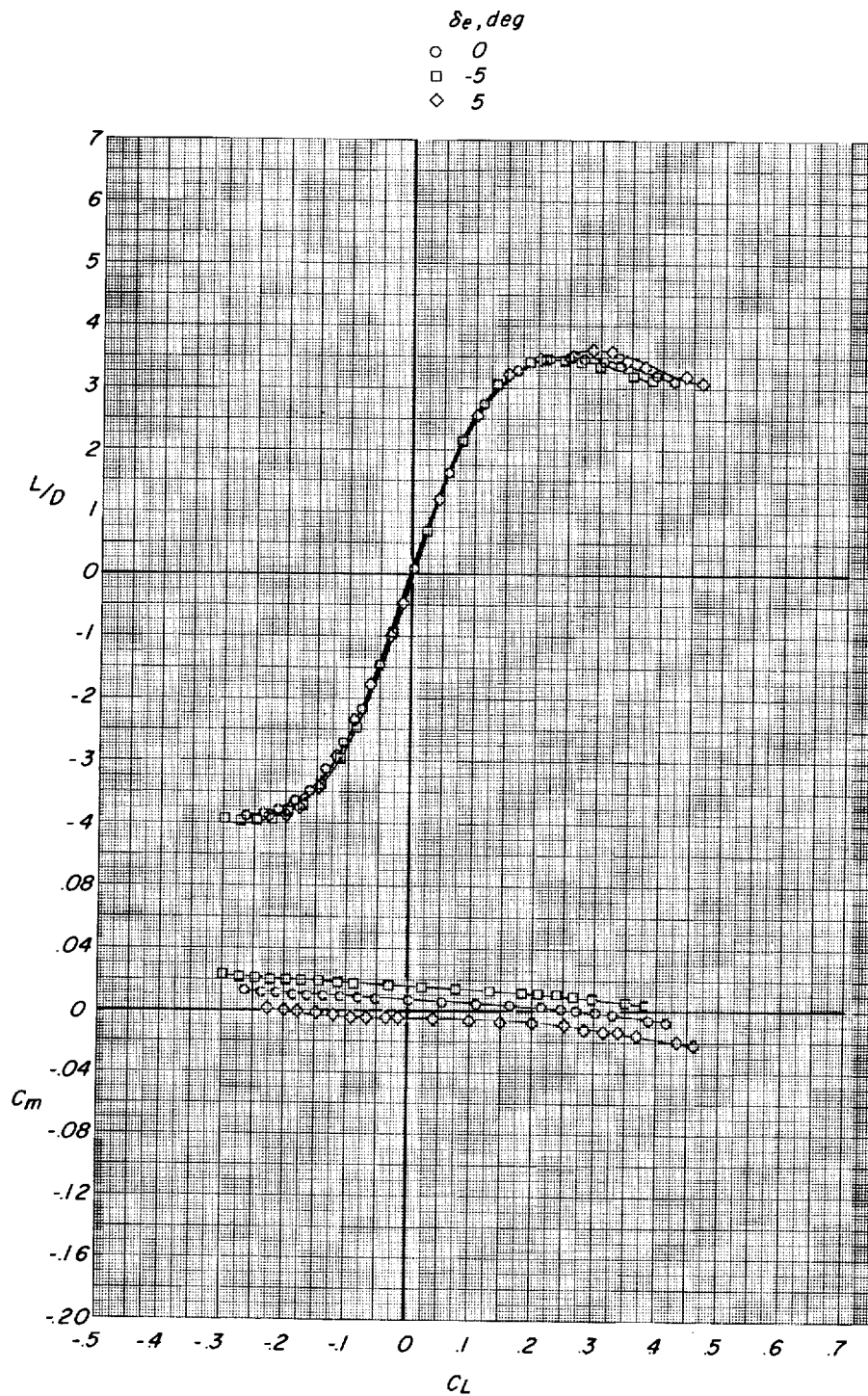
(a) Original fin E_2

Figure 11.- Longitudinal control characteristics associated with deflection of original HL-10 elevon. $\theta = 0^\circ$; vortex generators off; one-fin HL-10.



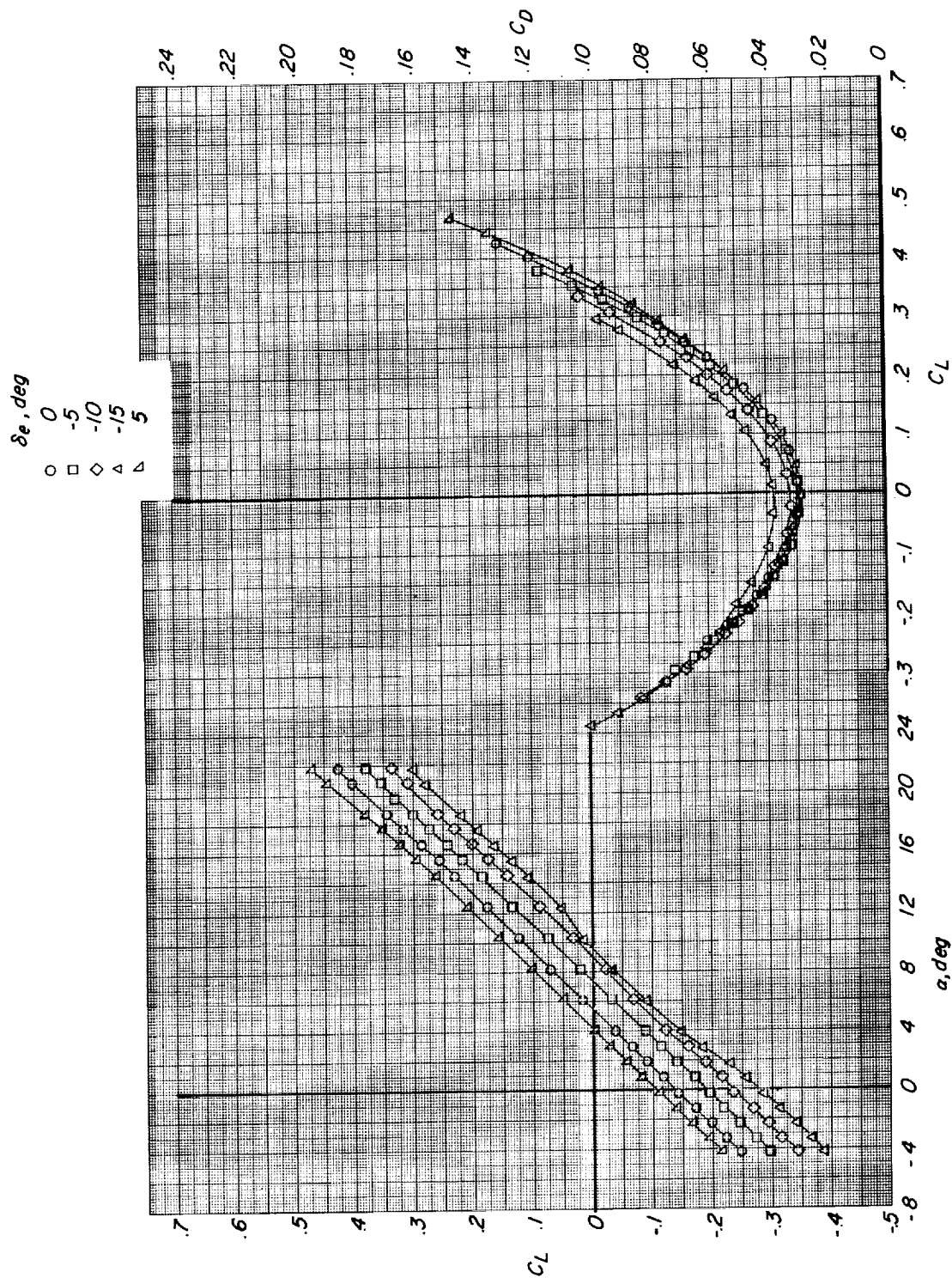
(a) Continued.

Figure 11.- Continued.



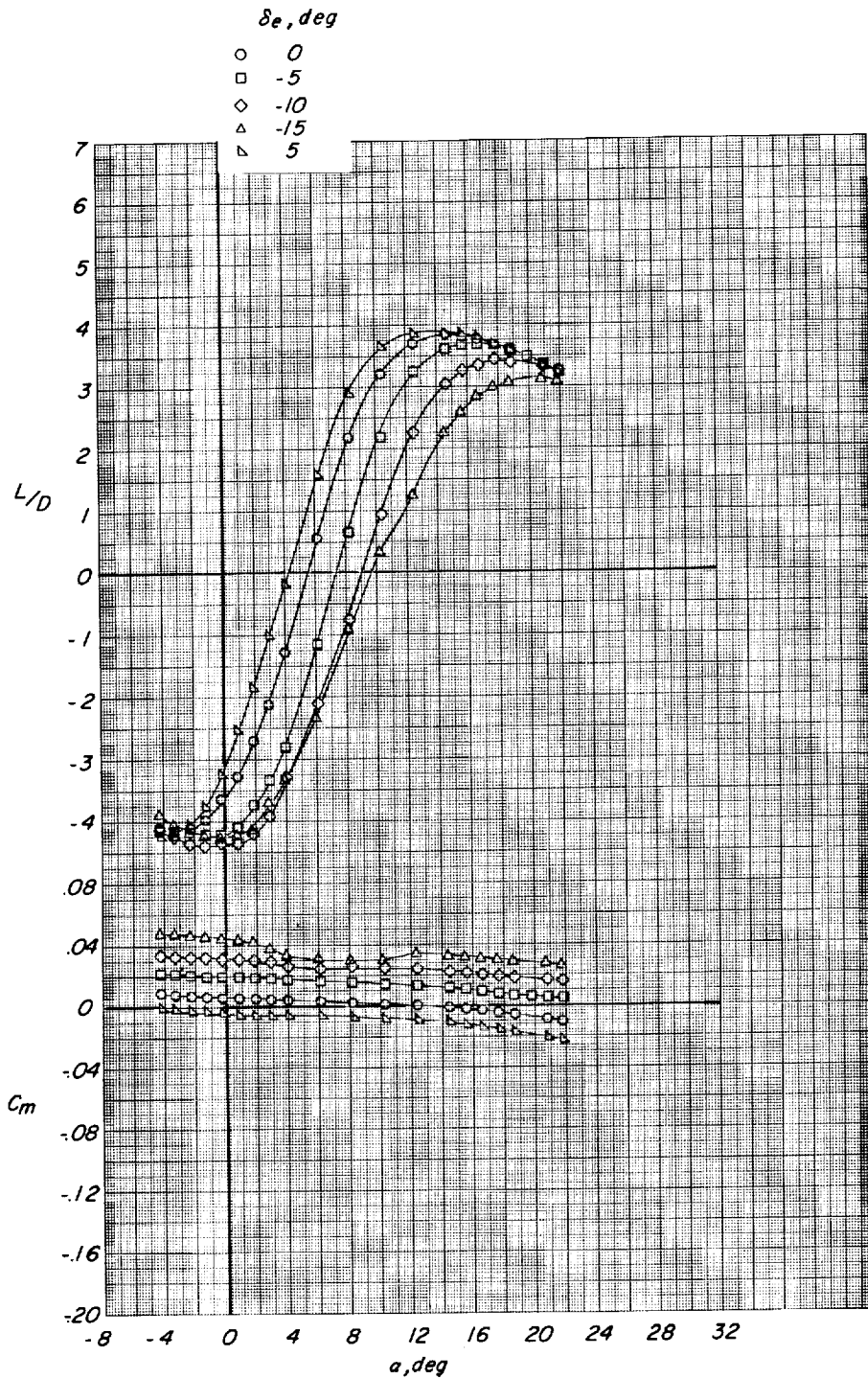
(a) Concluded.

Figure 11.- Continued.



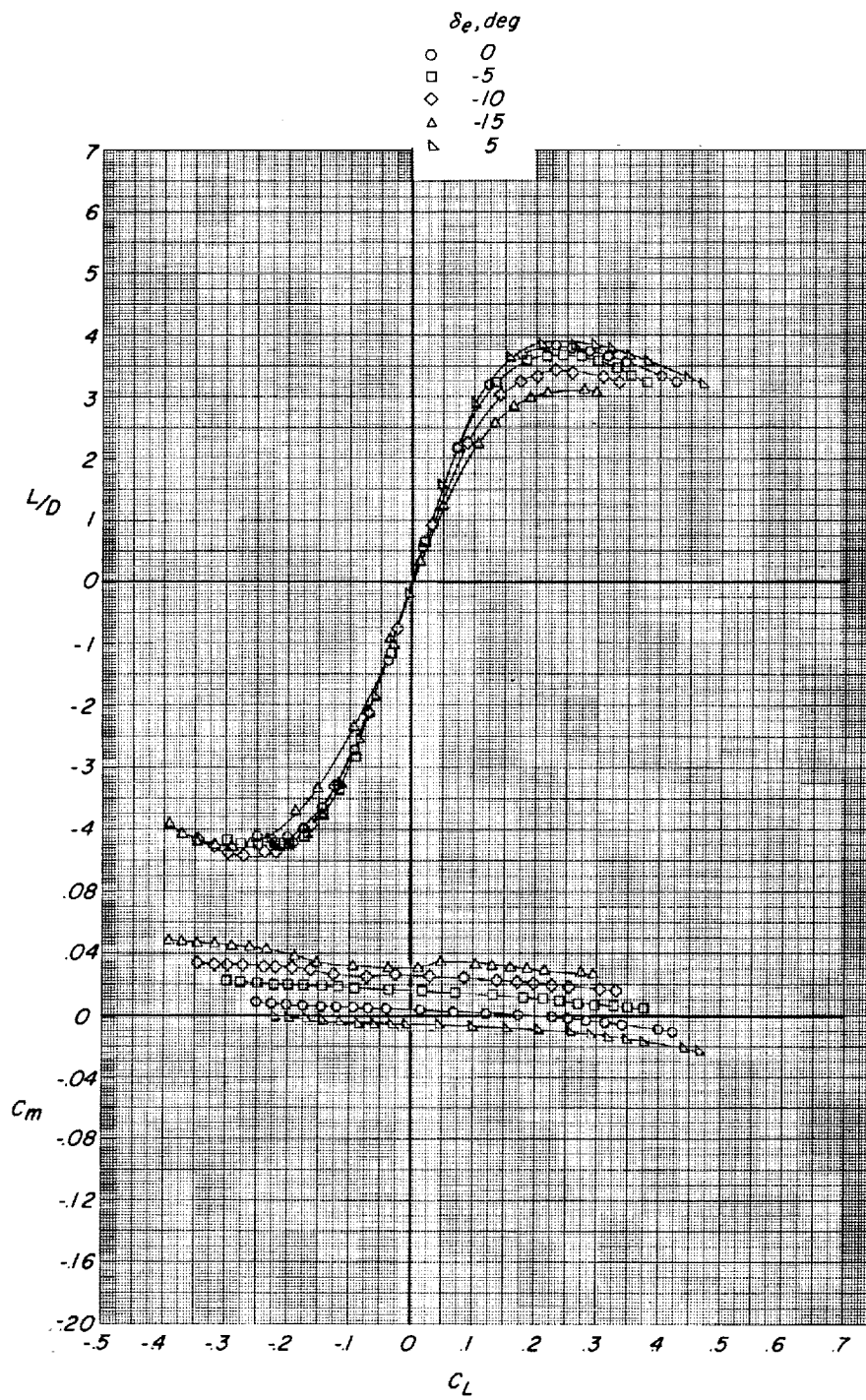
(b) Modified fin E2.

Figure 11.- Continued.



(b) Continued.

Figure 11.- Continued.



(b) Concluded.

Figure 11.- Concluded.

δ_e, deg Vortex generators

- \circ 0 Off
- \square 0 On
- \diamond -5 Off
- \triangle -5 On

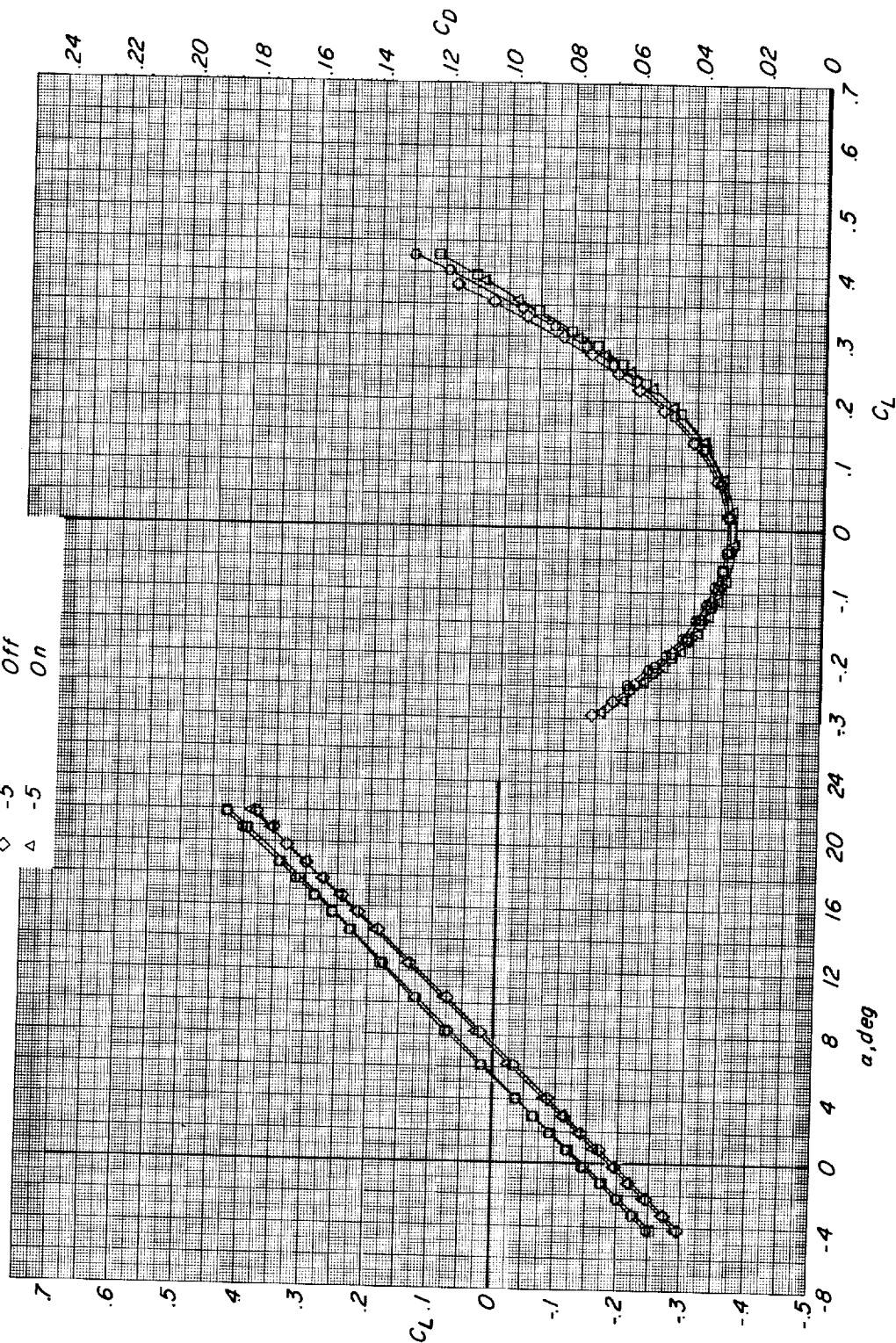


Figure 12.- Longitudinal control characteristics associated with deflection of original HL-10 elevon. $\theta = 0^\circ$; one-fin HL-10; modified fin E2.

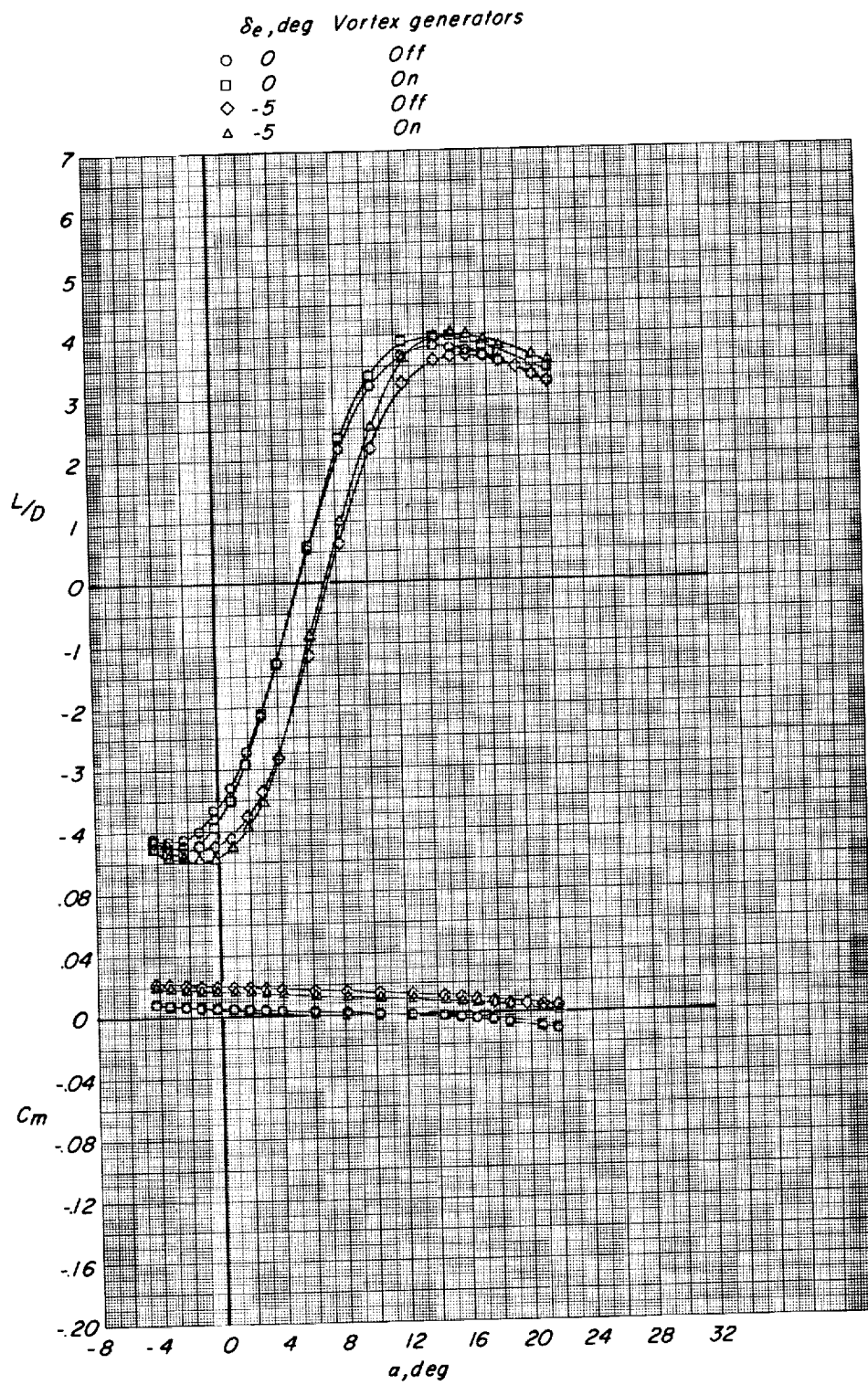


Figure 12.- Continued.

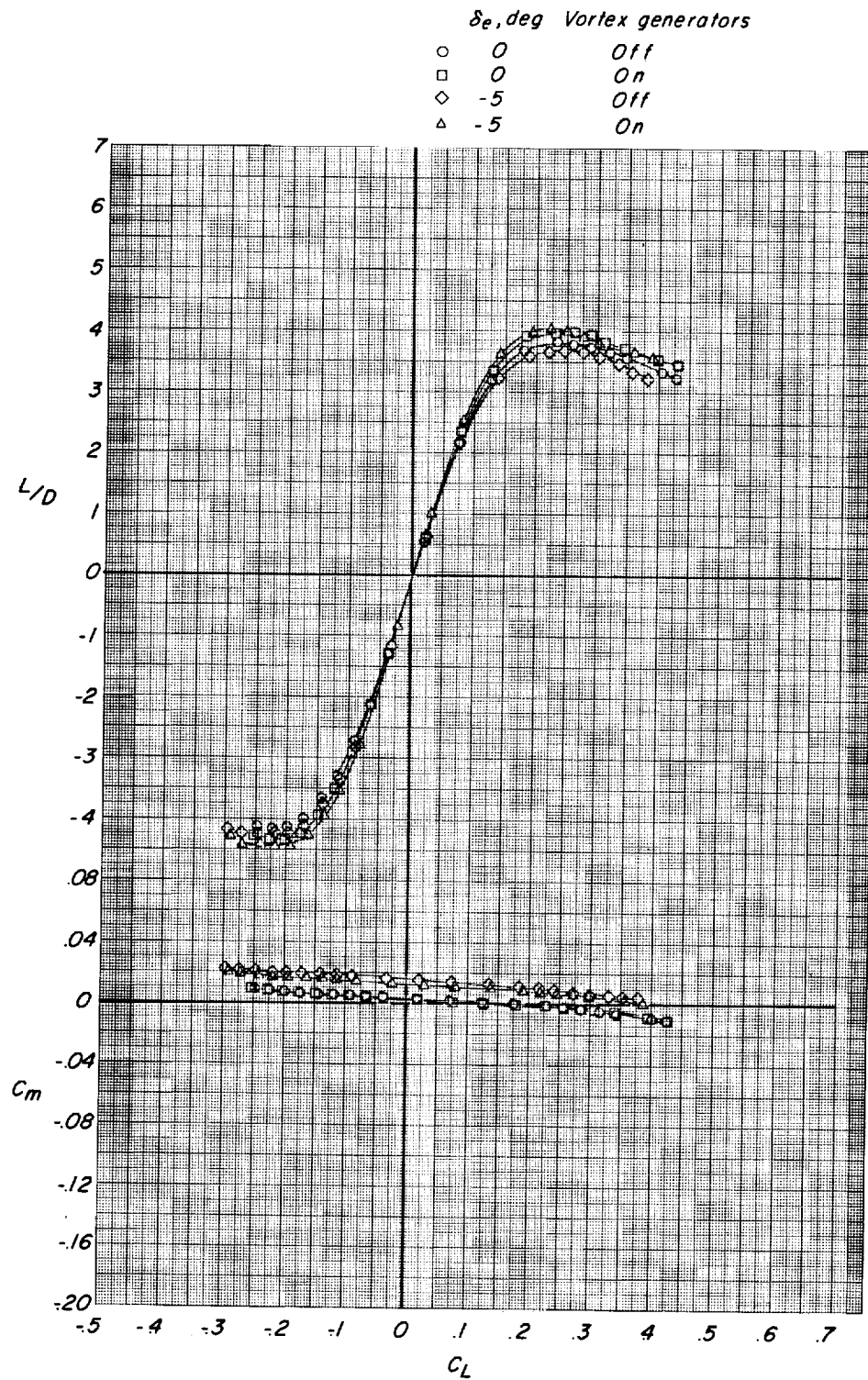
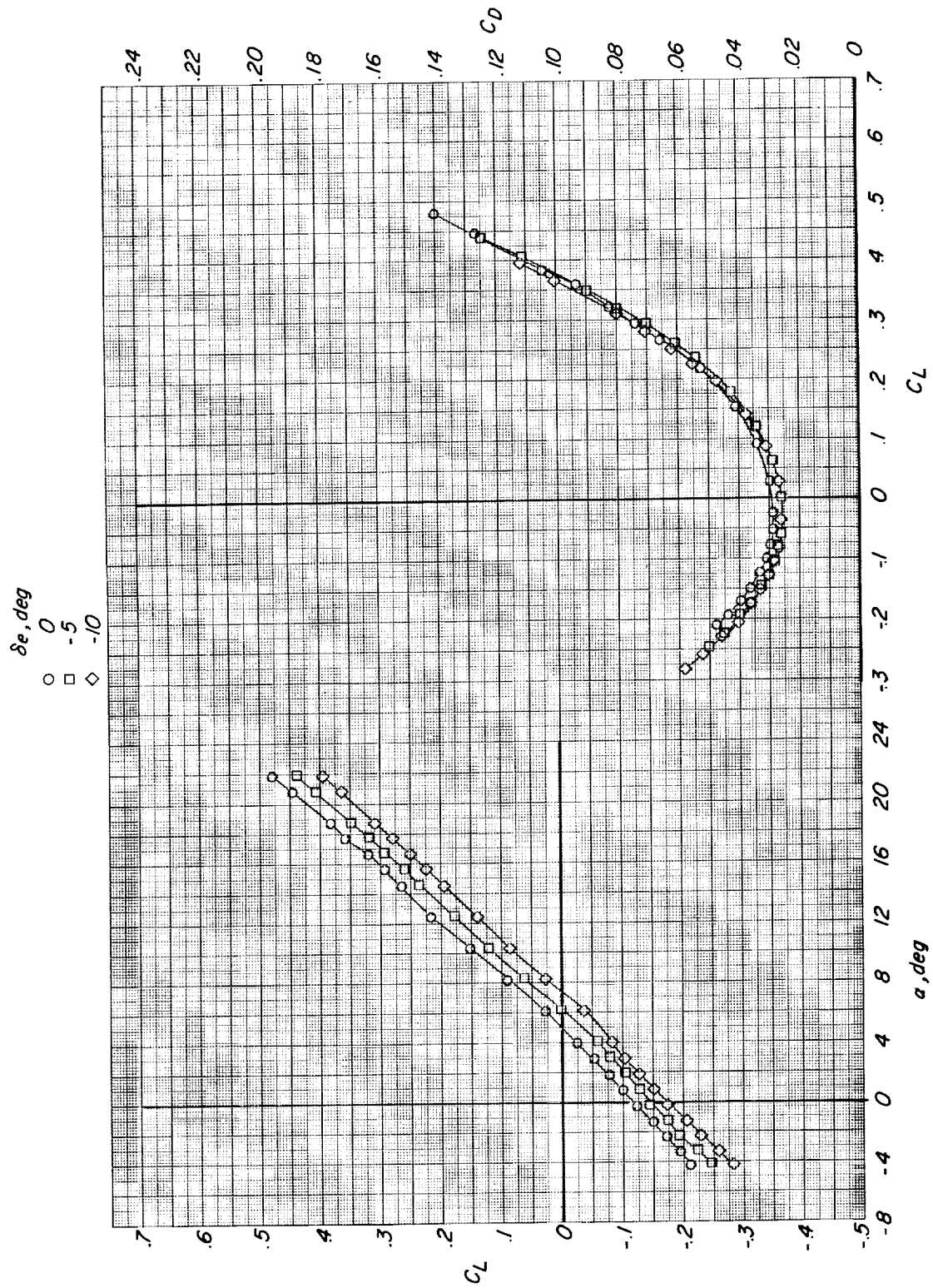
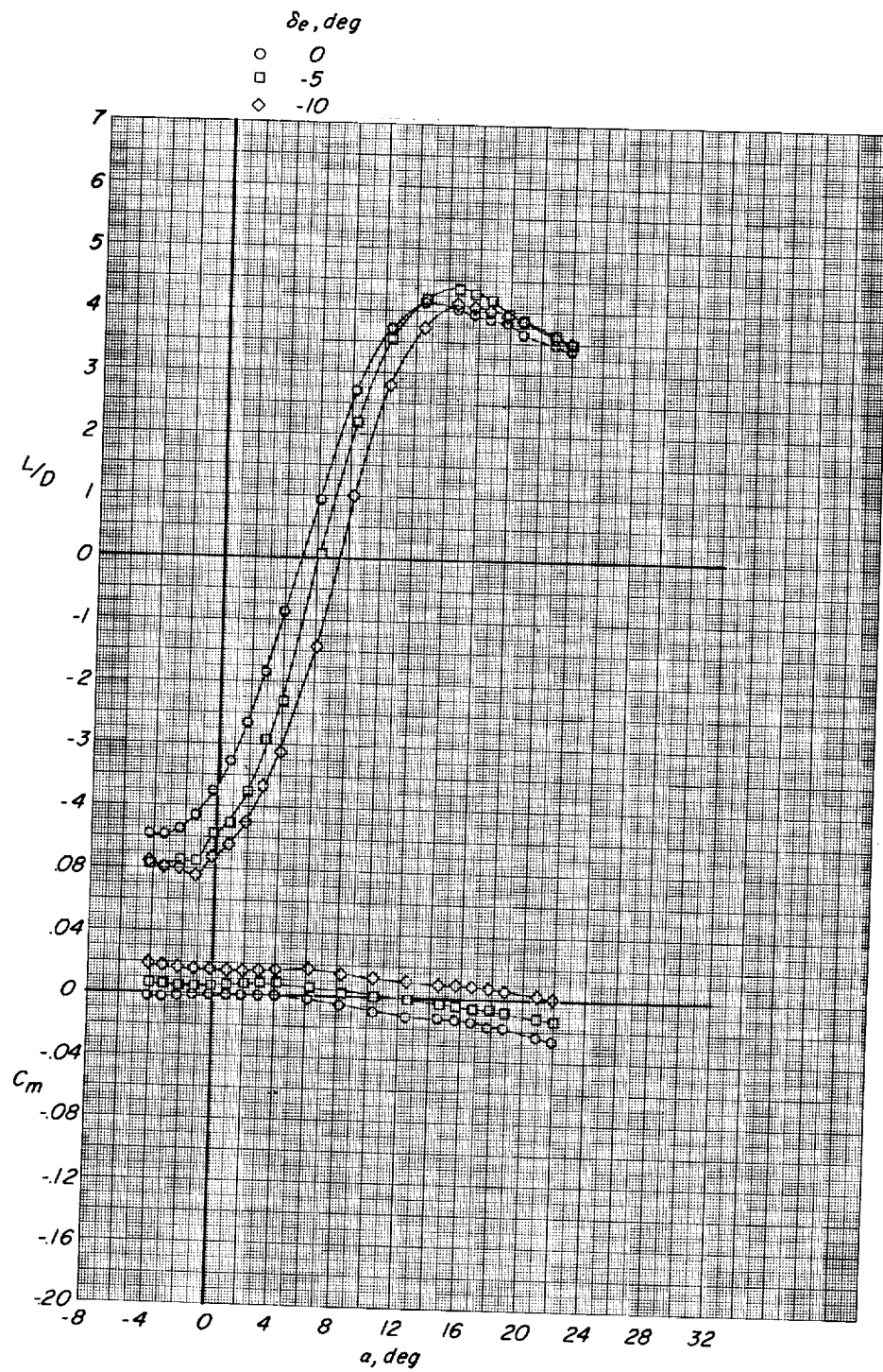


Figure 12.- Concluded.



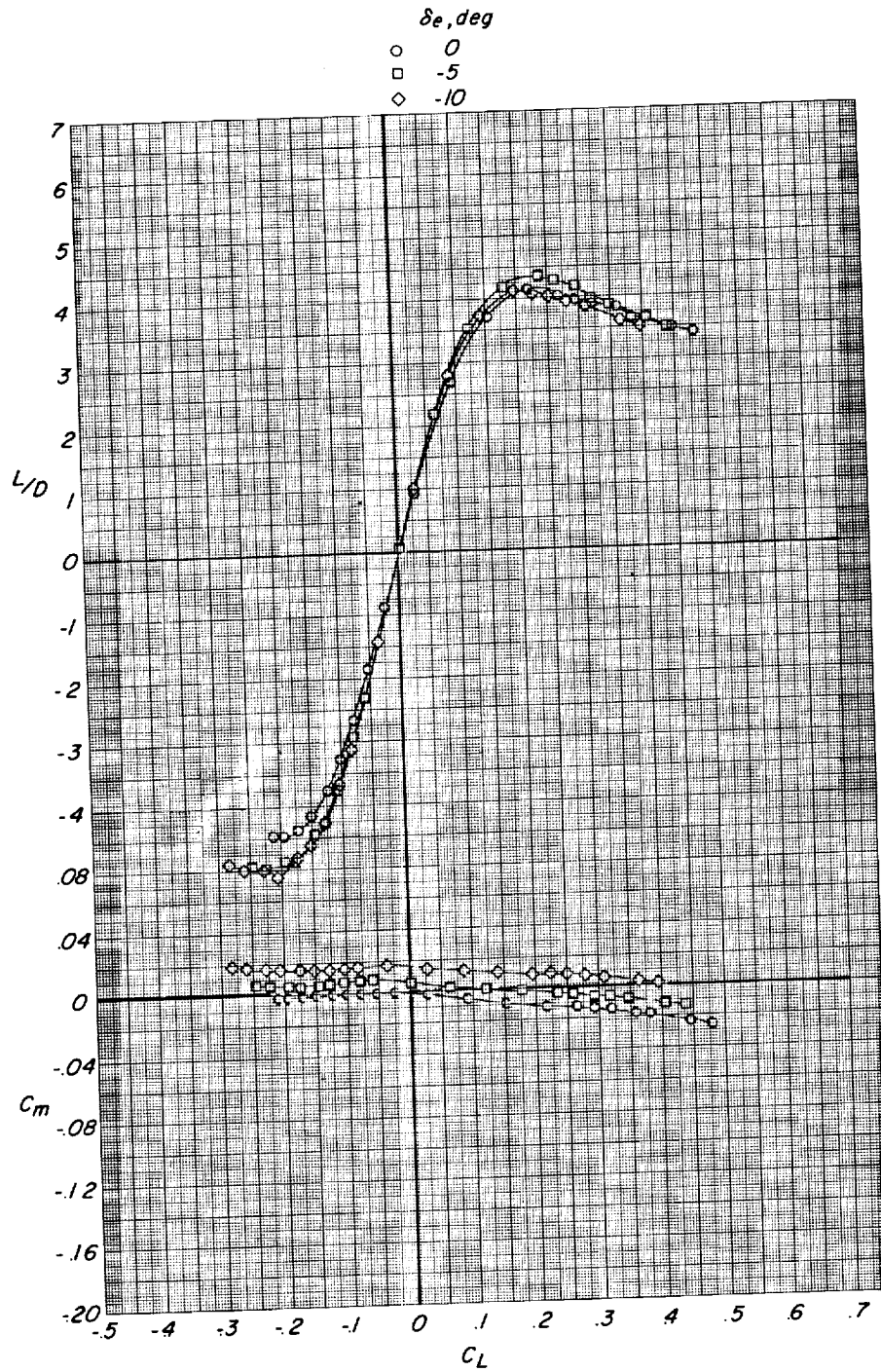
(a) Vortex generators off.

Figure 13.- Longitudinal control characteristics associated with deflection of modified HL-10 elevon. $\theta = 120^\circ$, one-fin HL-10; modified fin E2.



(a) Continued.

Figure 13.- Continued.

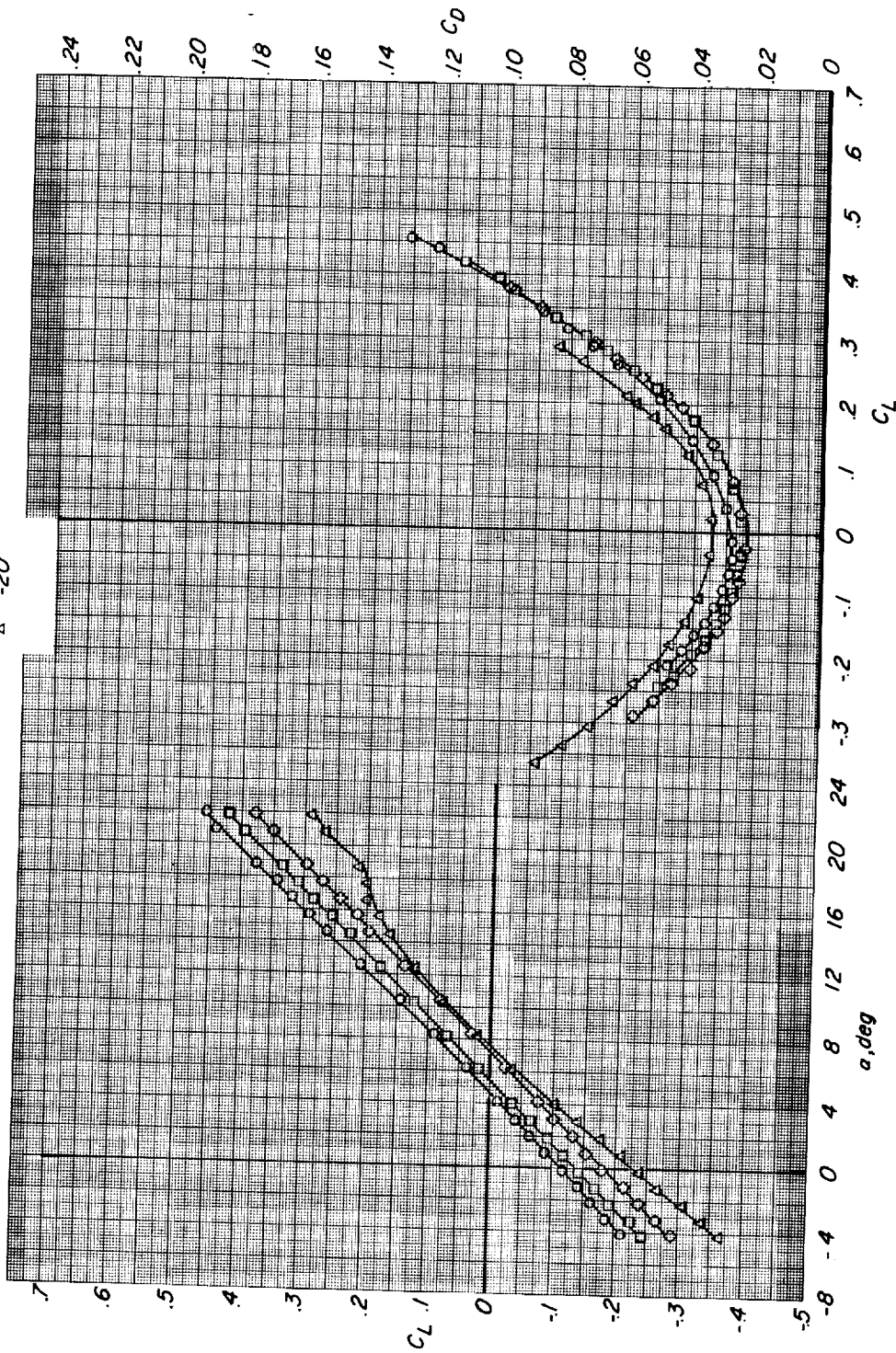


(a) Concluded.

Figure 13.- Continued.

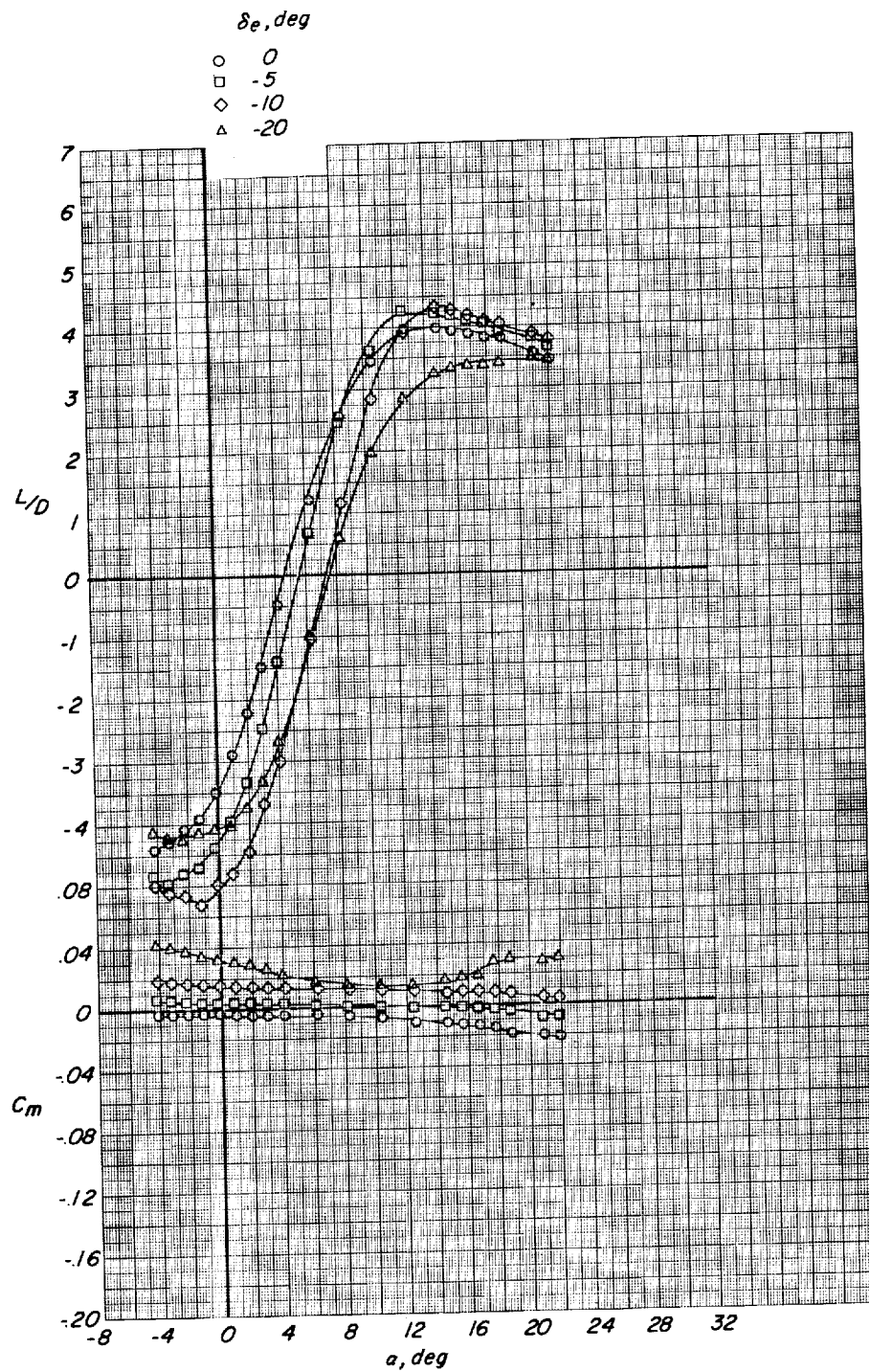
δ_e, deg

- 0
- -5
- ◇ -10
- △ -20



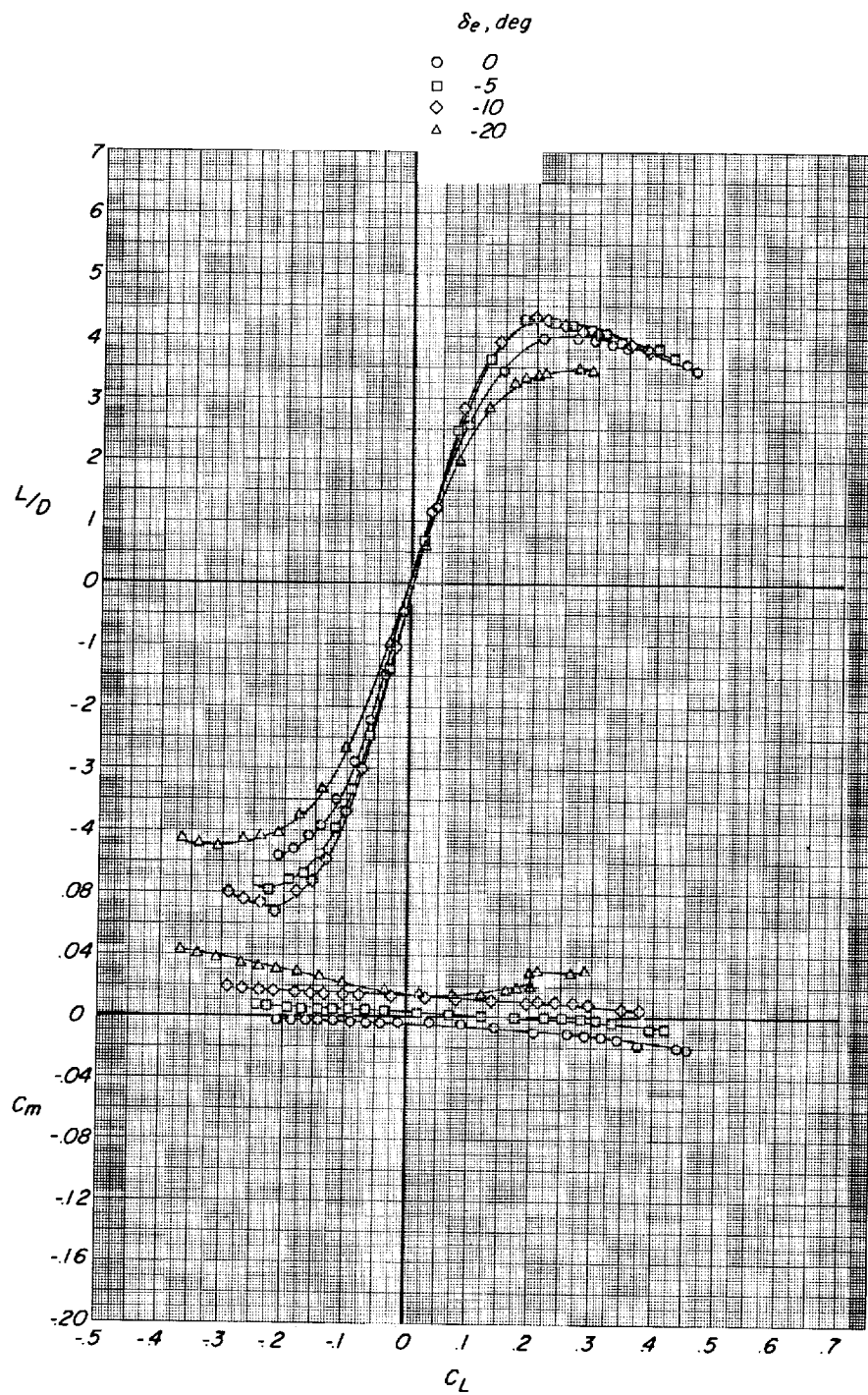
(b) Vortex generators on.

Figure 13.- Continued.



(b) Continued.

Figure 13.- Continued.



(b) Concluded.

Figure 13.- Concluded.

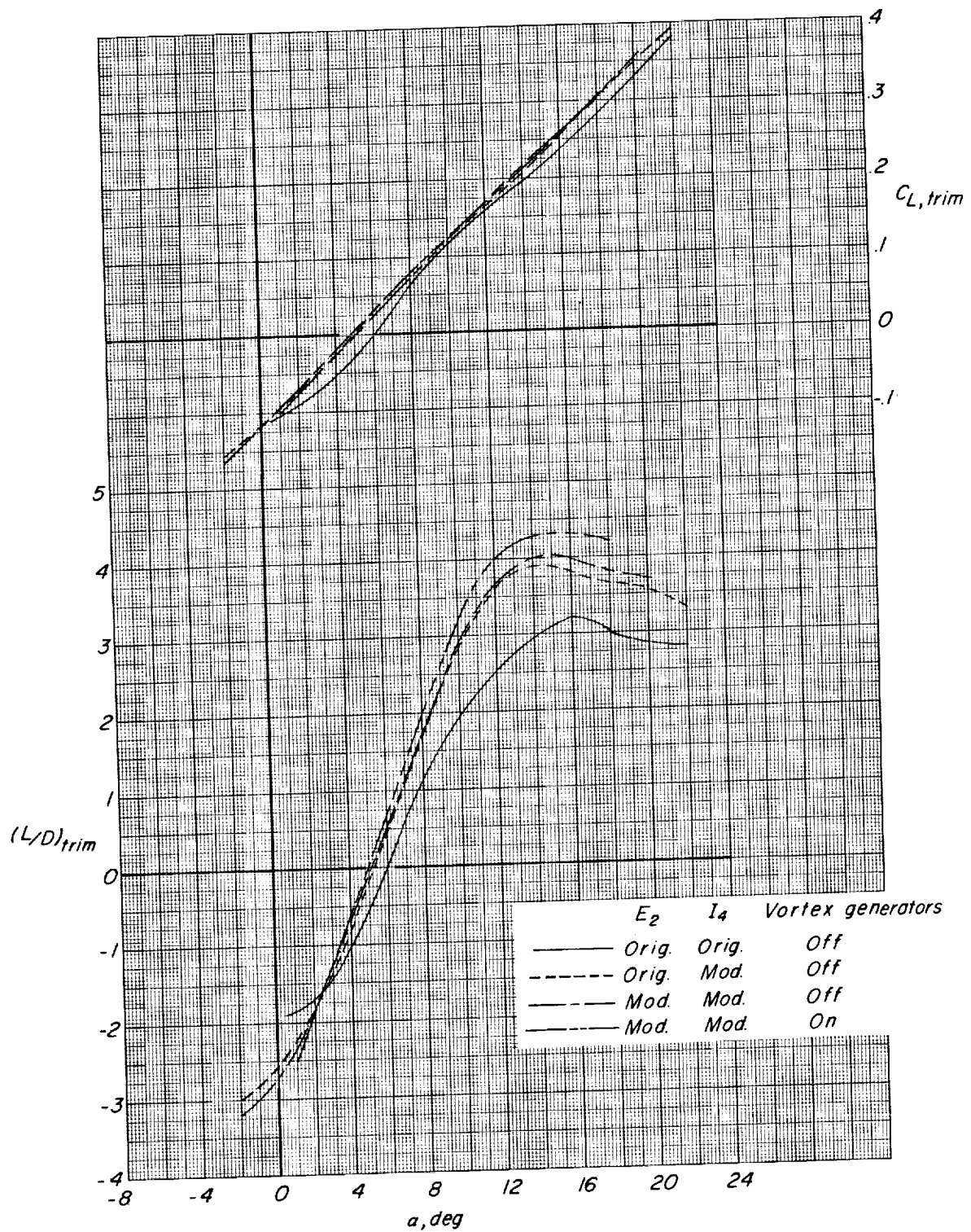


Figure 14.- Summary of effects of model components on trimmed characteristics. Three-fin HL-10 with original elevon; $\theta = 0^\circ$.

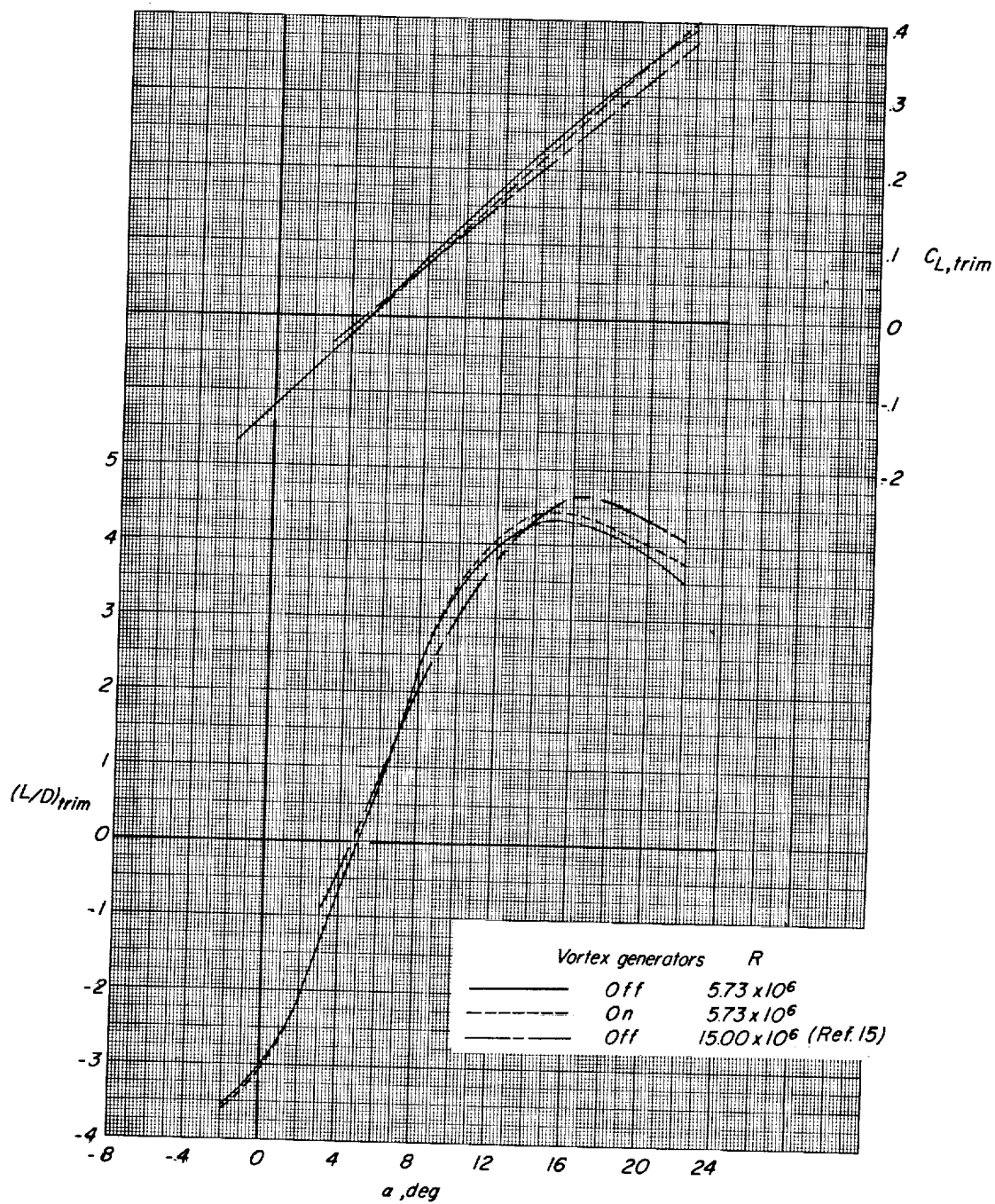


Figure 15.- Summary of effects of modified HL-10 elevon ($\theta = 40^\circ$) on trimmed characteristics and comparison with high Reynolds number results. Three-fin HL-10; modified fins E_2 plus I_4 .

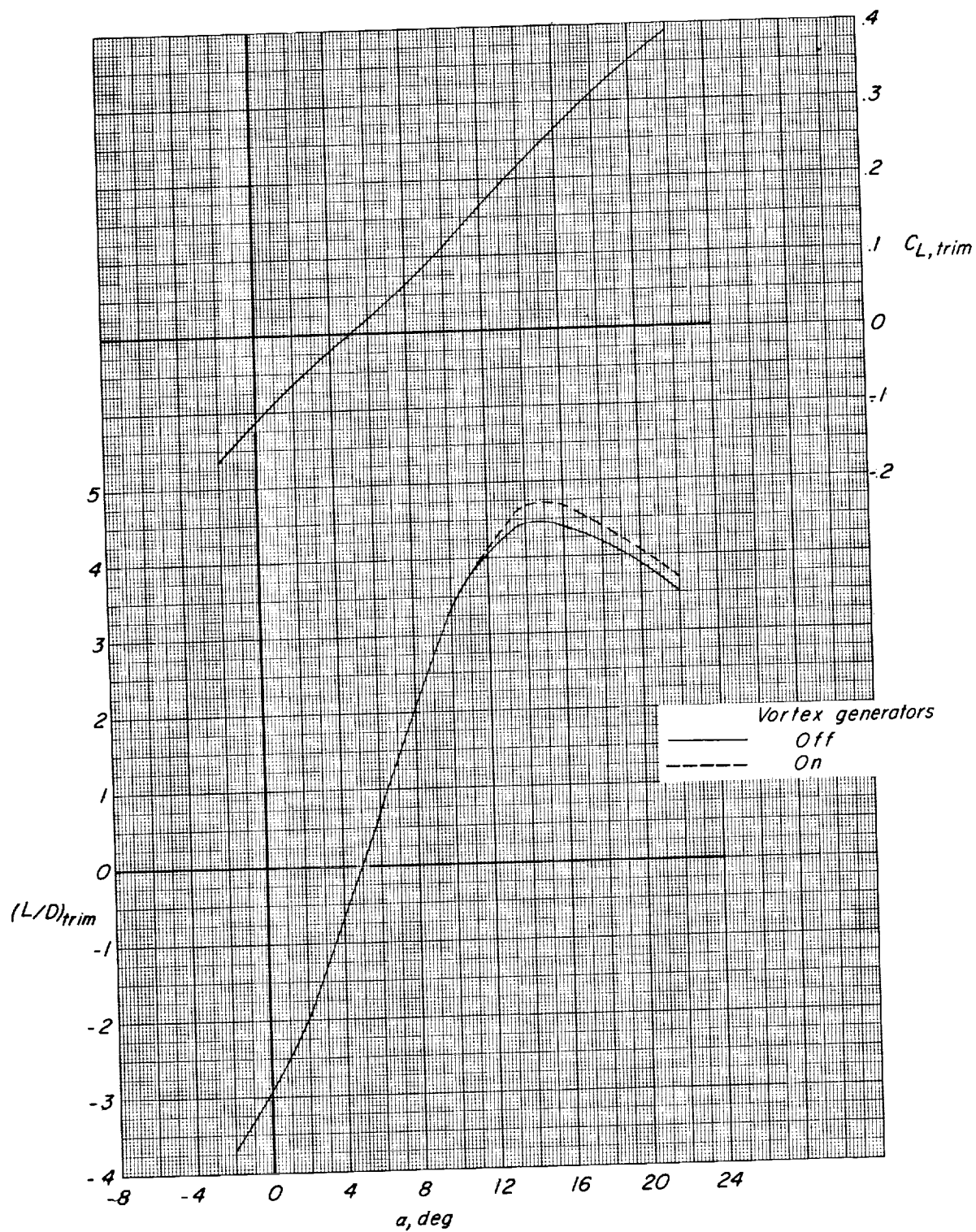


Figure 16.- Summary of effects of modified HL-10 elevon ($\theta = 80^\circ$) on trimmed characteristics. Three-fin HL-10; modified fins E₂ plus I₄.

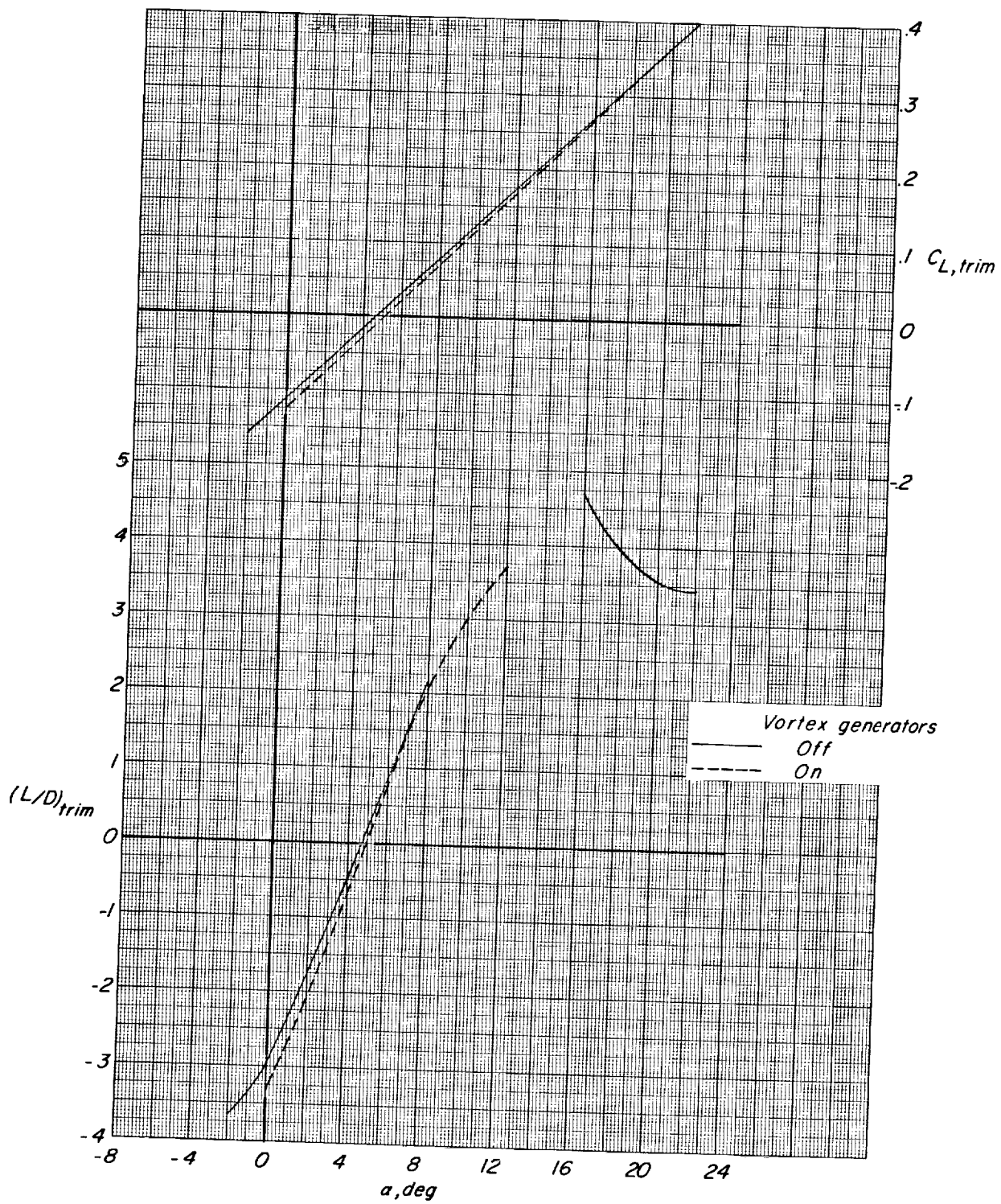


Figure 17.- Summary of effects of modified HL-10 elevon ($\theta = 12^\circ$) on trimmed characteristics. Three-fin HL-10; modified fins E_2 plus I_4 .

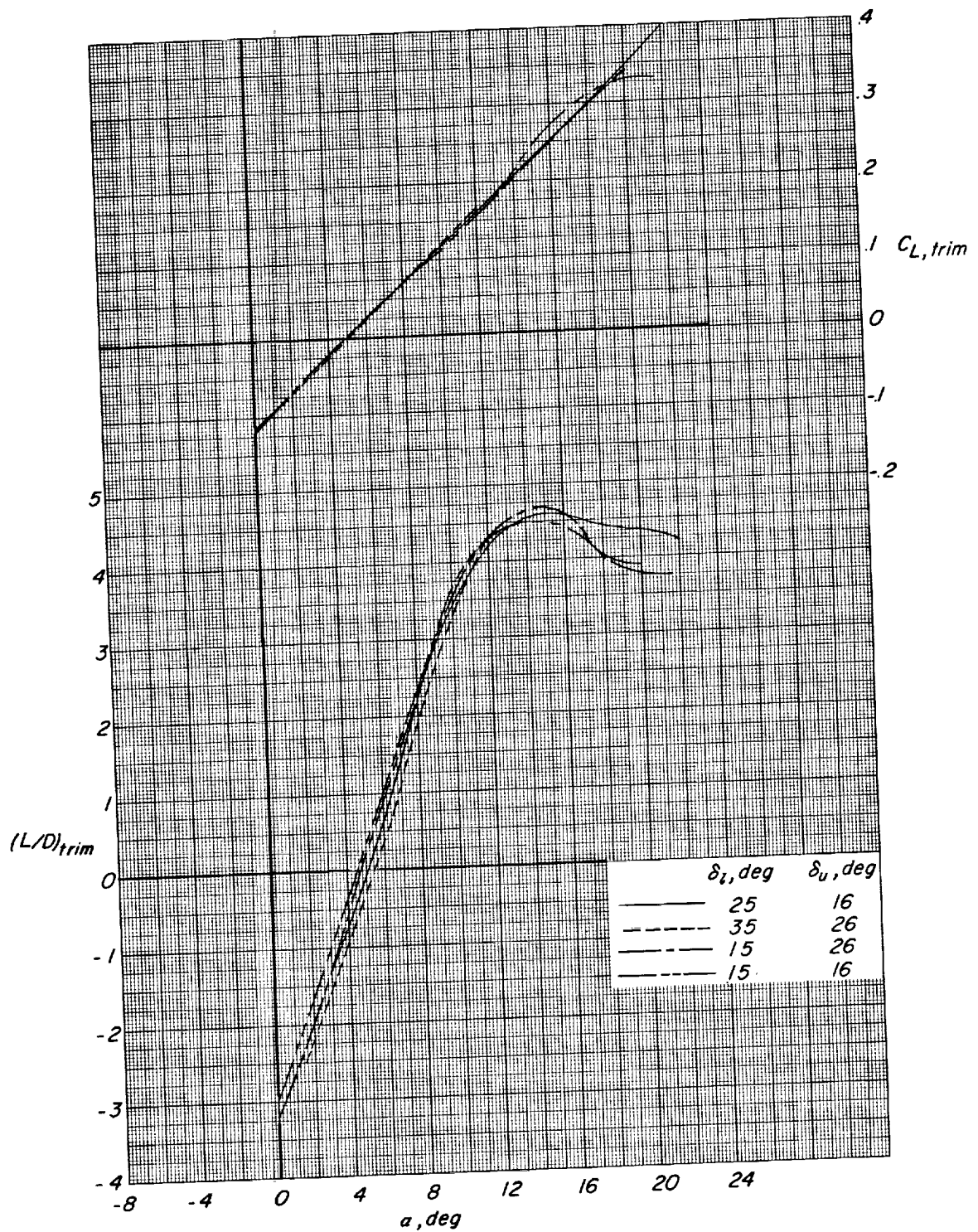


Figure 18.- Summary of effects of base extensions on trimmed characteristics. Three-fin HL-10 with original elevon ($\theta = 0^\circ$); modified fins E2 plus 14; vortex generators on.

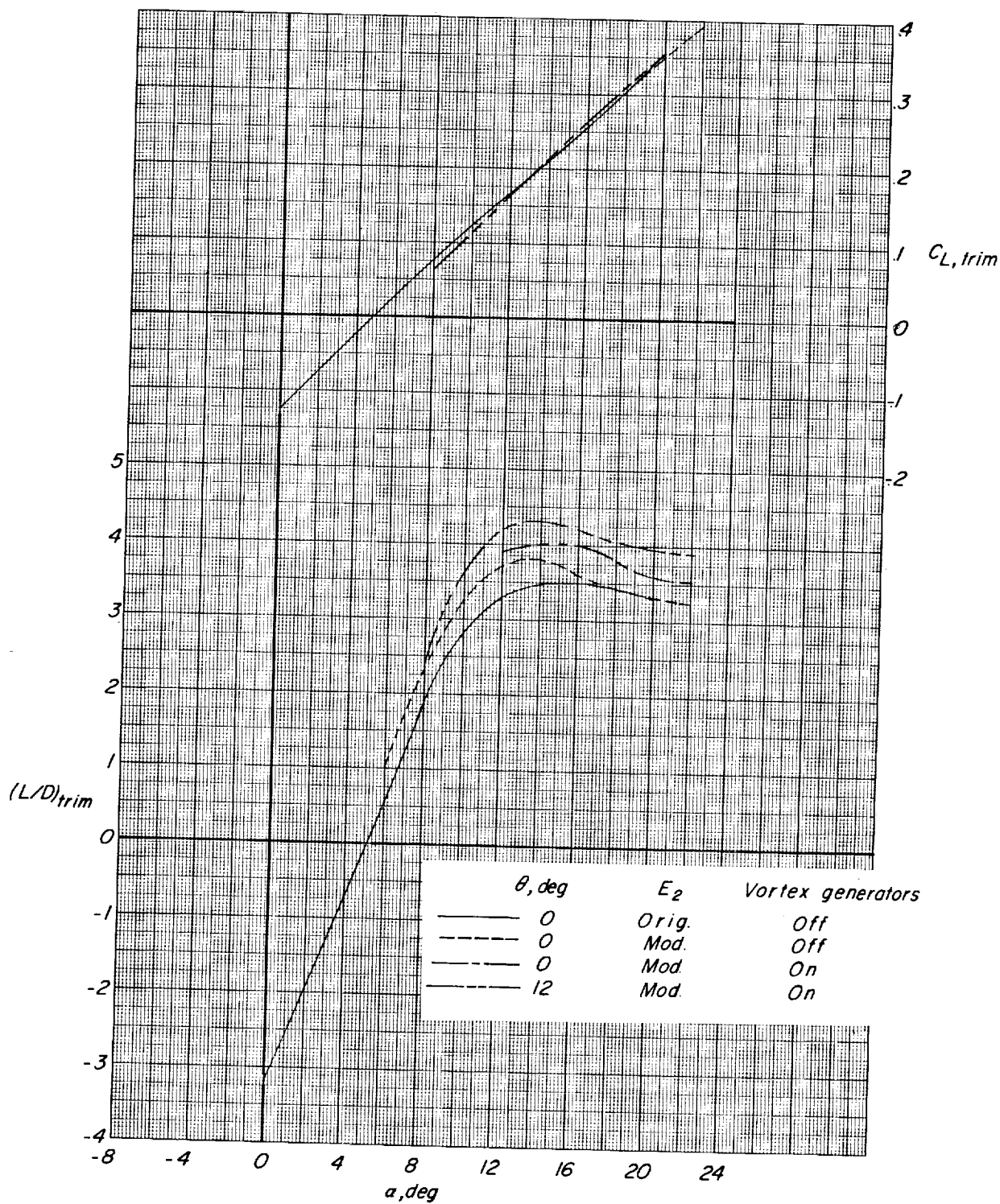


Figure 19.- Summary of effects of model components and elevon modifications on trimmed characteristics. One-fin HL-10.

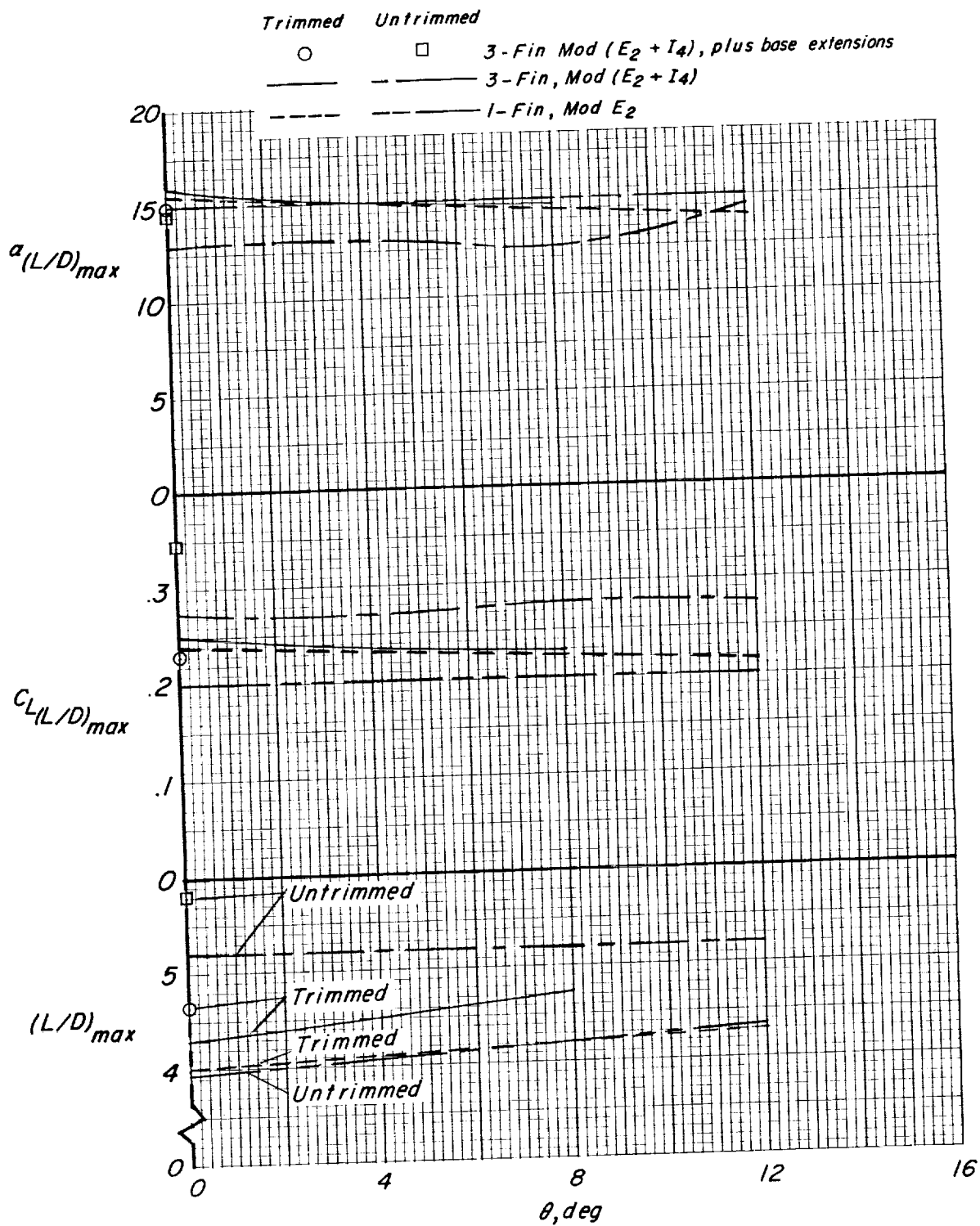


Figure 20.- Summary of effects of elevon modifications on trimmed and untrimmed characteristics at $(L/D)_{max}$. Vortex generators on.

[illegible]

CONFIDENTIAL

CONFIDENTIAL

22

[REDACTED]

[REDACTED]

CONFIDENTIAL

[REDACTED]

[REDACTED]